

Chapter 8

Mixing and Lifetimes

K. Anikeev, F. Azfar, N. Cason, H.W.K. Cheung, A. Dighe, I. Furic, G. Gutierrez, J. Hewett, R. Jesik, M. Jones, P. Kasper, J. Kroll, V.E. Kuznetsov, R. Kutschke, G. Majumder, M. Martin, U. Nierste, Ch. Paus, S. Rakitin, S. Stone, M. Tanaka, W. Taylor, J. Tseng, M. Voloshin, J. Wang, N. Xuan

8.1 Overview

In hadron colliders b -flavored hadrons are produced with a large boost. Therefore they are a fertile ground for measurements of decay time distributions. The neutral B_d^0 and B_s^0 mesons mix with their antiparticles, which leads to oscillations between the flavor eigenstates. A measurement of the oscillation frequency allows to determine the mass difference Δm_q , $q = d, s$, between the two physical mass eigenstates. The rapid oscillations in $B_s^0 - \bar{B}_s^0$ mixing have not been resolved yet and their discovery has a high priority for the B physics program at Run II. Once this has been achieved, the mass difference Δm_s will be known very precisely. By combining this information with the already measured Δm_d one will precisely determine the length of one side of the unitarity triangle. $\Delta m_d/\Delta m_s$ will have a larger impact on our knowledge of the unitarity triangle than any previously measured quantity and even than a precisely measured $\sin(2\beta)$. Accurately measured decay distributions will further reveal the pattern of b -hadron lifetimes. The large mass of the b quark compared to the QCD scale parameter Λ_{QCD} allows to expand the widths in terms of Λ_{QCD}/m_b . Differences among the total widths are dominated by terms of order $16\pi^2(\Lambda_{QCD}/m_b)^3$, the measurements of lifetime differences therefore probe the heavy quark expansion at the third order in the expansion parameter. From Run II we expect valuable new information on the lifetimes of the B^+ , B_d^0 and B_s^0 mesons, the width difference $\Delta\Gamma_s$ between the two physical B_s meson eigenstates the lifetimes of the Λ_b and eventually also of other b -flavored baryons.

From the current experimental situation it is not clear whether the heavy quark expansion can be applied to baryon lifetimes, and Run II data will help to settle this question.

This chapter first discusses the theory predictions for the various quantities in great detail. Where possible, we derive simple ‘pocket-calculator’ formulae to facilitate the analysis of the measurements. It is described which fundamental information can be gained from the various measurements. Some quantities are sensitive to physics beyond the Standard Model and we show how they are affected by new physics. Then we summarize the experimental techniques and present the results of the Monte Carlo simulations.

8.2 Theory of heavy hadron lifetimes[†]

The dominant weak decays of hadrons containing a heavy quark, c or b , are caused by the decay of the heavy quark. In the limit of a very large mass m_Q of a heavy quark Q the parton picture of the hadron decay should set in, where the inclusive decay rates of hadrons, containing Q , mesons ($Q\bar{q}$) and baryons (Qqq), are all the same and equal to the inclusive decay rate $\Gamma_{parton}(Q)$ of the heavy quark. Yet, the known inclusive decay rates [1] are conspicuously different for different hadrons, especially for charmed hadrons, whose lifetimes span a range of more than one order of magnitude from the shortest $\tau(\Omega_c) = 0.064 \pm 0.020$ ps to the longest $\tau(D^+) = 1.057 \pm 0.015$ ps, while the differences of lifetime among b hadrons are substantially smaller. The relation between the relative lifetime differences for charmed and b hadrons reflects the fact that the dependence of the inclusive decay rates on the light quark-gluon ‘environment’ in a particular hadron is a pre-asymptotic effect in the parameter m_Q , which effect vanishes as an inverse power of m_Q at large mass.

A theoretical framework for systematic description of the leading at $m_Q \rightarrow \infty$ term in the inclusive decay rate $\Gamma_{parton}(Q) \propto m_Q^5$ as well as of the terms relatively suppressed by inverse powers of m_Q is provided [2–4] by the operator product expansion (OPE) in m_Q^{-1} . Existing theoretical predictions for inclusive weak decay rates are in a reasonable agreement, within the expected range of uncertainty, with the data on lifetimes of charmed particles and with the so far available data on decays of B mesons. The only outstanding piece of present experimental data is on the lifetime of the Λ_b baryon: $\tau(\Lambda_b)/\tau(B_d) \approx 0.8$, for which ratio a theoretical prediction, given all the uncertainty involved, is unlikely to produce a number lower than 0.9. The number of available predictions for inclusive decay rates of charmed and b hadrons is sufficiently large for future experimental studies to firmly establish the validity status of the OPE based theory of heavy hadron decays, and, in particular, to find out whether the present contradiction between the theory and the data on $\tau(\Lambda_b)/\tau(B_d)$ is a temporary difficulty, or an evidence of fundamental flaws in theoretical understanding.

It is a matter of common knowledge that application of OPE to decays of charmed and b hadrons has potentially two caveats. One is that the OPE is used in the Minkowski kinematical domain, and therefore relies on the assumption of quark-hadron duality at the energies involved in the corresponding decays. In other words, it is assumed that sufficiently many exclusive hadronic channels contribute to the inclusive rate, so that the accidentals of the low-energy resonance structure do not affect the total rates of the inclusive processes. Theoretical attempts at understanding the onset of the quark-hadron duality are so far limited to model estimates [5,6], not yet suitable for direct quantitative evaluation of possible deviation from duality in charm and b decays. This point presents the most fundamental uncertainty of the OPE based approach, and presently can only be clarified by confronting theoretical predictions with experimental data. The second possible caveat in applying the OPE technique to inclusive charm decays is that the mass of the charm quark, m_c , may be insufficiently large for significant suppression of higher terms of the expansion in m_c^{-1} . The relative lightness of the charm quark, however, accounts for a qualitative, and even semi-quantitative, agreement of the OPE based predictions with the observed large

[†] Author: Mikhail Voloshin

spread of the lifetimes of charmed hadrons: the nonperturbative effects, formally suppressed by m_c^{-2} and m_c^{-3} are comparable with the ‘leading’ parton term and describe the hierarchy of the lifetimes.

Another uncertainty of a technical nature arises from poor knowledge of matrix elements of certain quark operators over hadron, arising as terms in OPE. These can be estimated within theoretical models, with inevitable ensuing model dependence, or, where possible, extracted from the experimental data. With these reservations spelled out, we discuss here the OPE based description of inclusive weak decays of charm and b hadrons, with emphasis on specific experimentally testable predictions, and on the measurements, which would less rely on model dependence of the estimates of the matrix elements, thus allowing to probe the OPE predictions at a fundamental level.

8.2.1 OPE for inclusive weak decay rates

The optical theorem of the scattering theory relates the total decay rate Γ_H of a hadron H_Q containing a heavy quark Q to the imaginary part of the ‘forward scattering amplitude’. For the case of weak decays the latter amplitude is described by the following effective operator

$$L_{eff} = 2 \operatorname{Im} \left[i \int d^4x e^{iqx} T \{ L_W(x), L_W(0) \} \right], \quad (8.1)$$

in terms of which the total decay rate is given by¹

$$\Gamma_H = \langle H_Q | L_{eff} | H_Q \rangle. \quad (8.2)$$

The correlator in equation (8.1) in general is a non-local operator. However at $q^2 = m_Q^2$ the dominating space-time intervals in the integral are of order m_Q^{-1} and one can expand the correlator in x , thus producing an expansion in inverse powers of m_Q . The leading term in this expansion describes the parton decay rate of the quark. For instance, the term in the nonleptonic weak Lagrangian $\sqrt{2} G_F V(\bar{q}_{1L} \gamma_\mu Q_L)(\bar{q}_{2L} \gamma_\mu q_{3L})$ with V being the appropriate combination of the CKM mixing factors, generates through Eq. (8.1) the leading term in the effective Lagrangian

$$L_{eff, nl}^{(0)} = |V|^2 \frac{G_F^2 m_Q^5}{64 \pi^3} \eta_{nl} (\bar{Q}Q), \quad (8.3)$$

where η_{nl} is the perturbative QCD radiative correction factor. This expression reproduces the well known formula for the inclusive nonleptonic decay rate of a heavy quark, associated with the underlying process $Q \rightarrow q_1 q_2 \bar{q}_3$, due to the relation $\langle H_Q | \bar{Q}Q | H_Q \rangle \approx \langle H_Q | Q^\dagger Q | H_Q \rangle = 1$, which is valid up to corrections of order m_Q^{-2} . One also sees from this example, that in order to separate individual semi-inclusive decay channels, e.g., nonleptonic with specific flavor quantum numbers, or semileptonic, one should simply pick up the corresponding relevant part of the weak Lagrangian L_W , describing the underlying process, to include in the correlator (8.1).

¹We use here the non-relativistic normalization for the *heavy* quark states: $\langle Q | Q^\dagger Q | Q \rangle = 1$.

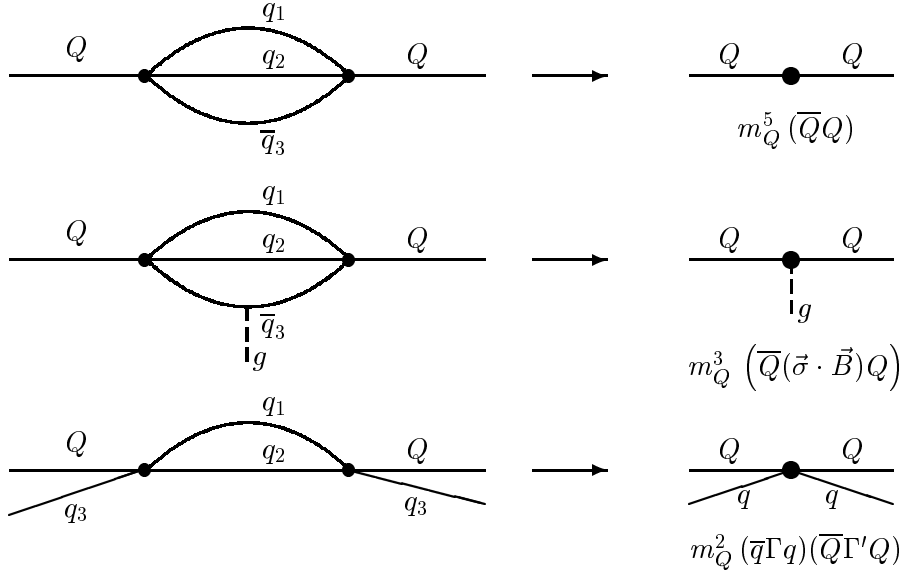


Figure 8.1: Graphs for three first terms in OPE for inclusive decay rates: the parton term, the chromomagnetic interaction, and the four-quark term.

The general expression for first three terms in the OPE for L_{eff} has the form

$$\begin{aligned}
 L_{eff} &= L_{eff}^{(0)} + L_{eff}^{(2)} + L_{eff}^{(3)} \\
 &= c^{(0)} \frac{G_F^2 m_Q^5}{64 \pi^3} (\bar{Q}Q) + c^{(2)} \frac{G_F^2 m_Q^3}{64 \pi^3} (\bar{Q} \sigma^{\mu\nu} G_{\mu\nu} Q) + \frac{G_F^2 m_Q^2}{4 \pi} \sum_i c_i^{(3)} (\bar{q}_i \Gamma_i q_i) (\bar{Q} \Gamma'_i Q),
 \end{aligned} \tag{8.4}$$

where the superscripts denote the power of m_Q^{-1} in the relative suppression of the corresponding term in the expansion with respect to the leading one, $G_{\mu\nu}$ is the gluon field tensor, q_i stand for light quarks, u , d , s , and, finally, Γ_i , Γ'_i denote spin and color structures of the four-quark operators. The coefficients $c^{(a)}$ depend on the specific part of the weak interaction Lagrangian L_W , describing the relevant underlying quark process.

One can notice the absence in the expansion (8.5) of a term suppressed by just one power of m_Q^{-1} , due to non-existence of operators of suitable dimension. Thus the decay rates receive no correction of relative order m_Q^{-1} in the limit of large m_Q , and the first pre-asymptotic corrections appear only in the order m_Q^{-2} .

The mechanisms giving rise to the three discussed terms in OPE are shown in Figure 8.1. The first, leading term corresponds to the parton decay, and does not depend on the light quark and gluon ‘environment’ of the heavy quark in a hadron. The second term describes the effect on the decay rate of the gluon field that a heavy quark ‘sees’ in a hadron. This term in fact is sensitive only to the chromomagnetic part of the gluon field, and contains the operator of the interaction of heavy quark chromomagnetic moment with the chromomagnetic field. Thus this term depends on the spin of the heavy quark, but does not depend on the flavors of the light quarks or antiquarks. Therefore this effect does not

split the inclusive decay rates within flavor $SU(3)$ multiplets of heavy hadrons, but generally gives difference of the rates, say, between mesons and baryons. The dependence on the light quark flavor arises from the third term in the expansion (8.5) which explicitly contains light quark fields. Historically, this part is interpreted in terms of two mechanisms [2,8,9]: the weak scattering (WS) and the Pauli interference (PI). The WS corresponds to a cross-channel of the underlying decay, generically $Q \rightarrow q_1 q_2 \bar{q}_3$, where either the quark q_3 is a spectator in a baryon and can undergo a weak scattering off the heavy quark: $q_3 Q \rightarrow q_1 q_2$, or an antiquark in meson, say \bar{q}_1 , weak-scatters (annihilates) in the process $\bar{q}_1 Q \rightarrow q_2 \bar{q}_3$. The Pauli interference effect arises when one of the final (anti)quarks in the decay of Q is identical to the spectator (anti)quark in the hadron, so that an interference of identical particles should be taken into account. The latter interference can be either constructive or destructive, depending on the relative spin-color arrangement of the (anti)quark produced in the decay and of the spectator one, thus the sign of the PI effect is found only as a result of specific dynamical calculation. In specific calculations, however, WS and PI arise from the same terms in OPE, depending on the hadron discussed, and technically there is no need to resort to the traditional terminology of WS and PI.

In what follows we discuss separately the effects of the three terms in the expansion (8.5) and their interpretation within the existing and future data.

8.2.2 The parton decay rate

The leading term in the OPE amounts to the perturbative expression for the decay rate of a heavy quark. In b hadrons the contribution of the subsequent terms in OPE is at the level of few percent, so that the perturbative part can be confronted with the data in its own right. In particular, for the B_d meson the higher terms in OPE contribute only about 1% of the total nonleptonic as well as of the semileptonic decay rate. Thus the data on these rates can be directly compared with the leading perturbative term in OPE.

The principal theoretical topic, associated with this term is the calculation of QCD radiative corrections, i.e. of the factor η_{nl} in Eq. (8.3) and of a similar factor, η_{sl} , for semileptonic decays. It should be noted, that even at this, perturbative, level there is a known long-standing problem between the existing data and the theory in that the current world average for the semileptonic branching ratio for the B mesons, $B_{sl}(B) = 10.45 \pm 0.21\%$, is somewhat lower than the value $B_{sl}(B) \geq 11.5$ preferred from the present knowledge of theoretical QCD radiative corrections to the ratio of nonleptonic to semileptonic decay rates (see, e.g., [10]). However, this apparent discrepancy may in fact be due to insufficient ‘depth’ of perturbative QCD calculation of the ratio η_{nl}/η_{sl} . In order to briefly elaborate on this point, we notice that the standard way of analyzing the perturbative radiative corrections in the nonleptonic decays is through the renormalization group (RG) summation of the leading log terms and the first next-to-leading terms [11,12] in the parameter $L \equiv \ln(m_W/m_b)$. For the semileptonic decays the logarithmic dependence on m_W/m_b is absent in all orders due to the weak current conservation at momenta larger than m_b , thus the correction is calculated by the standard perturbative technique, and a complete expression in the first order in α_s is available both for the total rate [13,14] and for the lepton spectrum [15]. In reality however the parameter $L \approx 2.8$ is not large, and non-logarithmic terms may well compete

with the logarithmic ones. This behavior is already seen from the known expression for the logarithmic terms: when expanded up to the order α_s^2 the result of Ref. [16] for the rate of decays with single final charmed quark takes the form

$$\frac{\Gamma(b \rightarrow c\bar{u}d) + \Gamma(b \rightarrow c\bar{u}s)}{3\Gamma(b \rightarrow ce\bar{\nu})} = 1 + \frac{\alpha_s}{\pi} + \frac{\alpha_s^2}{\pi^2} \left[4L^2 + \left(\frac{7}{6} + \frac{2}{3} c(m_c^2/m_b^2) \right) L \right], \quad (8.5)$$

where, in terms of notation of Ref. [16], $c(a) = c_{22}(a) - c_{12}(a)$. The behavior of the function $c(a)$ is known explicitly [16] and is quite weak: $c(0) = 19/2$, $c(1) = 6$, and $c(m_c^2/m_b^2) \approx 9.0$ for the realistic mass ratio $m_c/m_b \approx 0.3$. One can see that the term with the single logarithm L contributes about two thirds of that with L^2 in the term quadratic in α_s . Under such circumstances the RG summation of the terms with powers of L does not look satisfactory for numerical estimates of the QCD effects, at least at the so far considered level of the first next-to-leading order terms, and the next-to-next-to-leading terms can be equally important as the two known ones, which would eliminate the existing impasse between the theory and the data on $B_{sl}(B)$. One can present some arguments [17] that this is indeed the case for the b quark decay, although a complete calculation of these corrections is still unavailable.

8.2.3 Chromomagnetic and time dilation effects in decay rates

The corrections suppressed by two powers of m_Q^{-1} to inclusive decay rates arise from two sources [7]: the $O(m_Q^{-2})$ corrections to the matrix element of the leading operator, $(\bar{Q}Q)$, and the second term in OPE (8.5) containing the chromomagnetic interaction. The expression for the matrix element of the leading operator with the correction included is written in the form

$$\langle H_Q | \bar{Q}Q | H_Q \rangle = 1 - \frac{\mu_\pi^2(H_Q) - \mu_g^2(H_Q)}{2m_Q^2} + \dots, \quad (8.6)$$

where μ_π^2 and μ_g^2 are defined as

$$\begin{aligned} \mu_\pi^2 &= \langle H_Q | \bar{Q} (i\vec{D})^2 Q | H_Q \rangle, \\ \mu_g^2 &= \langle H_Q | \bar{Q} \frac{1}{2} \sigma^{\mu\nu} G_{\mu\nu} Q | H_Q \rangle, \end{aligned} \quad (8.7)$$

with D being the QCD covariant derivative. The correction in equation (8.6) in fact corresponds to the time dilation factor m_Q/E_Q , for the heavy quark decaying inside a hadron, where it has energy E_Q , which energy is contributed by the kinetic part ($\propto \mu_\pi^2$) and the chromomagnetic part ($\propto \mu_g^2$). The second term in OPE describes the effect of the chromomagnetic interaction in the decay process, and is also expressed through μ_g^2 .

The explicit formulas for the decay rates, including the effects up to the order m_Q^{-2} are found in [7] and for decays of the b hadrons read as follows. For the semileptonic decay rate

$$\Gamma_{sl}(H_b) = \frac{|V_{cb}|^2 G_F^2 m_b^5}{192 \pi^3} \langle H_b | \bar{b}b | H_b \rangle \left[1 + \frac{\mu_g^2}{m_b^2} \left(\frac{x}{2} \frac{d}{dx} - 2 \right) \right] \eta_{sl} I_0(x, 0, 0), \quad (8.8)$$

and for the nonleptonic decay rate

$$\Gamma_{nl}(H_b) = \frac{|V_{cb}|^2 G_F^2 m_b^5}{64 \pi^3} \langle H_b | \bar{b}b | H_b \rangle \left\{ \left[1 + \frac{\mu_g^2}{m_b^2} \left(\frac{x}{2} \frac{d}{dx} - 2 \right) \right] \eta_{nl} I(x) - 8\eta_2 \frac{\mu_g^2}{m_b^2} I_2(x) \right\}. \quad (8.9)$$

These formulas take into account only the dominant CKM mixing V_{cb} and neglect the small one, V_{ub} . The following notation is also used: $x = m_c/m_b$, $I_0(x, y, z)$ stands for the kinematical suppression factor in a three-body weak decay due to masses of the final fermions. In particular,

$$\begin{aligned} I_0(x, 0, 0) &= (1 - x^4)(1 - 8x^2 + x^4) - 24x^4 \ln x, \\ I_0(x, x, 0) &= (1 - 14x^2 - 2x^4 - 12x^6)\sqrt{1 - 4x^2} + 24(1 - x^4) \ln \frac{1 + \sqrt{1 - 4x^2}}{1 - \sqrt{1 - 4x^2}}. \end{aligned} \quad (8.10)$$

Furthermore, $I(x) = I_0(x, 0, 0) + I_0(x, x, 0)$, and

$$I_2(x) = (1 - x^2)^3 + \left(1 + \frac{1}{2}x^2 + 3x^4 \right) \sqrt{1 - 4x^2} - 3x^2(1 - 2x^4) \ln \frac{1 + \sqrt{1 - 4x^2}}{1 - \sqrt{1 - 4x^2}}.$$

Finally, the QCD radiative correction factor η_2 in Eq. (8.9) is known in the leading logarithmic approximation and is expressed in terms of the well known coefficients C_+ and C_- in the renormalization of the nonleptonic weak interaction: $\eta_2 = (C_+^2(m_b) - C_-^2(m_b))/6$ with

$$C_-(\mu) = C_+^{-2}(\mu) = \left[\frac{\alpha_s(\mu)}{\alpha_s(m_W)} \right]^{4/b}, \quad (8.11)$$

and b is the coefficient in the QCD beta function. The value of b relevant to b decays is $b = 23/3$.

Numerically, for $x \approx 0.3$, the expressions for the decay rates can be written as

$$\begin{aligned} \Gamma_{sl}(H_b) &= \Gamma_{sl}^{parton} \left(1 - \frac{\mu_\pi^2(H_b) - \mu_g^2(H_b)}{2m_b^2} - 2.6 \frac{\mu_g^2(H_b)}{m_b^2} \right), \\ \Gamma_{nl}(H_b) &= \Gamma_{nl}^{parton} \left(1 - \frac{\mu_\pi^2(H_b) - \mu_g^2(H_b)}{2m_b^2} - 1.0 \frac{\mu_g^2(H_b)}{m_b^2} \right), \end{aligned} \quad (8.12)$$

where Γ^{parton} is the perturbation theory value of the corresponding decay rate of b quark.

The matrix elements μ_π^2 and μ_g^2 are related to the spectroscopic formula for a heavy hadron mass M ,

$$M(H_Q) = m_Q + \bar{\Lambda}(H_Q) + \frac{\mu_\pi^2(H_Q) - \mu_g^2(H_Q)}{2m_Q} + \dots \quad (8.13)$$

Being combined with the spin counting for pseudoscalar and vector mesons, this formula allows to find the value of μ_g^2 in pseudoscalar mesons from the mass splitting:

$$\mu_g^2(B) = \frac{3}{4} (M_{B^*}^2 - M_B^2) \approx 0.36 \text{ GeV}^2. \quad (8.14)$$

The value of μ_π^2 for B mesons is less certain. It is constrained by the inequality [18], $\mu_\pi^2(H_Q) \geq \mu_g^2(H_Q)$, and there are theoretical estimates from the QCD sum rules [19]: $\mu_\pi^2(B) = 0.54 \pm 0.12 \text{ GeV}^2$ and from an analysis of spectroscopy of heavy hadrons [20]: $\mu_\pi^2(B) = 0.3 \pm 0.2 \text{ GeV}^2$. In any event, the discussed corrections are rather small for b hadrons, given that $\mu_g^2/m_b^2 \approx 0.015$. The largest, in relative terms, effect of these corrections in B meson decays is on the semileptonic decay rate, where it amounts to 4–5 % suppression of the rate, which rate however is only a moderate fraction of the total width. In the dominant nonleptonic decay rate the effect is smaller, and, according to the formula (8.12) amounts to about 1.5–2 %.

The effect of the m_Q^{-2} corrections can be evaluated with a somewhat better certainty for the ratio of the decay rates of Λ_b and B mesons. This is due to the fact that $\mu_g^2(\Lambda_b) = 0$, since there is no correlation of the spin of the heavy quark in Λ_b with the light component, having overall quantum numbers $J^P = 0^+$. Then, applying the formula (8.12) to B and Λ_b , we find for the ratio of the (dominant) nonleptonic decay rates:

$$\frac{\Gamma_{nl}(\Lambda_b)}{\Gamma_{nl}(B)} = 1 - \frac{\mu_\pi^2(\Lambda_b) - \mu_\pi^2(B)}{2 m_b^2} + 0.5 \frac{\mu_g^2(B)}{m_b^2}. \quad (8.15)$$

The difference of the kinetic terms, $\mu_\pi^2(\Lambda_b) - \mu_\pi^2(B)$, can be estimated from the mass formula:

$$\mu_\pi^2(\Lambda_b) - \mu_\pi^2(B) = \frac{2 m_b m_c}{m_b - m_c} [\overline{M}(B) - \overline{M}(D) - M(\Lambda_b) + M(\Lambda_c)] = 0 \pm 0.04 \text{ GeV}^2, \quad (8.16)$$

where \overline{M} is the spin-averaged mass of the mesons, e.g., $\overline{M}(B) = (M(B) + 3M(B^*))/4$. The estimated difference of the kinetic terms is remarkably small. Thus the effect in the ratio of the decay rates essentially reduces to the chromomagnetic term, which is also rather small and accounts for less than 1% difference of the rates. For the ratio of the semileptonic decay rates the chromomagnetic term is approximately four times larger, but then the contribution of the semileptonic rates to the total width is rather small. Thus one concludes that the terms of order m_b^{-2} in the OPE expansion for the decay rates can account only for about 1% difference of the lifetimes of Λ_b and the B mesons.

The significance of the m_Q^{-2} terms is substantially different for the decay rates of charmed hadrons, where these effects suppress the inclusive decays of the D mesons by about 40% with respect to those of the charmed hyperons in a reasonable agreement with the observed pattern of the lifetimes.

It should be emphasized once again that the m_Q^{-2} effects do not depend on the flavors of the spectator quarks or antiquarks. Thus the explanation of the variety of the inclusive decay rates within the flavor $SU(3)$ multiplets, observed for charmed hadrons and expected for the b ones, has to be sought among the m_Q^{-3} terms.

8.2.4 $L_{eff}^{(3)}$ Coefficients and operators

Although the third term in the expansion (8.5) is formally suppressed by an extra power of m_Q^{-1} , its effects are comparable to, or even larger than the effects of the second term. This

is due to the fact that the diagrams determining the third term (see Fig. 8.1) contain a two-body phase space, while the first two terms involve a three-body phase space. This brings in a numerical enhancement factor, typically $4\pi^2$. The enhanced numerical significance of the third term in OPE, generally, does not signal a poor convergence of the expansion in inverse heavy quark mass for decays of b , and even charmed, hadrons the numerical enhancement factor is a one time occurrence in the series, and there is no reason for similar ‘anomalous’ enhancement among the higher terms in the expansion.

Here we first present the expressions for the relevant parts of $L_{eff}^{(3)}$ for decays of b and c hadrons in the form of four-quark operators and then proceed to a discussion of hadronic matrix elements and the effects in specific inclusive decay rates. The consideration of the effects in decays of charmed hadrons is interesting in its own right, and leads to new predictions to be tested experimentally, and is also important for understanding the magnitude of the involved matrix elements using the existing data on charm decays.

We start with considering the term $L_{eff}^{(3)}$ in b hadron nonleptonic decays, $L_{eff,nl}^{(3,b)}$, induced by the underlying processes $b \rightarrow c\bar{u}d$, $b \rightarrow c\bar{c}s$, $b \rightarrow c\bar{u}s$, and $b \rightarrow c\bar{c}d$. Unlike the case of three-body decay, the kinematical difference between the two-body states $c\bar{c}$ and $c\bar{u}$, involved in calculation of $L_{eff,nl}^{(3,b)}$ is of the order of $m_c^2/m_b^2 \approx 0.1$ and is rather small. At present level of accuracy in discussing this term in OPE, one can safely neglect the effect of finite charmed quark mass². In this approximation the expression for $L_{eff,nl}^{(3,b)}$ reads as [4]

$$\begin{aligned} L_{eff,nl}^{(3,b)} = & |V_{cb}|^2 \frac{G_F^2 m_b^2}{4\pi} \left\{ \tilde{C}_1 (\bar{b}\Gamma_\mu b)(\bar{u}\Gamma_\mu u) + \tilde{C}_2 (\bar{b}\Gamma_\mu u)(\bar{u}\Gamma_\mu b) \right. \\ & + \tilde{C}_5 (\bar{b}\Gamma_\mu b + \frac{2}{3}\bar{b}\gamma_\mu\gamma_5 b)(\bar{q}\Gamma_\mu q) + \tilde{C}_6 (\bar{b}_i\Gamma_\mu b_k + \frac{2}{3}\bar{b}_i\gamma_\mu\gamma_5 b_k)(\bar{q}_k\Gamma_\mu q_i) \\ & + \frac{1}{3}\tilde{\kappa}^{1/2}(\tilde{\kappa}^{-2/9} - 1) \left[2(\tilde{C}_+^2 - \tilde{C}_-^2)(\bar{b}\Gamma_\mu t^a b)j_\mu^a \right. \\ & \left. \left. - (5\tilde{C}_+^2 + \tilde{C}_-^2 - 6\tilde{C}_+ \tilde{C}_-)(\bar{b}\Gamma_\mu t^a b + \frac{2}{3}\bar{b}\gamma_\mu\gamma_5 t^a b)j_\mu^a \right] \right\}, \end{aligned} \quad (8.17)$$

where the notation $(\bar{q}\Gamma q) = (\bar{d}\Gamma d) + (\bar{s}\Gamma s)$ is used, the indices i, k are the color triplet ones, $\Gamma_\mu = \gamma_\mu(1 - \gamma_5)$, and $j_\mu^a = \bar{u}\gamma_\mu t^a u + \bar{d}\gamma_\mu t^a d + \bar{s}\gamma_\mu t^a s$ is the color current of the light quarks with $t^a = \lambda^a/2$ being the generators of the color $SU(3)$. The notation \tilde{C}_\pm , is used as shorthand for the short-distance renormalization coefficients $C_\pm(\mu)$ at $\mu = m_b$: $\tilde{C}_\pm \equiv C_\pm(m_b)$. The expression (8.17) is written in the leading logarithmic approximation for the QCD radiative effects in a low normalization point μ such that $\mu \ll m_b$ (but still, at least formally, $\mu \gg \Lambda_{QCD}$). For such μ there arises so called ‘hybrid’ renormalization [22], depending on the factor $\tilde{\kappa} = \alpha_s(\mu)/\alpha_s(m_b)$. The coefficients \tilde{C}_A with $A = 1, \dots, 6$ in Eq. (8.17) have the following explicit expressions in terms of \tilde{C}_\pm and $\tilde{\kappa}$:

$$\begin{aligned} \tilde{C}_1 &= \tilde{C}_+^2 + \tilde{C}_-^2 + \frac{1}{3}(1 - \kappa^{1/2})(\tilde{C}_+^2 - \tilde{C}_-^2), \\ \tilde{C}_2 &= \kappa^{1/2}(\tilde{C}_+^2 - \tilde{C}_-^2), \end{aligned}$$

²The full expression for a finite charmed quark mass can be found in [21]

$$\begin{aligned}
\tilde{C}_3 &= -\frac{1}{4} \left[(\tilde{C}_+ - \tilde{C}_-)^2 + \frac{1}{3}(1 - \kappa^{1/2})(5\tilde{C}_+^2 + \tilde{C}_-^2 + 6\tilde{C}_+\tilde{C}_-) \right], \\
\tilde{C}_4 &= -\frac{1}{4} \kappa^{1/2} (5\tilde{C}_+^2 + \tilde{C}_-^2 + 6\tilde{C}_+\tilde{C}_-), \\
\tilde{C}_5 &= -\frac{1}{4} \left[(\tilde{C}_+ + \tilde{C}_-)^2 + \frac{1}{3}(1 - \kappa^{1/2})(5\tilde{C}_+^2 + \tilde{C}_-^2 - 6\tilde{C}_+\tilde{C}_-) \right], \\
\tilde{C}_6 &= -\frac{1}{4} \kappa^{1/2} (5\tilde{C}_+^2 + \tilde{C}_-^2 - 6\tilde{C}_+\tilde{C}_-).
\end{aligned} \tag{8.18}$$

The expression for the CKM dominant semileptonic decays of b hadrons, associated with the elementary process $b \rightarrow c \ell \nu$ does not look to be of an immediate interest. The reason is that this process is intrinsically symmetric under the flavor $SU(3)$, and one expects no significant splitting of the semileptonic decay rates within $SU(3)$ multiplets of the b hadrons. The only possible effect of this term, arising through a penguin-like mechanism can be in a small overall shift of semileptonic decay rates between B mesons and baryons. However, these effects are quite suppressed and are believed to be even smaller than the ones arising from the discussed m_b^{-2} terms.

For charm decays there is a larger, than for b hadrons, variety of effects associated with $L_{eff}^{(3)}$ that can be studied experimentally, and we present here the relevant parts of the effective Lagrangian. For the CKM dominant nonleptonic decays of charm, originating from the quark process $c \rightarrow s u \bar{d}$, the discussed term in OPE has the form

$$\begin{aligned}
L_{eff,nl}^{(3,\Delta C=\Delta S)} &= \cos^4 \theta_c \frac{G_F^2 m_c^2}{4\pi} \left\{ C_1 (\bar{c} \Gamma_\mu c) (\bar{d} \Gamma_\mu d) + C_2 (\bar{c} \Gamma_\mu d) (\bar{d} \Gamma_\mu c) \right. \\
&+ C_3 (\bar{c} \Gamma_\mu c + \frac{2}{3} \bar{c} \gamma_\mu \gamma_5 c) (\bar{s} \Gamma_\mu s) + C_4 (\bar{c}_i \Gamma_\mu c_k + \frac{2}{3} \bar{c}_i \gamma_\mu \gamma_5 c_k) (\bar{s}_k \Gamma_\mu s_i) \\
&+ C_5 (\bar{c} \Gamma_\mu c + \frac{2}{3} \bar{c} \gamma_\mu \gamma_5 c) (\bar{u} \Gamma_\mu u) + C_6 (\bar{c}_i \Gamma_\mu c_k + \frac{2}{3} \bar{c}_i \gamma_\mu \gamma_5 c_k) (\bar{u}_k \Gamma_\mu u_i) \\
&\left. + \frac{1}{3} \kappa^{1/2} (\kappa^{-2/9} - 1) \left[2 (C_+^2 - C_-^2) (\bar{c} \Gamma_\mu t^a c) j_\mu^a - (5C_+^2 + C_-^2) (\bar{c} \Gamma_\mu t^a c + \frac{2}{3} \bar{c} \gamma_\mu \gamma_5 t^a c) j_\mu^a \right] \right\},
\end{aligned} \tag{8.19}$$

where, θ_c is the Cabibbo angle, and the coefficients without the tilde are given by the same expressions as above for the b decays (i.e., those with tilde) with the replacement $m_b \rightarrow m_c$. The part of the notation in the superscript $\Delta C = \Delta S$ points to the selection rule for the dominant CKM unsuppressed nonleptonic decays. One can rather realistically envisage however a future study of inclusive rates for the once CKM suppressed decays of charmed hadrons³, satisfying the selection rule $\Delta S = 0$ and associated with the quark processes $c \rightarrow d u \bar{s}$ and $c \rightarrow d u \bar{d}$. The corresponding part of the effective Lagrangian for these processes reads as

³Even if the inclusive rate of these decays is not to be separated experimentally, they contribute about 10% of the total decay rate, and it is worthwhile to include their contribution in the balance of the total width.

$$\begin{aligned}
L_{eff, nl}^{(3, \Delta S=0)} = & \cos^2 \theta_c \sin^2 \theta_c \frac{G_F^2 m_c^2}{4\pi} \left\{ C_1 (\bar{c}\Gamma_\mu c)(\bar{q}\Gamma_\mu q) + C_2 (\bar{c}_i\Gamma_\mu c_k)(\bar{q}_k\Gamma_\mu q_i) \right. \\
& + C_3 (\bar{c}\Gamma_\mu c + \frac{2}{3}\bar{c}\gamma_\mu\gamma_5 c)(\bar{q}\Gamma_\mu q) + C_4 (\bar{c}_i\Gamma_\mu c_k + \frac{2}{3}\bar{c}_i\gamma_\mu\gamma_5 c_k)(\bar{q}_k\Gamma_\mu q_i) \\
& + 2 C_5 (\bar{c}\Gamma_\mu c + \frac{2}{3}\bar{c}\gamma_\mu\gamma_5 c)(\bar{u}\Gamma_\mu u) + 2 C_6 (\bar{c}_i\Gamma_\mu c_k + \frac{2}{3}\bar{c}_i\gamma_\mu\gamma_5 c_k)(\bar{u}_k\Gamma_\mu u_i) \\
& \left. + \frac{2}{3}\kappa^{1/2}(\kappa^{-2/9} - 1) \left[2(C_+^2 - C_-^2)(\bar{c}\Gamma_\mu t^a c)j_\mu^a - (5C_+^2 + C_-^2)(\bar{c}\Gamma_\mu t^a c + \frac{2}{3}\bar{c}\gamma_\mu\gamma_5 t^a c)j_\mu^a \right] \right\}, \tag{8.20}
\end{aligned}$$

where again the notation $(\bar{q}\Gamma q) = (\bar{d}\Gamma d) + (\bar{s}\Gamma s)$ is used.

The semileptonic decays of charm, the CKM dominant, associated with $c \rightarrow s \ell \nu$, and the CKM suppressed, originating from $c \rightarrow s \ell \nu$, contribute to the semileptonic decay rate, which certainly can be measured experimentally. The expression for the part of the effective Lagrangian, describing the m_Q^{-3} terms in these decays is [17,24,25]

$$\begin{aligned}
L_{eff, sl}^{(3)} = & \frac{G_F^2 m_c^2}{12\pi} \left\{ \cos^2 \theta_c \left[L_1 (\bar{c}\Gamma_\mu c + \frac{2}{3}\bar{c}\gamma_\mu\gamma_5 c)(\bar{s}\Gamma_\mu s) + L_2 (\bar{c}_i\Gamma_\mu c_k + \frac{2}{3}\bar{c}_i\gamma_\mu\gamma_5 c_k)(\bar{s}_k\Gamma_\mu s_i) \right] \right. \\
& + \sin^2 \theta_c \left[L_1 (\bar{c}\Gamma_\mu c + \frac{2}{3}\bar{c}\gamma_\mu\gamma_5 c)(\bar{d}\Gamma_\mu d) + L_2 (\bar{c}_i\Gamma_\mu c_k + \frac{2}{3}\bar{c}_i\gamma_\mu\gamma_5 c_k)(\bar{d}_k\Gamma_\mu d_i) \right] \\
& \left. - 2\kappa^{1/2}(\kappa^{-2/9} - 1)(\bar{c}\Gamma_\mu t^a c + \frac{2}{3}\bar{c}\gamma_\mu\gamma_5 t^a c)j_\mu^a \right\}, \tag{8.21}
\end{aligned}$$

with the coefficients L_1 and L_2 found as

$$L_1 = (\kappa^{1/2} - 1), \quad L_2 = -3\kappa^{1/2}. \tag{8.22}$$

8.2.5 Effects of $L_{eff}^{(3)}$ in mesons

The expressions for the terms in $L_{eff}^{(3)}$ still leave us with the problem of evaluating the matrix elements of the four-quark operators over heavy hadrons in order to calculate the effects in the decay rates according to the formula (8.2). In doing so only few conclusions can be drawn in a reasonably model independent way, i.e., without resorting to evaluation of the matrix elements using specific ideas about the dynamics of quarks inside hadrons. The most straightforward prediction can in fact be found for b hadrons. Namely, one can notice that the operator (8.17) is symmetric under the flavor U spin (an SU(2) subgroup of the flavor SU(3), which mixes s and d quarks). This is a direct consequence of neglecting the small kinematical effect of the charmed quark mass. However the usual (in)accuracy of the flavor SU(3) symmetry is likely to be a more limiting factor for the accuracy of this symmetry, than the corrections of order m_c^2/m_b^2 . Modulo this reservation the immediate prediction from this symmetry is the degeneracy of inclusive decay rates within U spin doublets:

$$\Gamma(B_d) = \Gamma(B_s), \quad \Gamma(\Lambda_b) = \Gamma(\Xi_b^0), \tag{8.23}$$

where $\Gamma(B_s)$ stands for the average rate over the two eigenstates of the $B_s - \bar{B}_s$ oscillations. The data on decay rates of the cascade hyperon Ξ_b^0 are not yet available, while the currently

measured lifetimes of B_d and B_s are within less than 2% from one another. Theoretically, the difference of the lifetimes, associated with possible violation of the $SU(3)$ symmetry and with breaking of the U symmetry of the effective Lagrangian (8.17), is expected to not exceed about 1%.

For the non-vanishing matrix elements of four-quark operators over pseudoscalar mesons one traditionally starts with the factorization formula and parameterizes possible deviation from factorization in terms of ‘bag constants’. Within the normalization convention adopted here the relations used in this parameterization read as

$$\begin{aligned}\langle P_{Q\bar{q}} | (\bar{Q} \Gamma_\mu q) (\bar{q} \Gamma_\mu Q) | P_{Q\bar{q}} \rangle &= \frac{1}{2} f_P^2 M_P B, \\ \langle P_{Q\bar{q}} | (\bar{Q} \Gamma_\mu Q) (\bar{q} \Gamma_\mu q) | P_{Q\bar{q}} \rangle &= \frac{1}{6} f_P^2 M_P \tilde{B},\end{aligned}\tag{8.24}$$

where $P_{Q\bar{q}}$ stands for pseudoscalar meson made of Q and \bar{q} , f_P is the annihilation constant for the meson, and B and \tilde{B} are bag constants. The parameters B and \tilde{B} generally depend on the normalization point μ for the operators, and this dependence is compensated by the μ dependence of the coefficients in $L_{eff}^{(3)}$, so that the results for the physical decay rate difference do not depend on μ . If the normalization point μ is chosen at the heavy quark mass (i.e. $\mu = m_b$ for B mesons, and $\mu = m_c$ for D mesons) the predictions for the difference of total decay rates take a simple form in terms of the corresponding bag constants (generally different between B and D):

$$\begin{aligned}\Gamma(B^\pm) - \Gamma(B^0) &= |V_{cb}|^2 \frac{G_F^2 m_b^3 f_B^2}{8\pi} \left[(\tilde{C}_+^2 - \tilde{C}_-^2) B(m_b) + \frac{1}{3} (\tilde{C}_+^2 + \tilde{C}_-^2) \tilde{B}(m_b) \right] \\ &\approx -0.025 \left(\frac{f_B}{200 \text{ MeV}} \right)^2 ps^{-1},\end{aligned}\tag{8.25}$$

$$\begin{aligned}\Gamma(D^\pm) - \Gamma(D^0) &= \cos^4 \theta_c \frac{G_F^2 m_c^3 f_D^2}{8\pi} \left[(C_+^2 - C_-^2) B(m_c) + \frac{1}{3} (C_+^2 + C_-^2) \tilde{B}(m_c) \right] \\ &\sim -0.8 \left(\frac{f_D}{200 \text{ MeV}} \right)^2 ps^{-1},\end{aligned}\tag{8.26}$$

where the numerical values are written in the approximation of exact factorization: $B = 1$, and $\tilde{B} = 1$. It is seen from the numerical estimates that, even given all the theoretical uncertainties, the presented approach is in reasonable agreement with the data on the lifetimes of D and B mesons. In particular, this approach describes, at least qualitatively, the strong suppression of the decay rate of D^\pm mesons relative to D^0 , the experimental observation of which has in fact triggered in early 80-s the theoretical study of preasymptotic in heavy quark mass effects in inclusive decay rates. For the B mesons the estimate (8.25) is also in a reasonable agreement with the current data for the discussed difference ($-0.043 \pm 0.017 ps^{-1}$).

8.2.6 Effects of $L_{eff}^{(3)}$ in baryons

The weakly decaying heavy hyperons, containing either c or b quark are: $\Lambda_Q \sim Qud$, $\Xi_Q^{(u)} \sim Qus$, $\Xi_Q^{(d)} \sim Qds$, and $\Omega_Q \sim Qss$. The first three baryons form an $SU(3)$ (anti)triplet. The light diquark in all three is in the state with quantum numbers $J^P = 0^+$, so that there is no correlation of the spin of the heavy quark with the light component of the baryon. On the contrary, in Ω_Q the two strange quarks form a $J^P = 1^+$ state, and a correlation between the spins of heavy and light quarks is present. The absence of spin correlation for the heavy quark in the triplet of hyperons somewhat reduces the number of independent four-quark operators, having nonvanishing diagonal matrix elements over these baryons. Indeed, the operators entering $L_{eff}^{(3)}$ contain both vector and axial bilinear forms for the heavy quarks. However the axial part requires a correlation of the heavy quark spin with that of a light quark, and is thus vanishing for the hyperons in the triplet. Therefore only the structures with vector currents are relevant for these hyperons. These structures are of the type $(\bar{c}\gamma_\mu c)(\bar{q}\gamma_\mu q)$ and $(\bar{c}_i\gamma_\mu c_k)(\bar{q}_k\gamma_\mu q_i)$ with q being d , s or u . The flavor $SU(3)$ symmetry then allows to express, for each of the two color combinations, the matrix elements of three different operators, corresponding to three flavors of q , over the baryons in the triplet in terms of only two combinations: flavor octet and flavor singlet. Thus all effects of $L_{eff}^{(3)}$ in the triplet of the baryons can be expressed in terms of four independent combinations of matrix elements. These can be chosen in the following way:

$$\begin{aligned}
 x &= \left\langle \frac{1}{2} (\bar{Q}\gamma_\mu Q) [(\bar{u}\gamma_\mu u) - (\bar{s}\gamma_\mu s)] \right\rangle_{\Xi_Q^{(d)} - \Lambda_Q} \\
 &= \left\langle \frac{1}{2} (\bar{Q}\gamma_\mu Q) [(\bar{s}\gamma_\mu s) - (\bar{d}\gamma_\mu d)] \right\rangle_{\Lambda_Q - \Xi_Q^{(u)}}, \\
 y &= \left\langle \frac{1}{2} (\bar{Q}_i\gamma_\mu Q_k) [(\bar{u}_k\gamma_\mu u_i) - (\bar{s}_k\gamma_\mu s_i)] \right\rangle_{\Xi_Q^{(d)} - \Lambda_Q} \\
 &= \left\langle \frac{1}{2} (\bar{Q}_i\gamma_\mu Q_k) [(\bar{s}_k\gamma_\mu s_i) - (\bar{d}_k\gamma_\mu d_i)] \right\rangle_{\Lambda_Q - \Xi_Q^{(u)}}, \tag{8.27}
 \end{aligned}$$

with the notation for the differences of the matrix elements: $\langle \mathcal{O} \rangle_{A-B} = \langle A | \mathcal{O} | A \rangle - \langle B | \mathcal{O} | B \rangle$, for the flavor octet part and the matrix elements:

$$\begin{aligned}
 x_s &= \frac{1}{3} \langle H_Q | (\bar{Q}\gamma_\mu Q) \left((\bar{u}\gamma_\mu u) + (\bar{d}\gamma_\mu d) + (\bar{s}\gamma_\mu s) \right) | H_Q \rangle \\
 y_s &= \frac{1}{3} \langle H_Q | (\bar{Q}_i\gamma_\mu Q_k) \left((\bar{u}_k\gamma_\mu u_i) + (\bar{d}_k\gamma_\mu d_i) + (\bar{s}_k\gamma_\mu s_i) \right) | H_Q \rangle \tag{8.28}
 \end{aligned}$$

for the flavor singlet part, where H_Q stands for any heavy hyperon in the (anti)triplet.

The initial, very approximate, theoretical estimates of the matrix elements [4] were essentially based on a non-relativistic constituent quark model, where these matrix elements are proportional to the density of a light quark at the location of the heavy one, i.e., in terms of the wave function, proportional to $|\psi(0)|^2$. Using then the same picture for the

matrix elements over pseudoscalar mesons, relating the quantity $|\psi(0)|^2$ to the annihilation constant f_P , and assuming that $|\psi(0)|^2$ is approximately the same in baryons as in mesons, one arrived at the estimate

$$y = -x = x_s = -y_s \approx \frac{f_D^2 M_D}{12} \approx 0.006 \text{ GeV}^2, \quad (8.29)$$

where the sign relation between x and y is inferred from the color antisymmetry of the constituent quark wave function for baryons. Since the constituent picture was believed to be valid at distances of the order of the hadron size, the estimate (8.29) was applied to the matrix elements in a low normalization point where $\alpha_s(\mu) \approx 1$. For the matrix elements of the operators, containing s quarks over the Ω_Q hyperon, this picture predicts an enhancement factor due to the spin correlation:

$$\langle \Omega_Q | (\bar{Q} \Gamma_\mu Q) (\bar{s} \Gamma_\mu s) | \Omega_Q \rangle = -\langle \Omega_Q | (\bar{Q}_i \Gamma_\mu Q_k) (\bar{s}_k \Gamma_\mu s_i) | \Omega_Q \rangle = \frac{10}{3} y \quad (8.30)$$

Although these simple estimates allowed to correctly predict [4] the hierarchy of lifetimes of charmed hadrons prior to establishing this hierarchy experimentally, they fail to quantitatively predict the differences of lifetimes of charmed baryons. We shall see that the available data indicate that the color antisymmetry relation is badly broken, and the absolute value of the matrix elements is larger, than the naive estimate (8.29), especially for the quantity x .

It should be emphasized that in the heavy quark limit the matrix elements (8.27) and (8.28) do not depend on the flavor of the heavy quark, provided that the same normalization point μ is used. Therefore, applying the OPE formulas to both charmed and b baryons, one can extract the values for the matrix elements from available data on charmed hadrons, and then make predictions for b baryons, as well as for other inclusive decay rates, e.g., semileptonic, for charmed hyperons.

The only data available so far, which would allow to extract the matrix elements, are on the lifetimes of charmed hyperons. Therefore, one has to take into account several essential types of inclusive decay, at least those that contribute to the total decay rate at the level of about 10%. Here we first concentrate on the differences of the decay rates within the $SU(3)$ triplet of the hyperons, which will allow us to extract the non-singlet quantities x and y , and then discuss the $SU(3)$ singlet shifts of the rates.

The differences of the dominant Cabibbo unsuppressed nonleptonic decay rates are given by

$$\begin{aligned} \delta_1^{nl,0} &\equiv \Gamma_{\Delta S=\Delta C}^{nl}(\Xi_c^0) - \Gamma_{\Delta S=\Delta C}^{nl}(\Lambda_c) = \cos^4 \theta_c \frac{G_F^2 m_c^2}{4\pi} [(C_5 - C_3)x + (C_6 - C_4)y], \\ \delta_2^{nl,0} &\equiv \Gamma_{\Delta S=\Delta C}^{nl}(\Lambda_c) - \Gamma_{\Delta S=\Delta C}^{nl}(\Xi_c^+) = \cos^4 \theta_c \frac{G_F^2 m_c^2}{4\pi} [(C_3 - C_1)x + (C_4 - C_2)y]. \end{aligned} \quad (8.31)$$

The once Cabibbo suppressed decay rates of Λ_c and Ξ_c^+ are equal, due to the $\Delta U = 0$ property of the corresponding effective Lagrangian $L_{eff,nl}^{(3,1)}$ (Eq. (8.21)). Thus the only difference for these decays in the baryon triplet is

$$\begin{aligned}\delta^{nl,1} &\equiv \Gamma_{\Delta S=0}^{nl}(\Xi_c^0) - \Gamma_{\Delta S=0}^{nl}(\Lambda_c) \\ &= \cos^2 \theta_c \sin^2 \theta_c \frac{G_F^2 m_c^2}{4\pi} [(2 C_5 - C_1 - C_3) x + (2 C_6 - C_2 - C_4) y] .\end{aligned}\quad (8.32)$$

The dominant semileptonic decay rates are equal among the two Ξ_c baryons due to the isotopic spin property $\Delta I = 0$ of the corresponding interaction Lagrangian, thus there is only one non-trivial splitting for these decays:

$$\delta^{sl,0} \equiv \Gamma_{\Delta S=-1}^{sl}(\Xi_c) - \Gamma_{\Delta S=-1}^{sl}(\Lambda_c) = -\cos^2 \theta_c \frac{G_F^2 m_c^2}{12\pi} [L_1 x + L_2 y] . \quad (8.33)$$

Finally, the Cabibbo suppressed semileptonic decay rates are equal for Λ_c and Ξ_c^0 , due to the $\Delta V = 0$ property of the corresponding interaction. Thus the only difference for these is

$$\delta^{sl,1} \equiv \Gamma_{\Delta S=0}^{sl}(\Lambda_c) - \Gamma_{\Delta S=0}^{sl}(\Xi_c^+) = -\sin^2 \theta_c \frac{G_F^2 m_c^2}{12\pi} [L_1 x + L_2 y] . \quad (8.34)$$

Using the relations (8.31)–(8.34) one can find expressions for two differences of the measured total decay rates, $\Delta_1 = \Gamma(\Xi_c^0) - \Gamma(\Lambda_c)$ and $\Delta_2 = \Gamma(\Lambda_c) - \Gamma(\Xi_c^+)$, in terms of the quantities x and y :

$$\begin{aligned}\Delta_1 &= \delta_1^{nl,0} + \delta^{nl,1} + 2 \delta^{sl,0} \\ &= \frac{G_F^2 m_c^2}{4\pi} \cos^2 \theta \left\{ x \left[\cos^2 \theta (C_5 - C_3) + \sin^2 \theta (2 C_5 - C_1 - C_3) - \frac{2}{3} L_1 \right] \right. \\ &\quad \left. + y \left[\cos^2 \theta (C_6 - C_4) + \sin^2 \theta (2 C_6 - C_2 - C_4) - \frac{2}{3} L_2 \right] \right\} ,\end{aligned}\quad (8.35)$$

and

$$\begin{aligned}\Delta_2 &= \delta_2^{nl,0} - 2 \delta^{sl,0} + 2 \delta^{sl,1} \\ &= \frac{G_F^2 m_c^2}{4\pi} \left\{ x \left[\cos^4 \theta (C_3 - C_1) + \frac{2}{3} (\cos^2 \theta - \sin^2 \theta) L_1 \right] \right. \\ &\quad \left. + y \left[\cos^4 \theta (C_4 - C_2) + \frac{2}{3} (\cos^2 \theta - \sin^2 \theta) L_2 \right] \right\} .\end{aligned}\quad (8.36)$$

By comparing these relations with the data, one can extract the values of x and y . Using the current data for the total decay rates: $\Gamma(\Lambda_c) = 4.85 \pm 0.28 \text{ ps}^{-1}$, $\Gamma(\Xi_c^0) = 10.2 \pm 2 \text{ ps}^{-1}$, and the updated value [26] $\Gamma(\Xi_c^+) = 3.0 \pm 0.45 \text{ ps}^{-1}$, we find for the μ independent matrix element x

$$x = -(0.04 \pm 0.01) \text{ GeV}^3 \left(\frac{1.4 \text{ GeV}}{m_c} \right)^2 , \quad (8.37)$$

while the dependence of the thus extracted matrix element y on the normalization point μ is shown in Fig. 8.2.⁴

⁴It should be noted that the curves at large values of κ , $\kappa > \sim 3$, are shown only for illustrative purpose. The coefficients in the OPE, leading to the equations (8.35,8.36), are purely perturbative. Thus, formally, they correspond to $\alpha_s(\mu) \ll 1$, i.e., to $\kappa \ll 1/\alpha_s(m_c) \sim (3-4)$.

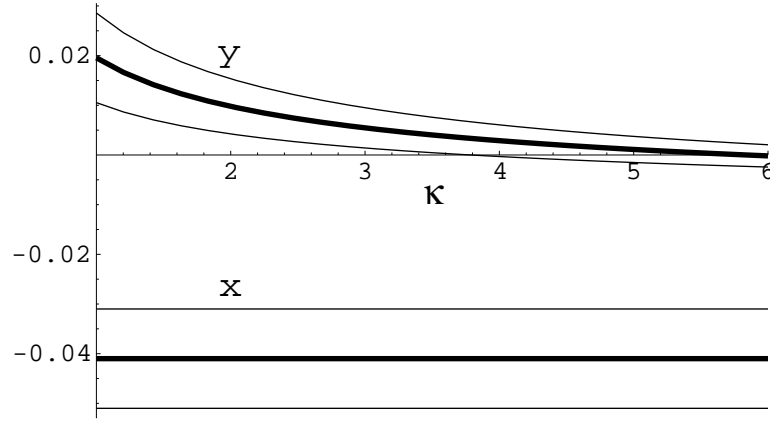


Figure 8.2: The values of the extracted matrix elements x and y in GeV^3 vs. the normalization point parameter $\kappa = \alpha_s(\mu)/\alpha_s(m_c)$. The thick lines correspond to the central value of the data on lifetimes of charmed baryons, and the thin lines show the error corridors. The extracted values of x and y scale as m_c^{-2} with the assumed mass of the charmed quark, and the plots are shown for $m_c = 1.4 \text{ GeV}$.

Notably, the extracted values of x and y are in a drastic variance with the simplistic constituent model: the color antisymmetry relation, $x = -y$, does not hold at any reasonable μ , and the absolute value of x is substantially enhanced⁵

Once the non-singlet matrix elements are determined, they can be used for predicting differences of other inclusive decay rates within the triplet of charmed hyperons as well as for the b baryons. Due to correlation of errors in x and y it makes more sense to express the predictions directly in terms of the total decay rates of the charmed hyperons. The thus arising relations between the rates do not depend on the normalization parameter μ . In this way one finds [28] for the difference of the Cabibbo dominant semileptonic decay rates between either of the Ξ_c hyperons and Λ_c :

$$\Gamma_{sl}(\Xi_c) - \Gamma_{sl}(\Lambda_c) \approx \delta^{sl,0} = 0.13 \Delta_1 - 0.065 \Delta_2 \approx 0.59 \pm 0.32 \text{ ps}^{-1}. \quad (8.38)$$

When compared with the data on the total semileptonic decay rate of Λ_c , $\Gamma_{sl}(\Lambda_c) = 0.22 \pm 0.08 \text{ ps}^{-1}$, this prediction implies that the semileptonic decay rate of the charmed cascade hyperons can be 2–3 times larger than that of Λ_c .

The predictions found in a similar way for the inclusive Cabibbo suppressed decay rates are [28]: for nonleptonic decays

$$\delta^{nl,1} = 0.082 \Delta_1 + 0.054 \Delta_2 \approx 0.55 \pm 0.22 \text{ ps}^{-1} \quad (8.39)$$

and for the semileptonic ones

$$\delta^{sl,1} = \tan^2 \theta_c \delta^{sl,0} \approx 0.030 \pm 0.016 \text{ ps}^{-1}. \quad (8.40)$$

⁵A similar, although with a smaller enhancement, behavior of the matrix elements was observed in a recent preliminary lattice study [27].

For the only difference of the inclusive rates in the triplet of b baryons, $\Gamma(\Lambda_b) - \Gamma(\Xi_b^-)$, one finds an expression in terms of x and y , or alternatively, in terms of the differences Δ_1 and Δ_2 between the charmed hyperons,

$$\begin{aligned} \Gamma(\Lambda_b) - \Gamma(\Xi_b^-) &= \cos^2 \theta_c |V_{cb}|^2 \frac{G_F^2 m_b^2}{4\pi} \left[(\tilde{C}_5 - \tilde{C}_1) x + (\tilde{C}_6 - \tilde{C}_2) y \right] \\ &\approx |V_{cb}|^2 \frac{m_b^2}{m_c^2} (0.85 \Delta_1 + 0.91 \Delta_2) \approx 0.015 \Delta_1 + 0.016 \Delta_2 \approx 0.11 \pm 0.03 \text{ ps}^{-1}. \end{aligned} \quad (8.41)$$

When compared with the data on the total decay rate of Λ_b this result predicts about 14% longer lifetime of Ξ_b^- than that of Λ_b .

The singlet matrix elements x_s and y_s (cf. Eq. (8.28)) are related to the shift of the average decay rate of the hyperons in the triplet:

$$\bar{\Gamma}_Q = \frac{1}{3} \left(\Gamma(\Lambda_Q) + \Gamma(\Xi_Q^1) + \Gamma(\Xi_Q^2) \right). \quad (8.42)$$

For the charmed baryons the shift of the dominant nonleptonic decay rate is given by [29]

$$\delta_{nl}^{(3,0)} \bar{\Gamma}_c = \cos^4 \theta \frac{G_F^2 m_c^2}{8\pi} (C_+^2 + C_-^2) \kappa^{5/18} (x_s - 3 y_s), \quad (8.43)$$

while for the b baryons the corresponding expression reads as

$$\delta^{(3)} \bar{\Gamma}_b = |V_{cb}|^2 \frac{G_F^2 m_b^2}{8\pi} (\tilde{C}_+ - \tilde{C}_-)^2 \tilde{\kappa}^{5/18} (x_s - 3 y_s). \quad (8.44)$$

The combination $x_s - 3 y_s$ of the $SU(3)$ singlet matrix elements cancels in the ratio of the shifts for b hyperons and the charmed ones:

$$\delta^{(3)} \bar{\Gamma}_b = \frac{|V_{cb}|^2}{\cos^4 \theta} \frac{m_b^2}{m_c^2} \frac{(\tilde{C}_+ - \tilde{C}_-)^2}{C_+^2 + C_-^2} \left[\frac{\alpha_s(m_c)}{\alpha_s(m_b)} \right]^{5/18} \delta_{nl}^{(3,0)} \bar{\Gamma}_c \approx 0.0025 \delta_{nl}^{(3,0)} \bar{\Gamma}_c. \quad (8.45)$$

(One can observe, with satisfaction, that the dependence on the unphysical parameter μ cancels out, as it should.) This equation shows that relatively to the charmed baryons the shift of the decay rates in the b baryon triplet is greatly suppressed by the ratio $(\tilde{C}_+ - \tilde{C}_-)^2 / (C_+^2 + C_-^2)$, which parametrically is of the second order in α_s , and numerically is only about 0.12.

An estimate of $\delta^{(3)} \bar{\Gamma}_b$ from Eq. (8.45) in absolute terms depends on evaluating the average shift $\delta_{nl}^{(3,0)} \bar{\Gamma}_c$ for charmed baryons. The latter shift can be conservatively bounded from above by the average total decay rate of those baryons: $\delta_{nl}^{(3,0)} \bar{\Gamma}_c < \bar{\Gamma}_c = 6.0 \pm 0.7 \text{ ps}^{-1}$, which then yields, using Eq. (8.45), an upper bound $\delta^{(3)} \bar{\Gamma}_b < 0.015 \pm 0.002 \text{ ps}^{-1}$. More realistically, one should subtract from the total average width $\bar{\Gamma}_c$ the contribution of the ‘parton’ term, which can be estimated from the decay rate of D_0 with account of the $O(m_c^{-2})$ effects, as amounting to about 3 ps^{-1} . (One should also take into account the semileptonic contribution to the total decay rates, which however is quite small at this level of accuracy). Thus a realistic evaluation of $\delta^{(3)} \bar{\Gamma}_b$ does not exceed 0.01 ps^{-1} , which constitutes only about

1% of the total decay rate of Λ_b . Thus the shift of the total decay rate of Λ_b due to the effects of $L_{eff}^{(3)}$ is dominantly associated with the $SU(3)$ non-singlet difference (8.42). The shift of the Λ_b decay rate with respect to the average width $\bar{\Gamma}_b$ due to the non-singlet operators is one third of the splitting (8.42), i.e., about 5%. Adding to this the 1% shift of the average width and another 1% difference from the meson decays due to the suppression of the latter by the m_b^{-2} chromomagnetic effects, one concludes that at the present level of theoretical understanding it looks impossible to explain a more than 10% enhancement of the total decay rate of Λ_b relative to B_d , where an ample 3% margin is added for the uncertainties of higher order terms in OPE as well as for higher order QCD radiative effects in the discussed corrections. In other words, the expected pattern of the lifetimes of the b hyperons in the triplet, relative to B_d , is

$$\tau(\Xi_b^0) \approx \tau(\Lambda_b) < \tau(B_d) < \tau(\Xi_b^-), \quad (8.46)$$

with the “best” theoretical estimate of the differences to be about 7% for each step of the inequality.

For the double strange hyperons Ω_c and Ω_b there is presently no better approach to evaluating the four-quark matrix elements, than the use of simplistic relations, like (8.30) based on constituent quark model. Such relations imply that the effects of the strange quark, WS and PI, in the Ω_Q baryons are significantly enhanced over the same effects in the cascade hyperons. In charmed baryons a presence of strange spectator quark enhances the decay through positive interference with the quark emerging from the $c \rightarrow s$ transition in the decay. For Ω_c this implies a significant enhancement of the total decay rate [4], which is in perfect agreement with the data on the Ω_c lifetime. Also a similar enhancement is expected for the semileptonic decay rate of Ω_c . In b baryons, on the contrary, the interference effect for a spectator strange quark is negative. Thus the nonleptonic decay rate of Ω_b is expected to be suppressed, leaving Ω_b most probably the longest-living particle among the b baryons.

8.2.7 Relation between spectator effects in baryons and the decays $\Xi_Q \rightarrow \Lambda_Q \pi$

Rather unexpectedly, the problem of four-quark matrix elements over heavy hyperons is related to decays of the type $\Xi_Q \rightarrow \Lambda_Q \pi$. The mass difference between the charmed cascade hyperons Ξ_c and Λ_c is about 180 MeV. The expected analogous mass splitting for the b hyperons should be very close to this number, since in the heavy quark limit

$$M(\Xi_b) - M(\Lambda_b) = M(\Xi_c) - M(\Lambda_c) + O(m_c^{-2} - m_b^{-2}). \quad (8.47)$$

Therefore in both cases are kinematically possible decays of the type $\Xi_Q \rightarrow \Lambda_Q \pi$, in which the heavy quark is not destroyed, and which are quite similar to decays of ordinary ‘light’ hyperons. Surprisingly, the rate of these decays for both Ξ_c and Ξ_b is not insignificantly small, but rather their branching fraction can reach a level of few per mill for Ξ_c and of one percent or more for Ξ_b [30].

The transitions $\Xi_Q \rightarrow \Lambda_Q \pi$ are induced by two underlying weak processes: the ‘spectator’ decay of a strange quark, $s \rightarrow u \bar{u} d$, which does not involve the heavy quark, and the ‘non-spectator’ weak scattering (WS)

$$s c \rightarrow c d \quad (8.48)$$

through the weak interaction of the $c \rightarrow d$ and $s \rightarrow c$ currents. One can also readily see that the WS mechanism contributes only to the decays $\Xi_c \rightarrow \Lambda_c \pi$ and is not present in the decays of the b cascade hyperons. An important starting point in considering these transitions is that in the heavy quark limit the spin of the heavy quark completely decouples from the spin of the light component of the baryon, and that the latter light component in both the initial and the final baryons forms a $J^P = 0^+$ state with quantum numbers of a diquark. Since the momentum transfer in the considered decays is small in comparison with the mass of the heavy quark the spin of the amplitudes with spin flip of the heavy quark, and thus of the baryon, are suppressed by m_Q^{-1} . In terms of the two possible partial waves in the decay $\Xi_Q \rightarrow \Lambda_Q \pi$, the S and P , this implies that the P wave is strongly suppressed and the decays are dominated by the S wave.

According to the well known current algebra technique, the S wave amplitudes of pion emission can be considered in the chiral limit at zero four-momentum of the pion, where they are described by the PCAC reduction formula (pole terms are absent in these processes):

$$\langle \Lambda_Q \pi_i(p=0) | H_W | \Xi_Q \rangle = \frac{\sqrt{2}}{f_\pi} \langle \Lambda_Q | [Q_i^5, H_W] | \Xi_Q \rangle, \quad (8.49)$$

where π_i is the pion triplet in the Cartesian notation, and Q_i^5 is the corresponding isotopic triplet of axial charges. The constant $f_\pi \approx 130 \text{ MeV}$, normalized by the charged pion decay, is used here, hence the coefficient $\sqrt{2}$ in Eq. (8.49). The Hamiltonian H_W in Eq. (8.49) is the nonleptonic strangeness-changing Hamiltonian:

$$\begin{aligned} H_W = \sqrt{2} G_F \cos \theta_c \sin \theta_c \Big\{ (C_+ + C_-) \Big[(\bar{u}_L \gamma_\mu s_L) (\bar{d}_L \gamma_\mu u_L) - (\bar{c}_L \gamma_\mu s_L) (\bar{d}_L \gamma_\mu c_L) \Big] \\ + (C_+ - C_-) \Big[(\bar{d}_L \gamma_\mu s_L) (\bar{u}_L \gamma_\mu u_L) - (\bar{d}_L \gamma_\mu s_L) (\bar{c}_L \gamma_\mu c_L) \Big] \Big\}. \end{aligned} \quad (8.50)$$

In this formula the weak Hamiltonian is assumed to be normalized (in LLO) at $\mu = m_c$. The terms in the Hamiltonian (8.50) without the charmed quark fields describe the ‘spectator’ nonleptonic decay of the strange quark, while those with the c quark correspond to the WS process (8.48).

It is straightforward to see from Eq. (8.49) that in the PCAC limit the discussed decays should obey the $\Delta I = 1/2$ rule. Indeed, the commutator of the weak Hamiltonian with the axial charges transforms under the isotopic SU(2) in the same way as the Hamiltonian itself. In other words, the $\Delta I = 1/2$ part of H_W after the commutation gives an $\Delta I = 1/2$ operator, while the $\Delta I = 3/2$ part after the commutation gives an $\Delta I = 3/2$ operator. The latter operator however cannot have a non vanishing matrix element between an isotopic singlet, Λ_Q , and an isotopic doublet, Ξ_Q . Thus the $\Delta I = 3/2$ part of H_W gives no contribution to the S wave amplitudes in the PCAC limit.

Once the isotopic properties of the decay amplitudes are fixed, one can concentrate on specific charge decay channels, e.g., $\Xi_b^- \rightarrow \Lambda_b \pi^-$ and $\Xi_c^0 \rightarrow \Lambda_c \pi^-$. An application of the PCAC relation (8.49) with the Hamiltonian from Eq. (8.50) to these decays, gives the expressions for the amplitudes at $p = 0$ in terms of baryonic matrix elements of four-quark operators:

$$\begin{aligned}
& \langle \Lambda_b \pi^-(p=0) | H_W | \Xi_b^- \rangle \\
&= \frac{\sqrt{2}}{f_\pi} G_F \cos \theta_c \sin \theta_c \langle \Lambda_b | (C_+ + C_-) \left[(\bar{u}_L \gamma_\mu s_L) (\bar{d}_L \gamma_\mu d_L) - (\bar{u}_L \gamma_\mu s_L) (\bar{u}_L \gamma_\mu u_L) \right] \\
&\quad + (C_+ - C_-) \left[(\bar{d}_L \gamma_\mu s_L) (\bar{u}_L \gamma_\mu d_L) - (\bar{u}_L \gamma_\mu s_L) (\bar{u}_L \gamma_\mu u_L) \right] | \Xi_b^- \rangle \\
&= \frac{\sqrt{2}}{f_\pi} G_F \cos \theta_c \sin \theta_c \langle \Lambda_b | C_- \left[(\bar{u}_L \gamma_\mu s_L) (\bar{d}_L \gamma_\mu d_L) - (\bar{d}_L \gamma_\mu s_L) (\bar{u}_L \gamma_\mu d_L) \right] \\
&\quad - \frac{C_+}{3} \left[(\bar{u}_L \gamma_\mu s_L) (\bar{d}_L \gamma_\mu d_L) + (\bar{d}_L \gamma_\mu s_L) (\bar{u}_L \gamma_\mu d_L) + 2 (\bar{u}_L \gamma_\mu s_L) (\bar{u}_L \gamma_\mu u_L) \right] | \Xi_b^- \rangle,
\end{aligned} \tag{8.51}$$

where in the last transition the operator structure with $\Delta I = 3/2$ giving a vanishing contribution is removed and only the structures with explicitly $\Delta I = 1/2$ are retained, and

$$\begin{aligned}
& \langle \Lambda_c \pi^-(p=0) | H_W | \Xi_c^0 \rangle = \langle \Lambda_b \pi^-(p=0) | H_W | \Xi_b^- \rangle + \frac{\sqrt{2}}{f_\pi} G_F \cos \theta_c \sin \theta_c \\
& \quad \times \langle \Lambda_c | (C_+ + C_-) (\bar{c}_L \gamma_\mu s_L) (\bar{u}_L \gamma_\mu c_L) + (C_+ - C_-) (\bar{u}_L \gamma_\mu s_L) (\bar{c}_L \gamma_\mu c_L) | \Xi_c^0 \rangle.
\end{aligned} \tag{8.52}$$

In the latter formula the first term on the r.h.s. expresses the fact that in the heavy quark limit the ‘spectator’ amplitudes do not depend on the flavor or the mass of the heavy quark. The rest of the expression (8.53) describes the ‘non-spectator’ contribution to the amplitude of the charmed hyperon decay. Using the flavor $SU(3)$ symmetry the latter contribution can be related to the non-singlet matrix elements (8.27) (normalized at $\mu = m_c$) as

$$\begin{aligned}
\Delta A &\equiv \langle \Lambda_c \pi^-(p=0) | H_W | \Xi_c^0 \rangle - \langle \Lambda_b \pi^-(p=0) | H_W | \Xi_b^- \rangle \\
&= \frac{G_F \cos \theta_c \sin \theta_c}{2\sqrt{2}f_\pi} [(C_- - C_+) x - (C_+ + C_-) y].
\end{aligned} \tag{8.53}$$

Furthermore, with the help of the equations (8.35) and (8.36) relating the matrix elements x and y to the differences of the total decay widths within the triplet of charmed hyperons, one can eliminate x and y in favor of the measured width differences. The resulting expression has the form

$$\begin{aligned}
\Delta A &\approx -\frac{\sqrt{2}\pi \cos \theta_c \sin \theta_c}{G_F m_c^2 f_\pi} \left[0.45 \left(\Gamma(\Xi_c^0) - \Gamma(\Lambda_c) \right) + 0.04 \left(\Gamma(\Lambda_c) - \Gamma(\Xi_c^+) \right) \right] \\
&= -10^{-7} \left[0.97 \left(\Gamma(\Xi_c^0) - \Gamma(\Lambda_c) \right) + 0.09 \left(\Gamma(\Lambda_c) - \Gamma(\Xi_c^+) \right) \right] \left(\frac{1.4 \text{ GeV}}{m_c} \right)^2 ps,
\end{aligned} \tag{8.54}$$

where, clearly, in the latter form the widths are assumed to be expressed in ps^{-1} , and $m_c = 1.4 \text{ GeV}$ is used as a ‘reference’ value for the charmed quark mass. It is seen from

Eq. (8.54) that the evaluation of the difference of the amplitudes within the discussed approach is mostly sensitive to the difference of the decay rates of Ξ_c^0 and Λ_c , with only very little sensitivity to the total decay width of Ξ_c^+ . Using the current data the difference ΔA is estimated as

$$\Delta A = -(5.4 \pm 2) \times 10^{-7}, \quad (8.55)$$

with the uncertainty being dominated by the experimental error in the lifetime of Ξ_c^0 . An amplitude A of the magnitude, given by the central value in Eq. (8.55) would produce a decay rate $\Gamma(\Xi_Q \rightarrow \Lambda_Q \pi) = |A|^2 p_\pi / (2\pi) \approx 0.9 \times 10^{10} \text{ s}^{-1}$, which result can also be written in a form of triangle inequality

$$\sqrt{\Gamma(\Xi_b^- \rightarrow \Lambda_b \pi^-)} + \sqrt{\Gamma(\Xi_c^0 \rightarrow \Lambda_c \pi^-)} \geq \sqrt{0.9 \times 10^{10} \text{ s}^{-1}}. \quad (8.56)$$

Although at present it is not possible to evaluate in a reasonably model independent way the matrix element in Eq. (8.52) for the ‘spectator’ decay amplitude, the inequality (8.56) shows that at least some of the discussed pion transitions should go at the level of 0.01 ps^{-1} , similar to the rates of analogous decays of ‘light’ hyperons.

8.2.8 Summary on predictions for lifetimes

We summarize here specific predictions for the inclusive decay rates, which can be argued with a certain degree of theoretical reliability, and which can be possibly experimentally tested in the nearest future.

B mesons:

$$\tau(B_d)/\tau(B_s) = 1 \pm 0.01. \quad (8.57)$$

Charmed hyperons:

$$\begin{aligned} \Gamma_{sl}(\Xi_c) &= (2 - 3) \Gamma_{sl}(\Lambda_c) & \Gamma_{sl}(\Omega_c) &> \Gamma_{sl}(\Xi_c), \\ \Gamma_{\Delta S=-1}^{nl}(\Xi_c^+) &\approx \Gamma_{\Delta S=-1}^{nl}(\Lambda_c), \\ \Gamma_{\Delta S=-1}^{nl}(\Xi_c^0) - \Gamma_{\Delta S=-1}^{nl}(\Lambda_c) &\approx 0.55 \pm 0.22 \text{ ps}^{-1}. \end{aligned} \quad (8.58)$$

b hyperons:

$$\begin{aligned} \tau(\Xi_b^0) &\approx \tau(\Lambda_b) < \tau(B_d) < \tau(\Xi_b^-) < \tau(\Omega_b), \\ \Gamma(\Lambda_b) - \Gamma(\Xi_b^-) &\approx 0.11 \pm 0.03 \text{ ps}^{-1}, \\ 0.9 &< \frac{\tau(\Lambda_b)}{\tau(B_d)} < 1. \end{aligned} \quad (8.59)$$

Strangeness decays $\Xi_Q \rightarrow \Lambda_Q \pi$: The $\Delta I = 1/2$ rule should hold in these decays, so that $\Gamma(\Xi_Q^{(d)} \rightarrow \Lambda_Q \pi^-) = 2 \Gamma(\Xi_Q^{(u)} \rightarrow \Lambda_Q \pi^0)$. The rates are constrained by the triangle inequality (8.56).

8.3 Theory of $B^0 - \bar{B}^0$ mixing[†]

In Sect. 1.3.2 the time evolution of the $B^0 - \bar{B}^0$ system has been discussed. $B^0 - \bar{B}^0$ mixing involves three physical, rephasing-invariant quantities: $|M_{12}|$, $|\Gamma_{12}|$ and the phase ϕ defined in (1.62). In the following we will discuss how they are related to physical observables. The discussed quantities are summarized in Table 8.1.

8.3.1 Mass difference

The mass difference Δm can be measured from the tagged time evolutions in (1.73-1.77) from any decay $B^0 \rightarrow f$, unless $\lambda_f = \pm 1$, in which case the oscillatory terms vanish. The time evolution is especially simple for flavor-specific decays, which are characterized by $\lambda_f = 0$. The corresponding formulae can be found in (1.79) and (1.80). Interesting flavor-specific modes are tabulated in Table 8.4. Time integrated measurements determine $x_q = \Delta m_q / \Gamma_q = \Delta m_q \tau_{B_q}$, $q = d, s$, defined in (1.93). While unfortunately it is common practice to quote measurements of Δm_q in terms of x_q , it should be clear that the measured oscillation frequencies determine Δm_d and Δm_s and not x_d and x_s . Fundamental physics quantities like CKM elements are related to Δm_d and Δm_s , so that the errors of the lifetimes entering x_q are irrelevant.

In order to predict the mass difference Δm_q within the Standard Model or one of its extensions, one must first calculate the $|\Delta B|=2$ transition amplitude, which triggers $B^0 - \bar{B}^0$ mixing. The lowest order contribution to this amplitude in the Standard Model is the box diagram in Fig. 1.2. Then one must match the result to an effective field theory, in which the interactions mediated by heavy particles are described by local operators represented by pointlike vertices. In the Standard Model only one operator, Q in (1.118), emerges. This procedure separates short- and long-distance physics and is described in Sect. 1.5.1. It results in the effective Hamiltonian in (1.117). The interesting short-distance physics is contained in the Wilson coefficient C in (1.119). New physics can modify C and can introduce new operators in addition to Q in (1.118). The Standard Model prediction is readily obtained from (1.117) to (1.121):

$$\Delta m_q = 2|M_{12}^q| = \frac{|\langle B_q^0 | H^{|\Delta B|=2} | \bar{B}_q^0 \rangle|}{m_{B_q}} = \frac{G_F^2}{6\pi^2} \eta_B m_{B_q} \hat{B}_{B_q} f_{B_q}^2 M_W^2 S\left(\frac{m_t^2}{M_W^2}\right) |V_{tb}V_{tq}^*|^2. \quad (8.60)$$

where $q = s$ or d .

Next we discuss the phenomenology of Δm_d in the Standard Model. We first insert the numerical values of those quantities which are well-known into (8.60). The QCD factor $\eta_B = 0.55$ [31] corresponds to the $\overline{\text{MS}}$ scheme for m_t . The $\overline{\text{MS}}$ value of $m_t = 167 \text{ GeV}$ is numerically smaller than the pole mass measured at the Tevatron by roughly 7 GeV. Solving (8.60) for $|V_{td}|$ one finds:

$$|V_{td}| = 0.0078 \sqrt{\frac{\Delta m_d}{0.49 \text{ ps}^{-1}}} \frac{200 \text{ MeV}}{f_{B_d}} \sqrt{\frac{1.3}{\hat{B}_{B_d}}}. \quad (8.61)$$

[†]Author: Ulrich Nierste

observable	defined in	SM prediction for	
		B_d in	B_s in
$\Delta m \simeq 2 M_{12} $	(1.64a)	(8.60),(8.69)	(8.60),(8.65),(8.69)
ϕ	(1.62)	(8.83)	(8.83)
$\Delta\Gamma \simeq 2 \Gamma_{12} \cos\phi$	(1.64b)	(8.87),(8.89)	(8.86),(8.87)
$\Delta\Gamma_{\text{CP}} \simeq 2 \Gamma_{12} $	(8.98)		
$\Delta\Gamma'_{\text{CP}} \simeq 2 \Gamma_{12} \cos^2\phi$	(8.113)		
$\Delta\Gamma_{\text{CP}}^{cc} = 2 \xi_c^{d2}\Gamma_{12}^{cc} $	(8.133)	(8.134)	
$a = \left \frac{\Gamma_{12}}{M_{12}}\right \sin\phi$	(1.65)	(8.138)	(8.138)

Table 8.1: Observables related to $|M_{12}|$, $|\Gamma_{12}|$ and ϕ discussed in Sect. 8.3.

The relation of $|V_{td}|$ to the improved Wolfenstein parameters is

$$|V_{td}| = A\lambda^3 R_t \left(1 + \mathcal{O}(\lambda^4)\right) = |V_{cb}| \lambda R_t \left(1 + \mathcal{O}(\lambda^4)\right) \quad (8.62)$$

and

$$R_t = \sqrt{(1 - \bar{\rho})^2 + \bar{\eta}^2} \quad (8.63)$$

is the length of one side of the unitarity triangle. Hence the measurement of Δm_d defines a circle in the $(\bar{\rho}, \bar{\eta})$ plane centered around $(1, 0)$. Yet the hadronic uncertainties associated with $f_{B_d}\sqrt{\hat{B}_{B_d}}$ obscure a clean extraction of $|V_{td}|$ and R_t from the well-measured Δm_d . The summer 2000 world averages from lattice calculations are $f_{B_d} = (200 \pm 30) \text{ MeV}$ and $\hat{B}_{B_d} = 1.30 \pm 0.17$ [32]. This gives $|V_{td}| = 0.0078 \pm 0.0013$ and, with $|V_{cb}| = (40.4 \pm 1.8) \times 10^{-3}$, $R_t = 0.88 \pm 0.15$.

For the discussion of Δm_s we first note that the corresponding CKM element in (8.60) is fixed from CKM unitarity:

$$|V_{ts}| = |V_{cb}| \left[1 + \lambda^2 \left(\bar{\rho} - \frac{1}{2} \right) + \mathcal{O}(\lambda^4) \right]. \quad (8.64)$$

$|V_{ts}|$ is smaller than $|V_{cb}|$ by roughly 1%. Hence within the Standard Model a measurement of Δm_s directly probes the calculation of the hadronic matrix element. (8.60) specifies to

$$\Delta m_s = 17.2 \text{ ps}^{-1} \left(\frac{|V_{ts}|}{0.04} \frac{f_{B_s}}{230 \text{ MeV}} \right)^2 \frac{\hat{B}_{B_s}}{1.3}. \quad (8.65)$$

This can be rewritten as

$$f_{B_s} \sqrt{\hat{B}_{B_s}} = \sqrt{\frac{\Delta m_s}{14.9 \text{ ps}^{-1}}} \frac{0.04}{|V_{cb}|} 247 \text{ MeV}. \quad (8.66)$$

The present 95% C.L. limit of $\Delta m_s \geq 14.9 \text{ ps}^{-1}$ [33] implies a lower bound on $f_{B_s} \sqrt{\hat{B}_{B_s}}$ which is only marginally consistent with some of the quenched lattice calculations. Hence global fits of the unitarity triangle (using $\Delta m_d/\Delta m_s$ to constrain R_t) which use too small

values of $f_{B_s} \sqrt{\widehat{B}_{B_s}}$ confine the apex of the triangle to a too small region of the $(\overline{\rho}, \overline{\eta})$ plane or may even be in conflict with the measured lower bound on Δm_s .

The determination of R_t profits enormously from a measurement of Δm_s , because the ratio of the hadronic matrix elements entering $\Delta m_d/\Delta m_s$ can be calculated with a much higher accuracy than the individual matrix elements:

$$\xi = \frac{f_{B_s} \sqrt{\widehat{B}_{B_s}}}{f_{B_d} \sqrt{\widehat{B}_{B_d}}} \quad (8.67)$$

is equal to 1 in the limit of exact $SU(3)_F$ symmetry. Hence the theorists' task is reduced to the calculation of the deviation from 1. The current world average from lattice calculations is [32]

$$\xi = 1.16 \pm 0.05. \quad (8.68)$$

Further $|V_{cb}|$ drops out from the ratio

$$\frac{\Delta m_d}{\Delta m_s} = \lambda^2 R_t^2 \left(1 + \lambda^2 (1 - 2\overline{\rho}) + \mathcal{O}(\lambda^4) \right) \frac{m_{B_d}}{m_{B_s}} \frac{1}{\xi^2}. \quad (8.69)$$

With the expected experimental accuracy of $\Delta m_{d,s}$ and the anticipation of progress in the determination of ξ in (8.68) a determination of R_t at the level of 1-3% is possible. Then, eventually, even the uncertainty in λ cannot be neglected anymore. Keeping the overall factor of λ^2 while inserting $\lambda = 0.22$ in the subleading terms one finds from (8.69):

$$R_t = 0.880 \sqrt{\frac{\Delta m_d}{0.49 \text{ ps}^{-1}}} \sqrt{\frac{17 \text{ ps}^{-1}}{\Delta m_s}} \frac{0.22}{\lambda} \frac{\xi}{1.16} (1 + 0.05 \overline{\rho}). \quad (8.70)$$

Here the omission of $\mathcal{O}(\lambda^4)$ terms induces a negligible error of less than 0.1%. At present R_t is obtained from a global fit of the unitarity triangle and (8.69) is used to predict $\Delta m_s = 17.3_{-0.7}^{+1.5}$ [34]. One should be aware that some of the quantities entering the global fit, especially ϵ_K , are sensitive to new physics. Hence the measurement of a Δm_s well above the quoted range would be very exciting. In a large class of extensions of the Standard model Δm_d and Δm_s change, while their ratio does not. In these models Δm_s could be in conflict with (8.66) without affecting R_t in (8.70). Therefore it is desirable to gain additional experimental information on f_{B_s} , so that the dependence on non-perturbative methods is reduced. This information can be obtained from the B_s width difference discussed in Sect. 8.3.2.

8.3.2 Width difference

8.3.2.1 Calculation

The two mass eigenstates B_L and B_H in (1.54) differ not only in their masses but also in their widths. The prediction of the width difference $\Delta\Gamma = \Gamma_L - \Gamma_H \simeq 2|\Gamma_{12}|\cos\phi$

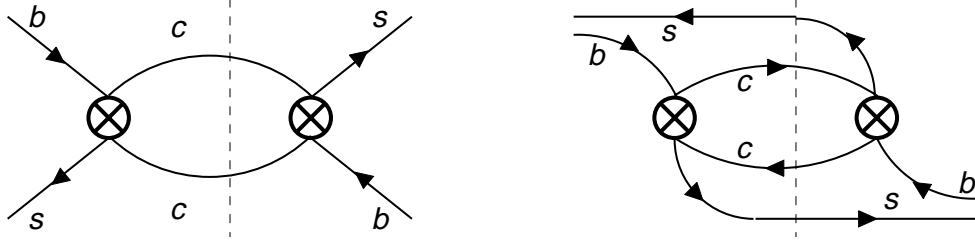


Figure 8.3: Leading order diagrams determining Γ_{12}^s . Only the CKM-favored contribution $\xi_c^{s*2}\Gamma_{12}^{cc}$ is shown. The left diagram is the *weak annihilation diagram* and the right one is the *spectator interference diagram*. The dashed line indicates the cut through the final state.

in (1.64b) requires the calculation of $|\Gamma_{12}|$ and ϕ . Γ_{12} is determined from the absorptive part of the $|\Delta B| = 2$ transition amplitude. It receives contributions from all final states which are common to B^0 and \bar{B}^0 as shown in the first line of (1.146). The leading order (LO) diagrams contributing to Γ_{12} in the B_s system are shown in Fig. 8.3. The dominant contribution comes from the spectator interference diagram, the weak annihilation diagram is color-suppressed. We write

$$\Gamma_{12}^q = - \left[\xi_c^{q*2} \Gamma_{12,q}^{cc} + 2\xi_u^{q*} \xi_c^{q*} \Gamma_{12,q}^{uc} + \xi_u^{q*2} \Gamma_{12,q}^{uu} \right], \quad q = d, s, \quad (8.71)$$

where the three terms denote the contributions from the diagram with (anti-)quarks i and j in the final state. The ξ_i^q 's denote the corresponding CKM factors:

$$\xi_u^q = V_{uq} V_{ub}^*, \quad \xi_c^q = V_{cq} V_{cb}^*, \quad \xi_t^q = V_{tq} V_{tb}^*. \quad (8.72)$$

They satisfy $\xi_u^q + \xi_c^q + \xi_t^q = 0$ from CKM unitarity and read in terms of the improved Wolfenstein parameters [35]:

$$\begin{aligned} \xi_u^d &= A\lambda^3 (\bar{\rho} + i\bar{\eta}) + \mathcal{O}(\lambda^5), & \xi_c^d &= -A\lambda^3 + \mathcal{O}(\lambda^5), \\ \xi_t^d &= A\lambda^3 (1 - \bar{\rho} - i\bar{\eta}) + \mathcal{O}(\lambda^5), \\ \xi_u^s &= A\lambda^4 (1 + \frac{\lambda^2}{2}) (\bar{\rho} + i\bar{\eta}) + \mathcal{O}(\lambda^8), & \xi_c^s &= A\lambda^2 (1 - \frac{\lambda^2}{2}) + \mathcal{O}(\lambda^6), \\ \xi_t^s &= -A\lambda^2 \left[1 - \lambda^2 (\frac{1}{2} - \bar{\rho} - i\bar{\eta}) \right] + \mathcal{O}(\lambda^6), \end{aligned} \quad (8.73)$$

$-\xi_u^d/\xi_c^d$ and $-\xi_t^d/\xi_c^d$ define two sides of the standard unitarity triangle depicted in Fig. 1.1. One has

$$-\frac{\xi_u^d}{\xi_c^d} = R_b e^{i\gamma}, \quad -\frac{\xi_t^d}{\xi_c^d} = R_t e^{-i\beta}, \quad (8.74)$$

where $R_b = \sqrt{\bar{\rho}^2 + \bar{\eta}^2}$ and R_t is defined in (8.63). The ratio ξ_t^s/ξ_c^s involves the phase β_s measured from the mixing-induced CP asymmetry in $B_s \rightarrow D_s^+ D_s^-$:

$$-\frac{\xi_t^s}{\xi_c^s} = [1 + \bar{\rho}\lambda^2 + \mathcal{O}(\lambda^4)] e^{i\beta_s} \quad \text{with} \quad \beta_s = \bar{\eta}\lambda^2 [1 + (1 - \bar{\rho})\lambda^2] + \mathcal{O}(\lambda^6). \quad (8.75)$$

The coefficients Γ_{12}^{ij} in (8.71) are positive. They are inclusive quantities and can be calculated using the heavy quark expansion described for the heavy hadron lifetimes in Sect. 8.2. The leading term of the power expansion in Λ_{QCD}/m_b contains two Dirac structures, each of which can be factorized into a short-distance Wilson coefficient and the matrix element of a local operator:

$$\Gamma_{12,q}^{ij} = \frac{G_F^2 m_b^2}{6\pi} f_{B_q}^2 M_{B_q} \left[F^{ij}(z) \frac{2}{3} B_{B_q} - F_S^{ij}(z) \frac{5}{12} B_{B_q}^{S'} \right] \left[1 + \mathcal{O}\left(\frac{\Lambda_{QCD}}{m_b}\right) \right]. \quad (8.76)$$

Here $z = m_c^2/m_b^2$. The operator Q , which we already encountered in the discussion of Δm , was defined in (1.118). When Q occurs in the context of $B_s^0 - \bar{B}_s^0$ mixing, we understand that the d quarks in (1.118) are appropriately replaced by s quarks. In $\Gamma_{12,q}$ a second operator occurs:

$$Q_S = \bar{q}_L b_R \bar{q}_L b_R, \quad q = d \text{ or } s. \quad (8.77)$$

B_{B_q} and $B_{B_q}^{S'}$ (or, equivalently, $B_{B_q}^S$) are ‘bag’ parameters quantifying the hadronic matrix elements of Q and Q_S :

$$\langle B_q^0 | Q(\mu) | \bar{B}_q^0 \rangle = \frac{2}{3} f_{B_q}^2 m_{B_q}^2 B_{B_q}(\mu), \quad (8.78)$$

$$\langle B_q^0 | Q_S(\mu) | \bar{B}_q^0 \rangle = -\frac{5}{12} f_{B_q}^2 m_{B_q}^2 B_{B_q}^{S'}(\mu) = -\frac{5}{12} f_{B_q}^2 m_{B_q}^2 \frac{m_{B_q}^2}{[m_b(\mu) + m_q(\mu)]^2} B_{B_q}^S(\mu).$$

$B_{B_q}^S$ and $B_{B_q}^{S'}$ simply differ by the factor $m_{B_q}^2/[m_b(\mu) + m_q(\mu)]^2$. While lattice results are usually quoted for $B_{B_q}^S$, the forthcoming formulae are shorter when expressed in terms of $B_{B_q}^{S'}$. These ‘bag’ factors depend on the renormalization scale μ and the renormalization scheme. In the literature on $\Delta\Gamma$ it is customary to use B_{B_q} and $B_{B_q}^S$ in the $\overline{\text{MS}}$ scheme as defined in [36]. Numerical values obtained in lattice calculations are usually quoted for $\mu = m_b$. The invariant bag factor \hat{B}_{B_q} defined in (1.121) is related to $B_{B_q}(\mu)$ by

$$\begin{aligned} \hat{B}_{B_q} &= B_{B_q}(\mu) b_B(\mu) \\ b_B(\mu) &= [\alpha_s(\mu)]^{-6/23} \left[1 + \frac{\alpha_s(\mu)}{4\pi} \frac{5165}{3174} \right], \quad b_B(m_b) = 1.52 \pm 0.03. \end{aligned} \quad (8.79)$$

A recent preliminary lattice calculation with two dynamical flavors found $B_{B_s}(m_b) = 0.83 \pm 0.08$ and $B_{B_s}^S(m_b) = 0.84 \pm 0.08$ [37]. No deviation of B_{B_s}/B_{B_d} and $B_{B_s}^S/B_{B_d}^S$ from 1 is seen. The quoted value for $B_{B_q}(m_b)$ corresponds to $\hat{B}_{B_q} = 1.26 \pm 0.12$. The short distance physics entering Γ_{12}^q in (8.76) is contained in $F(z)$ and $F_S(z)$. To leading order in α_s they read:

$$\begin{aligned} F^{cc}(z) &= \sqrt{1-4z} \left[(1-z)K_1 + \frac{1-4z}{2}K_2 \right] \\ F_S^{cc}(z) &= \sqrt{1-4z} (1+2z) (K_1 - K_2) \\ F^{uc}(z) &= (1-z)^2 \left[\frac{2+z}{2}K_1 + \frac{1-z}{2}K_2 \right] \\ F_S^{uc}(z) &= (1-z)^2 (1+2z) (K_1 - K_2) \end{aligned}$$

$$\begin{aligned} F^{uu}(z) &= F^{cc}(0) = F^{uc}(0) = K_1 + \frac{1}{2}K_2 \\ F_S^{uu}(z) &= F_S^{cc}(0) = F_S^{uc}(0) = K_1 - K_2. \end{aligned} \quad (8.80)$$

K_1 and K_2 are combinations of the Wilson coefficients C_1 and C_2 , which are tabulated in Table 1.3:

$$K_1 = 3C_1^2 + 2C_1C_2, \quad K_2 = C_2^2. \quad (8.81)$$

The scale at which the Wilson coefficients are evaluated must equal the scale used in $B_{B_q}(\mu)$ and $B_{B_q}^S(\mu)$. In (8.76) and (8.80) we have neglected the small contributions from penguin coefficients, which can be found in [36].

It is instructive to eliminate $\xi_c^q = -\xi_t^q - \xi_u^q$ in favor of ξ_u^q and ξ_t^q in (8.71):

$$\Gamma_{12}^q = -\xi_t^{q*2} \left[\Gamma_{12,q}^{cc} + 2 \frac{\xi_u^{q*}}{\xi_t^{q*}} \left(\Gamma_{12,q}^{cc} - \Gamma_{12,q}^{uc} \right) + \frac{\xi_u^{q*2}}{\xi_t^{q*2}} \left(\Gamma_{12,q}^{cc} - 2\Gamma_{12,q}^{uc} + \Gamma_{12,q}^{uu} \right) \right]. \quad (8.82)$$

In the limit $z = 0$ all the Γ_{12}^{ij} 's become equal and $\arg M_{12} = \arg(-\Gamma_{12}) = \arg(\xi_t^{q*2})$, so that ϕ vanishes in this limit. With (8.73) one verifies that $\phi_d = \mathcal{O}(\bar{\eta}z)$ and $\phi_s = \mathcal{O}(\lambda^2 \bar{\eta}z)$. This GIM suppression is lifted, if new physics contributes to $\arg M_{12}^q$ spoiling the cancellation between $\arg M_{12}$ and $\arg(-\Gamma_{12}^q)$. Therefore ϕ is extremely sensitive to new physics.

Combining (8.82) and (8.80) we find the Standard Model predictions for $\phi_d = \phi(B_d)$ and $\phi_s = \phi(B_s)$:

$$\begin{aligned} \phi_d &= -\frac{2\bar{\eta}}{R_t^2} \frac{\Gamma_{12,d}^{uc} - \Gamma_{12,d}^{cc}}{\Gamma_{12,d}^{cc}} \left[1 + \mathcal{O}(\bar{\eta}z^2, \bar{\eta}\lambda^4) \right] \approx -\frac{24}{5} \frac{\bar{\eta}}{R_t^2} \frac{B_{B_d}}{B_{B_d}^{S'}} \frac{K_1 + K_2}{K_2 - K_1} z \approx -0.1 = -5^\circ, \\ \phi_s &= 2\lambda^2 \bar{\eta} \frac{\Gamma_{12,s}^{uc} - \Gamma_{12,s}^{cc}}{\Gamma_{12,s}^{cc}} \left[1 + \mathcal{O}(\bar{\eta}z^2, \bar{\eta}\lambda^4) \right] \approx \frac{24}{5} \bar{\eta} \lambda^2 \frac{B_{B_s}}{B_{B_s}^{S'}} \frac{K_1 + K_2}{K_2 - K_1} z \approx 3 \times 10^{-3} = 0.2^\circ. \end{aligned} \quad (8.83)$$

That is, in the Standard Model, we can safely neglect the factor of $\cos \phi_q$ in the relation $\Delta\Gamma_q = 2|\Gamma_{12}^q| \cos \phi_q$ (see (1.64b)). For Γ_{12}^s the CKM-suppressed contributions $\Gamma_{12,s}^{uc}$ and $\Gamma_{12,s}^{uu}$ are completely irrelevant. Γ_{12}^d is also dominated by the double-charm contribution $\Gamma_{12,d}^{cc}$, with up to $\mathcal{O}(5\%)$ corrections from the second term in (8.82):

$$\begin{aligned} \Delta\Gamma_s^{\text{SM}} &= 2|\Gamma_{12}^s| = |\xi_t^s|^2 2|\Gamma_{12,s}^{cc}| \\ \Delta\Gamma_d^{\text{SM}} &= 2|\Gamma_{12}^d| = |\xi_t^d|^2 2|\Gamma_{12,d}^{cc}| \left| 1 + 2 \frac{R_t^2 + \bar{\rho} - 1}{R_t^2} \frac{\Gamma_{12,d}^{uc} - \Gamma_{12,d}^{cc}}{\Gamma_{12,d}^{cc}} + \mathcal{O}\left(\frac{R_B^4}{R_t^4} z^2\right) \right|. \end{aligned} \quad (8.84)$$

$\Gamma_{12,s}^{cc}$ has been calculated in the next-to-leading order of α_s [36] and Λ_{QCD}/m_b [38]. The result gives the following prediction for $\Delta\Gamma_s^{\text{SM}}$:

$$\frac{\Delta\Gamma_s^{\text{SM}}}{\Gamma} = \frac{2|\Gamma_{12}^s|}{\Gamma} = \left(\frac{f_{B_s}}{245 \text{ MeV}} \right)^2 \left[(0.234 \pm 0.035) B_{B_s}^S - 0.080 \pm 0.020 \right]. \quad (8.85)$$

Here the coefficient of $B_{B_s}^S$ has been updated to $m_b(m_b) + m_s(m_b) = 4.3 \text{ GeV}$ (in the $\overline{\text{MS}}$ scheme) compared to [36]. Since the coefficient $F^{cc}(z)$ of B_{B_s} in (8.76) is very small, B_{B_s} in (8.85) has been fixed to $B_{B_s}(m_b) = 0.85 \pm 0.05$ obtained in quenched lattice QCD [37]. Recently the KEK–Hiroshima group succeeded in calculating f_{B_s} in an unquenched lattice QCD calculation with two dynamical fermions [39]. The result is $f_{B_s} = (245 \pm 30) \text{ MeV}$. With this number and $B_{B_s}^S(m_b) = 0.87 \pm 0.09$ from quenched lattice QCD [37,40] one finds from (8.85):

$$\frac{\Delta\Gamma_s^{\text{SM}}}{\Gamma} = 0.12 \pm 0.06. \quad (8.86)$$

Here we have conservatively added the errors from the two lattice quantities linearly. f_{B_s} drops out from the ratio

$$\frac{\Delta\Gamma_s^{\text{SM}}}{\Delta m_s^{\text{SM}}} \simeq \frac{5\pi}{6} \frac{m_b^2}{M_W^2 \eta_B b_B S(m_t^2/M_W^2)} |F_S(z)| \frac{B_{B_s}^{S'}}{B_{B_s}} \left[1 + \mathcal{O}\left(\frac{\Lambda_{QCD}}{m_b}\right) \right]. \quad (8.87)$$

The full result with next-to-leading order corrections in α_s and Λ_{QCD}/m_b can be found in [36]. Including these corrections one finds [36]:

$$\frac{\Delta\Gamma_s^{\text{SM}}}{\Delta m_s^{\text{SM}}} = \left(3.7_{-1.5}^{+0.8}\right) \times 10^{-3}. \quad (8.88)$$

The uncertainty in (8.88) is dominated by the renormalization scale dependence. Its reduction requires a painful three-loop calculation. The numerical value in (8.88) is obtained with $B_{B_s}^S/B_{B_s} = 1.0 \pm 0.1$ [37], which is larger than the one used in [36].

Next we consider the width difference in the B_d meson system: since the second term in (8.84) is negligible in view of the other uncertainties, (8.87) also holds for $\Delta\Gamma_d^{\text{SM}}/\Delta m_d^{\text{SM}}$ with the replacement $B_{B_s}^{S'}/B_{B_s} \rightarrow B_{B_d}^{S'}/B_{B_d}$. The $SU(3)_F$ breaking in these ‘bag’ factors and in the Λ_{QCD}/m_b corrections can safely be neglected, so that the numerical range (8.88) also holds for $\Delta\Gamma_d^{\text{SM}}/\Delta m_d^{\text{SM}}$. With $\Delta m_d = 0.49 \text{ ps}^{-1}$ and $\tau_{B_d} = 1.5 \text{ ps}$ one finds $\Delta\Gamma_d^{\text{SM}} \approx 3 \times 10^{-3} \Gamma_d$. Since $\Delta\Gamma_d$ and Δm_d are affected by new physics in different ways, it is instructive to consider the ratio of the two width differences: from (8.84) and (8.85) one finds

$$\frac{\Delta\Gamma_d^{\text{SM}}}{\Delta\Gamma_s^{\text{SM}}} = \frac{|\Gamma_{12}^d|}{|\Gamma_{12}^s|} \simeq \frac{f_{B_d}^2 B_{B_d}^S}{f_{B_s}^2 B_{B_s}^S} \left| \frac{\xi_t^d}{\xi_t^s} \right|^2 \simeq 0.04 R_t^2. \quad (8.89)$$

In the last line we have used $f_{B_s}/f_{B_d} = 1.16 \pm 0.05$ and $B_{B_s}^S = B_{B_d}^S$. The numerical predictions for $\Delta\Gamma_d$ from (8.88) and (8.89) are consistent with each other. Since $\Delta\Gamma_d$ stems from the CKM-suppressed decay modes, it can be substantially enhanced in models of new physics.

8.3.2.2 Phenomenology of $\Delta\Gamma_s$

Time Evolution: The width difference $\Delta\Gamma_s$ can be measured from the time evolution of an untagged B_s sample, as shown in sect. 1.3.3. In general the decay $\overline{B}_s \rightarrow f$ is governed

by the two-exponential formula in (1.85). With (1.54) and (1.72) we can calculate $\langle f | B_{L,H} \rangle$ and find from (1.85):

$$\Gamma[f, t] = \mathcal{N}_f \frac{|A_f|^2}{2} (1 + |\lambda_f|^2) \left[(1 - \mathcal{A}_{\Delta\Gamma}^f) e^{-\Gamma_L t} + (1 + \mathcal{A}_{\Delta\Gamma}^f) e^{-\Gamma_H t} \right] \quad (8.90)$$

with $\mathcal{A}_{\Delta\Gamma}^f$ defined in (1.83). Throughout this Sect. 8.3.2.2 we neglect small terms of order a . The time-independent prefactor of the square bracket can be eliminated in favor of the branching ratio $Br(\bar{B} \rightarrow f)$ using (1.84). In principle one could measure $\Delta\Gamma_s = \Gamma_L - \Gamma_H$ by fitting the decay distribution of any decay with $|\mathcal{A}_{\Delta\Gamma}^f| \neq 1$ to $\Gamma[f, t]$ in (8.90). In practice, however, one will at best be able to measure the deviation from a single exponential up to terms linear in $\Delta\Gamma_s t$. In (1.82) $\Gamma[f, t]$ is expressed in terms of $\Gamma_s = (\Gamma_L + \Gamma_H)/2$ and $\Delta\Gamma_s$. With (1.84) one finds

$$\Gamma[f, t] = 2 \text{BR}(\bar{B}_s \rightarrow f) \Gamma_s e^{-\Gamma_s t} \left[1 + \frac{\Delta\Gamma_s}{2} \mathcal{A}_{\Delta\Gamma}^f \left(t - \frac{1}{\Gamma_s} \right) \right] + \mathcal{O}((\Delta\Gamma_s t)^2). \quad (8.91)$$

That is, unless one is able to resolve quadratic $\mathcal{O}((\Delta\Gamma_s)^2)$ terms, one can only determine the product $\mathcal{A}_{\Delta\Gamma}^f \Delta\Gamma_s$ from the time evolution. A flavor-specific decay mode like $B_s \rightarrow D_s^- \pi^+$ is characterized by $\lambda_f = 0$ and therefore has $\mathcal{A}_{\Delta\Gamma}^f = 0$. In these decay modes the term involving $\Delta\Gamma_s$ in (8.91) vanishes. Flavor-specific decays therefore determine Γ_s up to corrections of order $(\Delta\Gamma_s)^2$. For those decays $\Gamma[f, t]$ is insensitive to new physics in M_{12} , because $\lambda_f = 0$. In order to gain information on $\Delta\Gamma_s$ from (8.91), one must consider decays with $\lambda_f \neq 0$. But λ_f and $\mathcal{A}_{\Delta\Gamma}^f$ depend on the mixing phase ϕ_M (see (1.67)) and therefore change in the presence of new physics in M_{12} . In the Standard Model we can calculate ϕ_M and then extract $\Delta\Gamma_s$ from the measured $\mathcal{A}_{\Delta\Gamma}^f \Delta\Gamma_s$. In the presence of new physics, however, one needs additional information. We therefore discuss these two cases independently below.

Lifetimes are conventionally measured by fitting the decay distribution to a single exponential. We now write the two-exponential formula of (8.90) as

$$\begin{aligned} \Gamma[f, t] &= A e^{-\Gamma_L t} + B e^{-\Gamma_H t} \\ &= e^{-\Gamma_s t} \left[(A + B) \cosh \frac{\Delta\Gamma_s t}{2} + (B - A) \sinh \frac{\Delta\Gamma_s t}{2} \right], \end{aligned} \quad (8.92)$$

where $A = A(f)$ and $B = B(f)$ can be read off from (8.90). If one uses a maximum likelihood fit of (8.92) to a single exponential,

$$F[f, t] = \Gamma_f e^{-\Gamma_f t}, \quad (8.93)$$

it will yield the following result [41]:

$$\Gamma_f = \frac{A/\Gamma_L + B/\Gamma_H}{A/\Gamma_L^2 + B/\Gamma_H^2}. \quad (8.94)$$

We expand this to second order in $\Delta\Gamma_s$:

$$\Gamma_f = \Gamma_s + \frac{A - B}{A + B} \frac{\Delta\Gamma_s}{2} - \frac{2AB}{(A + B)^2} \frac{(\Delta\Gamma_s)^2}{\Gamma_s} + \mathcal{O}\left(\frac{(\Delta\Gamma_s)^3}{\Gamma_s^2}\right). \quad (8.95)$$

In flavor-specific decays we have $A = B$ (see (1.82)). We see from (8.95) that here a single-exponential fit determines

$$\Gamma_{\text{fs}} = \Gamma_s - \frac{(\Delta\Gamma_s)^2}{2\Gamma_s} + \mathcal{O}\left(\frac{(\Delta\Gamma_s)^3}{\Gamma_s^2}\right). \quad (8.96)$$

Heavy quark symmetry predicts that the average *widths* Γ_s and Γ_d are equal up to corrections of less than one percent [38,42]. From (8.96) we then realize that the average B_s *lifetime* (defined as $1/\Gamma_f$) can exceed the B_d lifetime by more than one percent, if $\Delta\Gamma_s$ is sizable.

CP Properties and Branching Ratios: In the B_s system $\Delta\Gamma$ is dominated by $\Gamma_{12}^{s,cc}$. In the following we will neglect the Cabibbo-suppressed contributions from $\Gamma_{12}^{s,uc}$ and $\Gamma_{12}^{s,uu}$. We also specify to the PDG phase convention for the CKM matrix, in which $\arg(V_{cb}V_{cs}^*) = \mathcal{O}(\lambda^6)$, see (8.75). For the discussion in the forthcoming paragraphs it will be useful to define the CP eigenstates

$$|B_s^{\text{even}}\rangle = \frac{1}{\sqrt{2}} (|B_s\rangle + |\overline{B}_s\rangle), \quad \text{and} \quad |B_s^{\text{odd}}\rangle = \frac{1}{\sqrt{2}} (|B_s\rangle - |\overline{B}_s\rangle). \quad (8.97)$$

Here we have used the standard convention for the CP transformation: $CP|B_s\rangle = -|\overline{B}_s\rangle$.

Interestingly, one can measure $\Delta\Gamma_s$ from branching ratios, without information from lifetime fits. We define

$$\Delta\Gamma_{\text{CP}}^s \equiv 2|\Gamma_{12}^s| = 2 \sum_{f \in X_{c\overline{c}}} [\Gamma(B_s \rightarrow f_{\text{CP}+}) - \Gamma(B_s \rightarrow f_{\text{CP}-})]. \quad (8.98)$$

Here $X_{c\overline{c}}$ represents the final states containing a (c, \overline{c}) pair, which constitute the dominant contribution to $\Delta\Gamma_{\text{CP}}^s$ stemming from the decay $b \rightarrow c\overline{c}s$. In (8.98) we have decomposed any final state f into its CP -even and CP -odd component, $|f\rangle = |f_{\text{CP}+}\rangle + |f_{\text{CP}-}\rangle$ ⁶ and defined

$$\Gamma(B_s \rightarrow f_{\text{CP}\pm}) = \mathcal{N}_f |\langle f_{\text{CP}\pm} | B_s \rangle|^2 = \frac{|\langle f_{\text{CP}\pm} | B_s \rangle|^2}{|\langle f | B_s \rangle|^2} \Gamma(B_s \rightarrow f). \quad (8.99)$$

\mathcal{N}_f is the usual normalization factor originating from the phase-space integration. $\Delta\Gamma_{\text{CP}}^s$ equals $\Delta\Gamma_s$ in the Standard Model, but these quantities differ by a factor of $\cos\phi_s$ in models of new physics, see (1.64b). We will later exploit this feature to probe the Standard Model and to determine $|\cos\phi_s|$.

We now prove the second equality in (8.98) and subsequently discuss how $\Gamma(B_s \rightarrow f_{\text{CP}\pm})$ can be measured. Start from the definition of Γ_{12}^s :

$$\Gamma_{12}^s = \sum_f \mathcal{N}_f \langle B_s | f \rangle \langle f | \overline{B}_s \rangle = \frac{1}{2} \sum_f \mathcal{N}_f [\langle B_s | f \rangle \langle f | \overline{B}_s \rangle + \langle B_s | \overline{f} \rangle \langle \overline{f} | \overline{B}_s \rangle]. \quad (8.100)$$

⁶The factor of 2 in (8.98) is an artifact of our normalization of $|f_{\text{CP}\pm}\rangle$.

In the second equation we have paired the final state $|f\rangle$ with its CP conjugate $|\bar{f}\rangle = -CP|f\rangle$. In the next step we trade f for f_{CP+} and f_{CP-} and use the CP transformation

$$\langle f_{CP\pm} | \bar{B}_s \rangle = \mp \langle f_{CP\pm} | B_s \rangle \quad (8.101)$$

in our phase convention with $\arg(V_{cb}V_{cs}^*) = 0$. Then (8.100) becomes

$$\begin{aligned} -\Gamma_{12}^s &= \sum_{f \in X_{c\bar{c}}} \mathcal{N}_f \left[|\langle f_{CP+} | B_s \rangle|^2 - |\langle f_{CP-} | B_s \rangle|^2 \right] \\ &= \sum_{f \in X_{c\bar{c}}} [\Gamma(B_s \rightarrow f_{CP+}) - \Gamma(B_s \rightarrow f_{CP-})]. \end{aligned} \quad (8.102)$$

Interference terms involving both $\langle f_{CP+} | B_s \rangle$ and $\langle f_{CP-} | B_s \rangle$ drop out when summing the two terms $\langle B_s | f \rangle \langle f | \bar{B}_s \rangle$ and $\langle B_s | \bar{f} \rangle \langle \bar{f} | \bar{B}_s \rangle$. An explicit calculation of Γ_{12}^s reveals that the overall sign of the LHS of (8.102) is positive, which completes the proof of (8.98).

Loosely speaking, $\Delta\Gamma_{CP}^s$ is measured by counting the CP -even and CP -odd double-charm final states in B_s decays. Our formulae become more transparent if we use the CP -eigenstates defined in (8.97). With $|B_s\rangle = (|B_s^{\text{even}}\rangle + |B_s^{\text{odd}}\rangle)/\sqrt{2}$ one easily finds from (8.102):

$$\Delta\Gamma_{CP}^s = 2|\Gamma_{12}^s| = \Gamma(B_s^{\text{even}}) - \Gamma(B_s^{\text{odd}}). \quad (8.103)$$

Here the RHS refers to the total widths of the CP -even and CP -odd B_s eigenstates. We stress that the possibility to relate $|\Gamma_{12}^s|$ to a measurable quantity in (8.98) crucially depends on the fact that Γ_{12}^s is dominated by a single weak phase. For instance, the final state K^+K^- is triggered by $b \rightarrow u\bar{u}s$ and involves a weak phase different from $b \rightarrow c\bar{c}s$. Although K^+K^- is CP -even, the decay $B_s^{\text{odd}} \rightarrow K^+K^-$ is possible. An inclusion of such CKM-suppressed modes into (8.102) would add interference terms that spoil the relation to measured quantities. The omission of these contributions to Γ_{12}^s induces a theoretical uncertainty of order 3–5% on (8.103).

A measurement of $\Delta\Gamma_{CP}^s$ has been performed by the ALEPH collaboration [43]. ALEPH has measured

$$2 \text{BR}(\bar{B}_s \rightarrow D_s^{(*)+} D_s^{(*)-}) = 0.26_{-0.15}^{+0.30} \quad (8.104)$$

and related it to $\Delta\Gamma_{CP}^s$. For this the following theoretical input has been used [44]:

- i) In the heavy quark limit $m_c \rightarrow \infty$ and neglecting certain terms of order $1/N_c$ (where $N_c = 3$ is the number of colors) the decay $B_s^{\text{odd}} \rightarrow D_s^\pm D_s^{*\mp}$ is forbidden. Hence in this limit the final state in $\bar{B}_s \rightarrow D_s^\pm D_s^{*\mp}$ is CP -even. Further in $\bar{B}_s \rightarrow D_s^{*+} D_s^{*-}$ the final state is in an S-wave.
- ii) In the small velocity limit when $m_c \rightarrow \infty$ with $m_b - 2m_c$ fixed [45], $\Delta\Gamma_{CP}^s$ is saturated by $\Gamma(\bar{B}_s \rightarrow D_s^{(*)+} D_s^{(*)-})$. With i) this implies that in the considered limit the width of B_s^{odd} vanishes. For $N_c \rightarrow \infty$ and in the SV limit, $\Gamma(\bar{B}_s \rightarrow D_s^{(*)+} D_s^{(*)-})$ further equals the parton model result for $\Delta\Gamma_{CP}^s$ (quark-hadron duality).

Identifying $\Gamma(B_s^{\text{even}} \rightarrow D_s^{(*)+} D_s^{(*)-}) \simeq \Delta\Gamma_{\text{CP}}^s$ and $\Gamma(B_s^{\text{odd}} \rightarrow D_s^{(*)+} D_s^{(*)-}) \simeq 0$ we can integrate $\Gamma[D_s^{(*)+} D_s^{(*)-}, t] = \Gamma(B_s^{\text{even}} \rightarrow D_s^{(*)+} D_s^{(*)-}) \exp(-\Gamma_L t)$ over t to find:

$$2 \text{BR}(\bar{B}_s \rightarrow D_s^{(*)+} D_s^{(*)-}) \simeq \frac{\Delta\Gamma_{\text{CP}}^s}{\Gamma_L}. \quad (8.105)$$

Thus the measurement in (8.104) is compatible with the theoretical prediction in (8.86).

When using (8.105) one should be aware that the corrections to the limits i) and ii) adopted in [44] can be numerically sizeable. For instance, in the SV limit there are no multibody final states like $D_s^{(*)} \bar{D} X_s$, which can modify (8.105). As serious would be the presence of a sizeable CP -odd component of the $D_s^{(*)+} D_s^{(*)-}$ final state, since it would be added with the wrong sign to $\Delta\Gamma_{\text{CP}}^s$ in (8.105). A method to control the corrections to the SV limit experimentally is proposed below in the paragraph on new physics. One feature of the SV limit is the absence of CP -odd double-charm final states. (Indeed there are only very few CP -odd final states in Table 8.5.) This has the consequence that $\Delta\Gamma_{\text{CP}}^s$ cannot be too small, because for $\Gamma(B_s^{\text{odd}} \rightarrow X_{\bar{c}c})$ the spectator contributions and non-spectator diagrams like those in Fig. 8.3 must sum to zero. This favors values of $\Delta\Gamma_{\text{CP}}^s = \Delta\Gamma_s^{\text{SM}}$ in the upper range of (8.86).

Standard Model: In the Standard Model the $B_s^0 - \bar{B}_s^0$ mixing phase $\phi_M^s = -2\beta_s$ can be safely neglected for the discussion of $\Delta\Gamma_s$. Then the mass eigenstates coincide with the CP eigenstates defined in (8.97) with $|B_L\rangle = |B_s^{\text{even}}\rangle$ and $|B_H\rangle = |B_s^{\text{odd}}\rangle$. Any $b \rightarrow c\bar{c}s$ decay into a CP -even final state like $D_s^+ D_s^-$ stems solely from the $|B_L\rangle$ component in the untagged B_s sample. A lifetime fit to this decay therefore determines Γ_L . Conversely, the $b \rightarrow c\bar{c}s$ decay into a CP -odd eigenstate determines Γ_H . We can easily verify this from (8.90) by calculating $\mathcal{A}_{\Delta\Gamma}^f$: q/p in (1.66) equals -1 and $\bar{A}_f/A_f = -\eta_f$, where η_f is the CP parity of the final state. Then (1.72) yields $\lambda_f = \eta_f$, so that $\mathcal{A}_{\Delta\Gamma}^f = -\eta_f$. Hence for any $b \rightarrow c\bar{c}s$ decay the coefficient of $\exp(-\Gamma_H t)$ in (8.90) vanishes for a CP -even final state, while the $\exp(-\Gamma_L t)$ term vanishes for a CP -odd final state. In practice one will encounter much more statistics in CP -even final states, so that the best determination of $\Delta\Gamma_s$ will combine Γ_L with Γ_{fs} measured in a flavor-specific decay. From (8.96) and $\Gamma_L = \Gamma_s + \Delta\Gamma_s/2$ one finds

$$\Delta\Gamma_s = 2(\Gamma_L - \Gamma_{\text{fs}}) \left(1 - 2 \frac{\Gamma_L - \Gamma_{\text{fs}}}{\Gamma_{\text{fs}}} \right) + \mathcal{O} \left(\frac{(\Delta\Gamma_s)^3}{\Gamma_s^2} \right). \quad (8.106)$$

Here we have expanded to second order in $\Delta\Gamma_s$, which should be sufficient for realistic values of $\Delta\Gamma_s$.

It should be stressed that every $b \rightarrow c\bar{c}s$ decay encodes the same information on $\Delta\Gamma_s$, once its CP parity is known. This is also true for $b \rightarrow c\bar{u}d$ decays into CP eigenstates, because the decay amplitude carries the same phase as the one in $b \rightarrow c\bar{c}s$. Therefore the extracted values for $\Delta\Gamma_s$ in these decays can be combined to gain statistics. Interesting decay modes are summarized in Table 8.5. Many of the listed modes, like $\bar{B}_s \rightarrow \psi\phi$, require an angular analysis to separate the CP -even from the CP -odd component. This procedure is described in detail in Sect. 8.3.5.

It is tempting to use $\bar{B}_s \rightarrow K^+ K^-$ to measure $\Delta\Gamma_s$ because of its nice experimental signature. But such CKM-suppressed decay modes cannot be used, because the weak phase of the decay amplitude is not known. If $B_s \rightarrow K^+ K^-$ were dominated by penguin loops and new physics were absent from these loops, $\lambda_{K^+ K^-}$ would indeed be equal to $+1$ and the coefficient of $\exp(-\Gamma_H t)$ in (8.90) would vanish. In practice, however, the tree-level amplitude $b \rightarrow u\bar{u}s$ is expected to give a non-negligible contribution. Since this amplitude carries a different phase, $2\arg(V_{ub}) = -2\gamma$, $\lambda_{K^+ K^-}$ deviates from ± 1 and both exponentials in (8.90) contribute.

New Physics: In the presence of new physics the CP-violating phase ϕ in (1.62) and (1.64b) can be large. Since various observables in untagged B_s decays depend on $\cos\phi_s$ in different ways, one can reveal new physics and determine $|\cos\phi_s|$ by combining different measurements. We have already seen above that $\Delta\Gamma_{\text{CP}}^s$ in (8.98) does not depend on ϕ_s at all, while $\Delta\Gamma_s$ is diminished in the presence of new physics:

$$\Delta\Gamma_s = \Delta\Gamma_{\text{CP}}^s \cos\phi_s. \quad (8.107)$$

On the other hand $\sin\phi_s$ can be obtained from CP asymmetries in B_s decays like $B_s \rightarrow \psi\phi$. Therefore measurements of $\Delta\Gamma$ are complementary to the study of CP asymmetries, which require tagging and the resolution of the rapid $B_s - \bar{B}_s$ oscillation and come with a loss in statistics, efficiency and purity. Both avenues should be pursued and their results combined, because they measure the same fundamental quantities. A detailed analysis of both tagged and untagged decays can be found in [46].

In our phase convention $\arg(V_{cb}V_{cs}^*) = 0$ we simply have

$$\arg(M_{12}) = \phi_s. \quad (8.108)$$

The mass eigenstates can be expressed as

$$\begin{aligned} |B_L\rangle &= \frac{1 + e^{i\phi}}{2} |B_s^{\text{even}}\rangle - \frac{1 - e^{i\phi}}{2} |B_s^{\text{odd}}\rangle, \\ |B_H\rangle &= -\frac{1 - e^{i\phi}}{2} |B_s^{\text{even}}\rangle + \frac{1 + e^{i\phi}}{2} |B_s^{\text{odd}}\rangle. \end{aligned} \quad (8.109)$$

Whenever we use B_s^{even} and B_s^{odd} we implicitly refer to our phase conventions for the CKM matrix and the CP transformation. If formulae involving B_s^{even} and B_s^{odd} are used to constrain models with an extended quark sector, the phase convention used for the enlarged CKM matrix must likewise be chosen such that $\arg(V_{cb}V_{cs}^*) \simeq 0$.

We next consider the time evolution of a $b \rightarrow c\bar{c}s$ decay into a CP eigenstate with CP parity η_f . $\mathcal{A}_{\Delta\Gamma}^f$ reads

$$\mathcal{A}_{\Delta\Gamma}^f = -\eta_f \cos\phi_s. \quad (8.110)$$

In the Standard Model, where $\phi_s \simeq 0$, $\Gamma[f, t]$ simplifies to a single-exponential law, which can be verified from (8.91) or by inserting (8.109) into (1.85).

Since $\Delta\Gamma_{\text{CP}}^s$ is unaffected by new physics and $\Delta\Gamma_{\text{CP}}^s > 0$, several facts hold beyond the Standard Model:

- i) There are more CP -even than CP -odd final states in B_s decays.
- ii) The shorter-lived mass eigenstate is always the one with the larger CP -even component in (8.109). Its branching ratio into a CP -even final state f_{CP+} exceeds the branching ratio of the longer-lived mass eigenstate into f_{CP+} , if the weak phase of the decay amplitude is close to $\arg V_{cb}V_{cs}^*$.
- iii) For $\cos \phi_s > 0$ B_L has a shorter lifetime than B_H , while for $\cos \phi_s < 0$ the situation is the opposite [47].

Allowing for a new physics phase ϕ_s the result in (8.105) is changed. In the SV limit one now predicts:

$$\begin{aligned} 2 \text{BR}(\overline{B}_s \rightarrow D_s^{(*)+} D_s^{(*)-}) &\simeq \Delta\Gamma_{\text{CP}}^s \left[\frac{1 + \cos \phi_s}{2\Gamma_L} + \frac{1 - \cos \phi_s}{2\Gamma_H} \right] \\ &= \frac{\Delta\Gamma_{\text{CP}}^s}{\Gamma_s} \left[1 + \mathcal{O}\left(\frac{\Delta\Gamma_s}{\Gamma_s}\right) \right]. \end{aligned} \quad (8.111)$$

The term in square brackets accounts for the fact that in general the CP -even eigenstate $|B_s^{\text{even}}\rangle$ is a superposition of $|B_L\rangle$ and $|B_H\rangle$. It is straightforward to obtain (8.105): inserting (8.109) into (1.85) expresses $\Gamma[f, t]$ in terms of $\Gamma(B_s^{\text{even}} \rightarrow f)$ and $\Gamma(B_s^{\text{odd}} \rightarrow f)$. After integrating over time the coefficient of $\Gamma(B_s^{\text{even}} \rightarrow f)$ is just the term in square brackets in (8.111). We verify from (8.111) that the measurement of $\text{BR}(\overline{B}_s \rightarrow D_s^{(*)+} D_s^{(*)-})$ determines $\Delta\Gamma_{\text{CP}}^s$. Its sensitivity to the new physics phase ϕ_s is suppressed by another factor of $\Delta\Gamma_s/\Gamma_s$ and is irrelevant in view of the theoretical uncertainties.

Next we discuss the determination of $\Delta\Gamma_s$ and $|\cos \phi_s|$. There are two generic ways to obtain information on $\Delta\Gamma_s$ and ϕ_s :

- i) The measurement of the B_s lifetime in two decay modes $\overline{B}_s \rightarrow f_1$ and $\overline{B}_s \rightarrow f_2$ with $\mathcal{A}_{\Delta\Gamma}^{f_1} \neq \mathcal{A}_{\Delta\Gamma}^{f_2}$.
- ii) The fit of the decay distribution of $\overline{B}_s \rightarrow f$ to the two-exponential formula in (1.82).

As first observed in [47], the two methods are differently affected by a new physics phase $\phi_s \neq 0$. Thus by combining the results of methods i) and ii) one can gain information on ϕ_s . In this paragraph we consider two classes of decays:

- flavor-specific decays, which are characterized by $\overline{A}_f = 0$ implying $\mathcal{A}_{\Delta\Gamma}^f = 0$. Examples are $B_s \rightarrow D_s^- \pi^+$ and $B_s \rightarrow X \ell^+ \nu_\ell$,
- the CP -specific decays of Table 8.5, with $\mathcal{A}_{\Delta\Gamma}^f = -\eta_f \cos \phi_s$.

In both cases the time evolution of the untagged sample in (1.82) is not sensitive to the sign of $\Delta\Gamma_s$ (or, equivalently, of $\cos \phi_s$). For the CP -specific decays of Table 8.5 this can be seen by noticing that

$$\mathcal{A}_{\Delta\Gamma}^f \sinh \frac{\Delta\Gamma_s t}{2} = -\eta_f |\cos \phi_s| \sinh \frac{|\Delta\Gamma_s| t}{2}. \quad (8.112)$$

Here we have used the fact that $\Delta\Gamma_s$ and $\cos\phi_s$ always have the same sign, because $\Delta\Gamma_{\text{CP}}^s > 0$. Hence our untagged studies can only determine $|\cos\phi_s|$ and therefore lead to a four-fold ambiguity in ϕ_s . The sign ambiguity in $\cos\phi_s$ reflects the fact that from the untagged time evolution in (1.82) one cannot distinguish, whether the heavier or the lighter eigenstate has the shorter lifetime. (Methods to resolve the discrete ambiguity can be found in [46].)

In order to experimentally establish a non-zero $\Delta\Gamma_s$ from the time evolution in (1.82) one needs sufficient statistics to resolve the deviation from a single-exponential decay law, see (8.91). As long as we are only sensitive to terms linear in $\Delta\Gamma_s t$ and $\Delta\Gamma_s/\Gamma_s$, we can only determine $\mathcal{A}_{\Delta\Gamma}^f \Delta\Gamma_s$ from (8.91). $\mathcal{A}_{\Delta\Gamma}^f \Delta\Gamma_s$ vanishes for flavor-specific decays and equals $-\eta_f \Delta\Gamma_s \cos\phi_s$ for CP-specific final states. Hence from the time evolution alone one can only determine the product $\Delta\Gamma_s \cos\phi_s$ in the first experimental stage.

Determination of Γ_s and $\Delta\Gamma_s \cos\phi_s$: In Eqs. (8.92) – (8.95) we have related the width found in a single-exponential fit to the parameters $A(f)$, $B(f)$, Γ_s and $\Delta\Gamma_s$ of the two-exponential formula.

In (8.96) we found that a single-exponential fit in flavor-specific decays (which have $A = B$) determines Γ_s up to corrections of order $(\Delta\Gamma_s)^2/\Gamma_s^2$.

With (1.82) and (8.92) we can read off A and B for the CP-specific decays of Table 8.5 and find $A(f_{\text{CP}+})/B(f_{\text{CP}+}) = (1 + \cos\phi)/(1 - \cos\phi)$ and $A(f_{\text{CP}-})/B(f_{\text{CP}-}) = (1 - \cos\phi)/(1 + \cos\phi)$ for CP-even and CP-odd final states, respectively. Our key quantity for the discussion of CP-specific decays $\langle \bar{B}_s \rangle \rightarrow f_{\text{CP}}$ is

$$\Delta\Gamma_{\text{CP}}^{s'} \equiv -\eta_f \mathcal{A}_{\Delta\Gamma}^f \Delta\Gamma_s = \Delta\Gamma_s \cos\phi_s = \Delta\Gamma_{\text{CP}}^s \cos^2\phi_s. \quad (8.113)$$

With this definition (8.95) reads for the decay rate $\Gamma_{\text{CP},\eta_f}$ measured in $\langle \bar{B}_s \rangle \rightarrow f_{\text{CP}}$ [46]:

$$\Gamma_{\text{CP},\eta_f} = \Gamma_s + \eta_f \frac{\Delta\Gamma_{\text{CP}}^{s'}}{2} - \sin^2\phi_s \frac{(\Delta\Gamma_s)^2}{2\Gamma_s} + \mathcal{O}\left(\frac{(\Delta\Gamma_s)^3}{\Gamma_s^2}\right). \quad (8.114)$$

That is, to first order in $\Delta\Gamma_s$, comparing the $\langle \bar{B}_s \rangle$ lifetimes measured in a flavor-specific and a CP-specific final state determines $\Delta\Gamma_{\text{CP}}^{s'}$. The first term in (8.114) agrees with the result in [47], which has been found by expanding the time evolution in (8.92) and (8.93) for small $\Delta\Gamma_s t$.

From (8.96) and (8.114) one finds

$$\Gamma_{\text{CP},\eta_f} - \Gamma_{\text{fs}} = \frac{\Delta\Gamma_{\text{CP}}^{s'}}{2} \left(\eta_f + \frac{\Delta\Gamma_{\text{CP}}^{s'}}{\Gamma} \right) + \mathcal{O}\left(\frac{(\Delta\Gamma)^3}{\Gamma^2}\right). \quad (8.115)$$

Hence for a CP-even (CP-odd) final state the quadratic corrections enlarge (diminish) the difference between the two measured widths. A measurement of $\Delta\Gamma_{\text{CP}}^{s'}$ has a high priority at Run II of the Tevatron. The LHC experiments ATLAS, CMS and LHCb expect to measure $\Delta\Gamma_{\text{CP}}^{s'}/\Gamma_s$ with absolute errors between 0.012 and 0.018 for $\Delta\Gamma_{\text{CP}}^{s'}/\Gamma_s = 0.15$ [48]. An upper bound on $\Delta\Gamma_{\text{CP}}^{s'}$ would be especially interesting. If the lattice calculations entering (8.86)

mature and the theoretical uncertainty decreases, an upper bound on $|\Delta\Gamma_{\text{CP}}^{s'}/\Gamma_s|$ may show that $\phi_s \neq 0, \pi$ through

$$\frac{\Delta\Gamma_{\text{CP}}^{s'}}{\Delta\Gamma_{\text{CP}}^s} = \cos^2 \phi_s. \quad (8.116)$$

Note that conversely the experimental establishment of a non-zero $\Delta\Gamma_{\text{CP}}^{s'}$ immediately helps to constrain models of new physics, because it excludes values of ϕ_s around $\pi/2$.

The described method to obtain $\Delta\Gamma_{\text{CP}}^{s'}$ can also be used, if the sample contains a known ratio of CP -even and CP -odd components. This situation occurs e.g. in decays to $J/\psi\phi$, if no angular analysis is performed or in final states, which are neither flavor-specific nor CP eigenstates. We discuss this case below for $\overline{B}_s \rightarrow D_s^\pm D_s^{(*)\mp}$. Further note that the comparison of the lifetimes measured in CP -even and CP -odd final states determines $\Delta\Gamma_{\text{CP}}^{s'}$ up to corrections of order $(\Delta\Gamma_s/\Gamma_s)^3$.

The theoretical uncertainty in (8.86) dilutes the extraction of $|\cos \phi_s|$ from a measurement of $\Delta\Gamma_{\text{CP}}^{s'}$ alone. One can bypass the theory prediction in (8.86) altogether by measuring both $\Delta\Gamma_{\text{CP}}^{s'}$ and $|\Delta\Gamma_s|$ and determine $|\cos \phi_s|$ through

$$\frac{\Delta\Gamma_{\text{CP}}^{s'}}{|\Delta\Gamma_s|} = |\cos \phi_s|. \quad (8.117)$$

To obtain additional information on $\Delta\Gamma_s$ and ϕ_s from the time evolution in (1.82) requires more statistics: the coefficient of t in (8.91), $\Delta\Gamma_s \mathcal{A}_{\Delta\Gamma}^f/2$, vanishes in flavor-specific decays and is equal to $-\eta_f \Delta\Gamma_{\text{CP}}^{s'}/2$ in the CP -specific decays of Table 8.5. Therefore the data sample must be large enough to be sensitive to the terms of order $(\Delta\Gamma_s t)^2$ in order to get new information on $\Delta\Gamma_s$ and ϕ_s . We now list three methods to determine $|\Delta\Gamma_s|$ and $|\cos \phi_s|$ separately [46]. The theoretical uncertainty decreases and the required experimental statistics increases from method 1 to method 3. Hence as the collected data sample grows, one can work off our list downwards. The first method exploits information from branching ratios and needs no information from the quadratic $(\Delta\Gamma_s t)^2$ terms.

Method 1: We assume that $\Delta\Gamma_{\text{CP}}^{s'}$ has been measured as described on page 365. The method presented now is a measurement of $\Delta\Gamma_{\text{CP}}^s$ using the information from branching ratios. With (8.116) one can then find $|\cos \phi_s|$ and subsequently $|\Delta\Gamma_s|$ from (8.117). In the SV limit the branching ratio $\text{BR}(\overline{B}_s \rightarrow D_s^{(*)+} D_s^{(*)-})$ equals $\Delta\Gamma_{\text{CP}}^s/(2\Gamma_s)$ up to corrections of order $\Delta\Gamma_s/\Gamma_s$, as discussed above [44]. Corrections to the SV limit, however, can be sizeable. Yet we stress that one can control the corrections to this limit experimentally, successively arriving at a result which does not rely on the validity of the SV limit. For this it is of prime importance to determine the CP -odd component of the final states $D_s^\pm D_s^{*\mp}$ and $D_s^{*+} D_s^{*-}$. We now explain how the CP -odd and CP -even component of any decay $\overline{B}_s \rightarrow f$ corresponding to the quark level transition $b \rightarrow c\bar{c}s$ can be obtained. This simply requires a fit of the time evolution of the decay to a single exponential, as in (8.93). Define the contributions of the CP -odd and CP -even eigenstate to $B_s \rightarrow f$:

$$\Gamma(B_s^{\text{odd}} \rightarrow f) \equiv \mathcal{N}_f |\langle f | B_s^{\text{odd}} \rangle|^2, \quad \Gamma(B_s^{\text{even}} \rightarrow f) \equiv \mathcal{N}_f |\langle f | B_s^{\text{even}} \rangle|^2. \quad (8.118)$$

It is useful to define the CP -odd fraction x_f by

$$\frac{\Gamma(B_s^{\text{odd}} \rightarrow f)}{\Gamma(B_s^{\text{even}} \rightarrow f)} = \frac{|\langle f|B_s^{\text{odd}}\rangle|^2}{|\langle f|B_s^{\text{even}}\rangle|^2} = \frac{|\langle \bar{f}|B_s^{\text{odd}}\rangle|^2}{|\langle \bar{f}|B_s^{\text{even}}\rangle|^2} = \frac{x_f}{1-x_f}. \quad (8.119)$$

The time evolution $(\Gamma[f, t] + \Gamma[\bar{f}, t])/2$ of the CP -averaged untagged decay $\bar{B}_s \rightarrow f, \bar{f}$ is governed by a two-exponential formula:

$$\frac{\Gamma[f, t] + \Gamma[\bar{f}, t]}{2} = A(f) e^{-\Gamma_L t} + B(f) e^{-\Gamma_H t}. \quad (8.120)$$

With (8.109) and (1.85) one finds

$$\begin{aligned} A(f) &= \frac{\mathcal{N}_f}{2} |\langle f|B_L\rangle|^2 + \frac{\mathcal{N}_f}{2} |\langle \bar{f}|B_L\rangle|^2 \\ &= \frac{1+\cos\phi}{2} \Gamma(B_s^{\text{even}} \rightarrow f) + \frac{1-\cos\phi}{2} \Gamma(B_s^{\text{odd}} \rightarrow f), \\ B(f) &= \frac{\mathcal{N}_f}{2} |\langle f|B_H\rangle|^2 + \frac{\mathcal{N}_f}{2} |\langle \bar{f}|B_H\rangle|^2 \\ &= \frac{1-\cos\phi}{2} \Gamma(B_s^{\text{even}} \rightarrow f) + \frac{1+\cos\phi}{2} \Gamma(B_s^{\text{odd}} \rightarrow f). \end{aligned} \quad (8.121)$$

With (8.119) we arrive at

$$\frac{A(f)}{B(f)} = \frac{(1+\cos\phi)\Gamma(B_s^{\text{even}} \rightarrow f) + (1-\cos\phi)\Gamma(B_s^{\text{odd}} \rightarrow f)}{(1-\cos\phi)\Gamma(B_s^{\text{even}} \rightarrow f) + (1+\cos\phi)\Gamma(B_s^{\text{odd}} \rightarrow f)} = \frac{1+(1-2x_f)\cos\phi}{1-(1-2x_f)\cos\phi}. \quad (8.122)$$

In (8.121) and (8.122) it is crucial that we average the decay rates for $\bar{B}_s \rightarrow f$ and the CP -conjugate process $\bar{B}_s \rightarrow \bar{f}$. This eliminates the interference term $\langle B_s^{\text{odd}}|f\rangle\langle f|B_s^{\text{even}}\rangle$, so that $A(f)/B(f)$ only depends on x_f . The single-exponential fit with (8.93) determines Γ_f . Equations (8.95) and (8.122) combine to give

$$2(\Gamma_f - \Gamma_s) = (1-2x_f)\Delta\Gamma_s \cos\phi_s = (1-2x_f)\Delta\Gamma_{\text{CP}}^s \cos^2\phi_s = (1-2x_f)\Delta\Gamma_{\text{CP}}^{s'}, \quad (8.123)$$

up to corrections of order $(\Delta\Gamma_s)^2/\Gamma_s$. In order to determine x_f from (8.123) we need $\Delta\Gamma_{\text{CP}}^{s'}$ from the lifetime measurement in a CP -specific final state like $D_s^+ D_s^-$ or from the angular separation of the CP components in $\bar{B}_s \rightarrow \psi\phi$. The corrections of order $(\Delta\Gamma_s)^2/\Gamma_s$ to (8.123) can be read off from (8.95) with (8.122) as well. Expressing the result in terms of Γ_f and the rate Γ_{fs} measured in flavor-specific decays, we find

$$1-2x_f = 2 \frac{\Gamma_f - \Gamma_{\text{fs}}}{\Delta\Gamma_{\text{CP}}^{s'}} \left[1 - 2 \frac{\Gamma_f - \Gamma_{\text{fs}}}{\Gamma_s} \right] + \mathcal{O}\left(\frac{(\Delta\Gamma_s)^2}{\Gamma_s^2}\right). \quad (8.124)$$

In order to solve for $\Gamma(B_s^{\text{even}} \rightarrow f)$ and $\Gamma(B_s^{\text{odd}} \rightarrow f)$ we also need the branching ratio $\text{BR}(\bar{B}_s \rightarrow f) + \text{BR}(\bar{B}_s \rightarrow \bar{f})$. Recalling (1.84) one finds from (8.120) and (8.121):

$$\begin{aligned} \text{BR}(\bar{B}_s \rightarrow f) + \text{BR}(\bar{B}_s \rightarrow \bar{f}) &= \Gamma(B_s^{\text{even}} \rightarrow f) \left[\frac{1+\cos\phi_s}{2\Gamma_L} + \frac{1-\cos\phi_s}{2\Gamma_H} \right] \\ &\quad + \Gamma(B_s^{\text{odd}} \rightarrow f) \left[\frac{1-\cos\phi_s}{2\Gamma_L} + \frac{1+\cos\phi_s}{2\Gamma_H} \right]. \end{aligned} \quad (8.125)$$

By combining (8.119) and (8.125) we can solve for the two CP components:

$$\begin{aligned}
\Gamma(B_s^{\text{even}} \rightarrow f) &= \left[\Gamma_s^2 - (\Delta\Gamma_s/2)^2 \right] \left(\text{BR}(\bar{B}_s \rightarrow f) + \text{BR}(\bar{B}_s \rightarrow \bar{f}) \right) \frac{1 - x_f}{2\Gamma_s - \Gamma_f} \\
&= (1 - x_f) \left(\text{BR}(\bar{B}_s \rightarrow f) + \text{BR}(\bar{B}_s \rightarrow \bar{f}) \right) \Gamma_s + \mathcal{O}(\Delta\Gamma_s) \\
\Gamma(B_s^{\text{odd}} \rightarrow f) &= \left[\Gamma_s^2 - (\Delta\Gamma_s/2)^2 \right] \left(\text{BR}(\bar{B}_s \rightarrow f) + \text{BR}(\bar{B}_s \rightarrow \bar{f}) \right) \frac{x_f}{2\Gamma_s - \Gamma_f} \\
&= x_f \left(\text{BR}(\bar{B}_s \rightarrow f) + \text{BR}(\bar{B}_s \rightarrow \bar{f}) \right) \Gamma_s + \mathcal{O}(\Delta\Gamma_s). \tag{8.126}
\end{aligned}$$

From (8.103) we now find the desired quantity by summing over all final states f :

$$\begin{aligned}
\Delta\Gamma_{\text{CP}}^s &= \Gamma(B_s^{\text{even}}) - \Gamma(B_s^{\text{odd}}) = 2 \left[\Gamma_s^2 - (\Delta\Gamma_s/2)^2 \right] \sum_{f \in X_{c\bar{c}}} \text{BR}(\bar{B}_s \rightarrow f) \frac{1 - 2x_f}{2\Gamma_s - \Gamma_f} \\
&= 2\Gamma_s \sum_{f \in X_{c\bar{c}}} \text{BR}(\bar{B}_s \rightarrow f) (1 - 2x_f) \left[1 + \mathcal{O}\left(\frac{\Delta\Gamma_s}{\Gamma_s}\right) \right]. \tag{8.127}
\end{aligned}$$

It is easy to find $\Delta\Gamma_{\text{CP}}^s$: first determine $1 - 2x_f$ from (8.124) for each studied decay mode, then insert the result into (8.127). The small quadratic term $(\Delta\Gamma_s/2)^2 = \Delta\Gamma_{\text{CP}}^s \Delta\Gamma_{\text{CP}}^{s'}/4$ is negligible. This procedure can be performed for $\text{BR}(\bar{B}_s \rightarrow D_s^\pm D_s^{*\mp})$ and $\text{BR}(\bar{B}_s \rightarrow D_s^{*+} D_s^{*-})$ to determine the corrections to the SV limit. In principle the CP-odd P-wave component of $\text{BR}(\bar{B}_s \rightarrow D_s^{*+} D_s^{*-})$ (which vanishes in the SV limit) could also be obtained by an angular analysis, but this is difficult in first-generation experiments at hadron colliders, because the photon from $D_s^* \rightarrow D_s \gamma$ cannot be detected. We emphasize that it is not necessary to separate the $D_s^{(*)+} D_s^{(*)-}$ final states; our method can also be applied to the semi-inclusive $D_s^{(*)\pm} D_s^{(*)\mp}$ sample, using $\Delta\Gamma_{\text{CP}}^{s'}$ obtained from an angular separation of the CP components in $\bar{B}_s \rightarrow \psi\phi$. Further one can successively include those double-charm final states which vanish in the SV limit into (8.127). If we were able to reconstruct all $b \rightarrow c\bar{c}s$ final states, we could determine $\Delta\Gamma_{\text{CP}}^s$ without invoking the SV limit. In practice a portion of these final states will be missed, but the induced error can be estimated from the corrections to the SV limit in the measured decay modes. By comparing $\Delta\Gamma_{\text{CP}}^s$ and $\Delta\Gamma_{\text{CP}}^{s'}$ one finds $|\cos\phi_s|$ from (8.116). The irreducible theoretical error of method 1 stems from the omission of CKM-suppressed decays and is of order $2|V_{ub}V_{us}|/(V_{cb}V_{cs}) \sim 3 - 5\%$.

Method 1 is experimentally simple: at the first stage (relying on the SV limit) it amounts to counting the \bar{B}_s decays into $D_s^{(*)+} D_s^{(*)-}$. The corrections to the SV limit are obtained by one-parameter fits to the time evolution of the collected double-charm data samples. This sample may include final states from decay modes which vanish in the SV limit, such as multiparticle final states. No sensitivity to $(\Delta\Gamma_s t)^2$ is needed. A further advantage is that $\Delta\Gamma_{\text{CP}}^s$ is not diminished by the presence of new physics.

Method 2: In the Standard Model the decay into a CP eigenstate f_{CP} is governed by a single exponential. If a second exponential is found in the time evolution of a CKM-favored decay $\bar{B}_s \rightarrow f_{\text{CP}}$, this will be clear evidence of new physics [49]. To this end we

must resolve the time evolution in (1.82) up to order $(\Delta\Gamma_s t)^2$. At first glance this seems to require a three-parameter fit to the data, because $\Gamma[f, t]$ in (1.82) depends on Γ_s , $\Delta\Gamma_s$ and (through $\mathcal{A}_{\Delta\Gamma}^f$, see (8.110)) on ϕ_s . It is possible, however, to choose these parameters in such a way that one of them enters $\Gamma[f_{\text{CP}}, t]$ at order $(\Delta\Gamma_s)^3$, with negligible impact. The fit parameters are Γ' and Y . They are chosen such that

$$\Gamma[f_{\text{CP}+}, t] = 2 \text{BR}(\bar{B}_s \rightarrow f_{\text{CP}+}) \Gamma' e^{-\Gamma' t} \left[1 + Y \Gamma' t \left(-1 + \frac{\Gamma' t}{2} \right) + \mathcal{O}((\Delta\Gamma_s)^3) \right]. \quad (8.128)$$

Here we have considered a CP -even final state, for which a lot more data are expected than for CP -odd states. With (8.128) we have generalized the lifetime fit method described in (8.91) – (8.96) to the order $(\Delta\Gamma t)^2$. A non-zero Y signals the presence of new physics. The fitted rate Γ' and Y are related to Γ_s , $\Delta\Gamma_s$ and ϕ_s by

$$Y = \frac{(\Delta\Gamma_s)^2}{4\Gamma'^2} \sin^2 \phi_s, \quad \Gamma' = \Gamma_s(1 - Y) + \frac{\cos \phi_s}{2} \Delta\Gamma_s. \quad (8.129)$$

Note that for $|\cos \phi_s| = 1$ the rate Γ' equals the rate of the shorter-lived mass eigenstate and the expansion in (8.128) becomes the exact single-exponential formula. After determining Γ' and Y we can solve (8.129) for Γ_s , $\Delta\Gamma_s$ and ϕ_s . To this end we need the width Γ_{fs} measured in flavor-specific decays. We find

$$\begin{aligned} |\Delta\Gamma_s| &= 2\sqrt{(\Gamma' - \Gamma_{\text{fs}})^2 + \Gamma_{\text{fs}}^2} \left[1 + \mathcal{O}\left(\frac{\Delta\Gamma_s}{\Gamma_s}\right) \right], \\ \Gamma_s &= \Gamma_{\text{fs}} + \frac{(\Delta\Gamma_s)^2}{2\Gamma_s} + \mathcal{O}\left(\left(\frac{\Delta\Gamma_s}{\Gamma_s}\right)^3\right) \\ \Delta\Gamma_{\text{CP}}^{s'} &= 2[\Gamma' - \Gamma_s(1 - Y)] \left[1 + \mathcal{O}\left(\left(\frac{\Delta\Gamma_s}{\Gamma_s}\right)^2\right) \right], \\ |\sin \phi_s| &= \frac{2\Gamma_s \sqrt{Y}}{|\Delta\Gamma_s|} \left[1 + \mathcal{O}\left(\frac{\Delta\Gamma_s}{\Gamma_s}\right) \right]. \end{aligned} \quad (8.130)$$

The quantity $\Delta\Gamma_{\text{CP}}^{s'}$, which we could already determine from single-exponential fits, is now found beyond the leading order in $\Delta\Gamma_s/\Gamma_s$. By contrast, $\Delta\Gamma_s$ and $|\sin \phi_s|$ in (8.130) are only determined to the first non-vanishing order in $\Delta\Gamma_s/\Gamma_s$.

In conclusion, method 2 involves a two-parameter fit and needs sensitivity to the quadratic term in the time evolution. The presence of new physics can be invoked from $Y \neq 0$ and does not require to combine lifetime measurements in different decay modes.

Method 3: Originally the following method has been proposed to determine $|\Delta\Gamma_s|$ [47,49]: The time evolution of a \bar{B}_s decay into a flavor-specific final state is fitted to two exponentials. This amounts to resolving the deviation of $\cosh(\Delta\Gamma_s t/2)$ from 1 in (1.82) in a two-parameter fit for Γ_s and $|\Delta\Gamma_s|$. If one adopts the same parameterization as in (8.128), Γ' and Y are obtained from (8.129) by replacing ϕ_s with $\pi/2$. The best suited flavor-specific decay modes at hadron colliders are $\bar{B}_s \rightarrow D_s^{(*)\pm} \pi^\mp$, $\bar{B}_s \rightarrow D_s^{(*)\pm} \pi^\mp \pi^+ \pi^-$

and $\bar{B}_s^- \rightarrow X \ell^\mp \nu$. Depending on the event rate in these modes, method 3 could be superior to method 2 in terms of statistics. On the other hand, to find the “smoking gun” of new physics, the $|\Delta\Gamma_s|$ obtained must be compared to $\Delta\Gamma_{\text{CP}}^{s'}$ from CP-specific decays to prove $|\cos\phi_s| \neq 1$ through (8.117). Since the two measurements are differently affected by systematic errors, this can be a difficult task. First upper bounds on $|\Delta\Gamma_s|$ using method 3 have been obtained in [50].

The L3 collaboration has determined an upper bound $|\Delta\Gamma_s|/\Gamma_s \leq 0.67$ by fitting the time evolution of fully inclusive decays to two exponentials [51]. This method is quadratic in $\Delta\Gamma_s$ as well. The corresponding formula for the time evolution can be simply obtained from (8.92) with $A = \Gamma_L$ and $B = \Gamma_H$.

8.3.2.3 Phenomenology of $\Delta\Gamma_d$

The Standard Model value $\Delta\Gamma_d^{\text{SM}}/\Gamma_d \approx 3 \times 10^{-3}$ derived before (8.89) is presumably too small to be measured from lifetime fits. In extension of the Standard Model, however, $\Delta\Gamma_d/\Gamma_d$ can be large, up to a few percent. The expected high statistics for the decay $B_d \rightarrow \psi K_S$ can be used to measure the lifetime $1/\Gamma_{B_d \rightarrow \psi K_S}$ in this channel with

$$\Gamma_{B_d \rightarrow \psi K_S} = \Gamma_d - \frac{\Delta\Gamma^d}{2} \cos(2\beta_{\psi K_S}) = \Gamma_d - |\Gamma_{12}^d| \cos(2\beta_{\psi K_S}) \cos\phi_d. \quad (8.131)$$

$\sin(2\beta_{\psi K_S})$ is the quantity characterizing the mixing-induced CP asymmetry measured from tagged $B_d \rightarrow \psi K_S$ decays. Γ_d is obtained from a lifetime measurements in flavor-specific decay modes. We stress that this measurement of $\Gamma_{B_d \rightarrow \psi K_S}$ can be done from the *untagged* $\bar{B}_d^- \rightarrow \psi K_S$ data sample. If Γ_{12}^d is dominated by new physics, its phase and therefore also ϕ_d is unknown. If one neglects the small SM contribution in (8.83) to ϕ_d , (8.131) reads

$$\Gamma_{B_d \rightarrow \psi K_S} \simeq \Gamma_d - |\Gamma_{12}^d| \cos(2\beta_{\psi K_S}) \cos(2\beta_{\psi K_S} - 2\beta) = \Gamma_d - |\Gamma_{12}^d| \cos(\phi_d + 2\beta) \cos\phi_d, \quad (8.132)$$

where β is the true angle of the unitarity triangle as defined in (1.32). Note that in the presence of new physics β is unknown. When combined with the CP asymmetry in flavor-specific decays discussed in Sect. 8.3.3 one can determine $|\Gamma_{12}^d|$ and $\sin\phi_d$. Then up to discrete ambiguities also $\beta = \beta_{\psi K_S} - \phi_d/2$ can be determined. Depending on whether the enhancement of Γ_{12}^d is due to $b \rightarrow \bar{c}cd$, $b \rightarrow \bar{u}cd$ or $b \rightarrow \bar{u}ud$, transitions, CP asymmetries in these channels can also help to disentangle $|\Gamma_{12}^d|$ and ϕ_d .

Interestingly, one can isolate the contribution to $|\Gamma_{12}^d|$ from $b \rightarrow \bar{c}cd$ decays. Define

$$\Delta\Gamma_{\text{CP}}^{d,cc} \equiv 2|\xi_c^d|^2 \Gamma_{12}^{d,cc} = 2 \sum_{f \in X_{c\bar{c}}} [\Gamma(B_d \rightarrow f_{\text{CP}+}) - \Gamma(B_d \rightarrow f_{\text{CP}-})]. \quad (8.133)$$

in analogy to (8.98). In the Standard Model $\Delta\Gamma_{\text{CP}}^{d,cc}$ is slightly larger than $2|\Gamma_{12}^d|$, by a factor of $1/R_t^2$. From (8.89) one finds

$$\frac{\Delta\Gamma_{\text{CP}}^{d,cc}}{\Delta\Gamma_{\text{CP}}^s} \simeq \frac{f_{B_d}^2 B_{B_d}^S}{f_{B_s}^2 B_{B_s}^S} \left| \frac{\xi_c^d}{\xi_t^s} \right|^2 \simeq 0.04, \quad (8.134)$$

i.e. $\Delta\Gamma_{\text{CP}}^{d,cc}/\Gamma_d \simeq 5 \times 10^{-3}$. Now $\Delta\Gamma_{\text{CP}}^{d,cc}$ can be measured by counting the CP -even and CP -odd final states in $b \rightarrow c\bar{c}d$ decays, just as described in Sect. 8.3.2.2 for $b \rightarrow c\bar{c}s$ decays of B_s mesons. Again, in the SV limit the inclusive decay $\bar{B}_d \rightarrow X_{c\bar{c}d}$ is exhausted by $\bar{B}_d \rightarrow D^{(*)+}D^{(*)-}$, which is purely CP -even in this limit. With (8.127) one can find $\Delta\Gamma_{\text{CP}}^{d,cc}$. That is, in the SV limit one just has to measure $Br(\bar{B}_d \rightarrow D^{(*)+}D^{(*)-})$, which equals $\Delta\Gamma_{\text{CP}}^{d,cc}/(2\Gamma_d)$. However, the lifetime method described in ‘Method 1’ above cannot be used to determine the corrections to the SV limit, because $\Delta\Gamma_d$ is too small. Yet in the limit of exact U-spin symmetry ($m_d = m_s$) the CP -odd components of $D^{(*)+}D^{(*)-}$ from B_d decay and $D_s^{(*)+}D_s^{(*)-}$ from B_s decay are the same. Finally in $b \rightarrow c\bar{c}d$ transitions CP violation in decay could be relevant. It results from penguin loops involving top- or up-quarks and spoils the relation (8.127) between branching ratios and $\Delta\Gamma_{\text{CP}}^{d,cc}$. This effect, however, is calculable for inclusive decays like $\bar{B}_d \rightarrow X_{c\bar{c}d}$. In the Standard Model CP violation in this inclusive decay is of order 1% and therefore negligible [52]. CP -violation from non-standard sources can be revealed by comparing CP -asymmetries in $b \rightarrow c\bar{c}d$ decays with those in $b \rightarrow c\bar{c}s$ decays (namely $\sin 2\beta$ from $B_d \rightarrow \psi K_S$). Since (8.134) depends on no CKM elements and the hadronic factor is known exactly in the $SU(3)_F$ limit, a combined measurement of $\Delta\Gamma_{\text{CP}}^{d,cc}$ and $\Delta\Gamma_{\text{CP}}^s$ provides an excellent probe of new physics in $b \rightarrow c\bar{c}d$ transitions.

8.3.3 CP Asymmetry in Flavor-specific Decays

In the preceding sections we have set the small parameter $a_q \equiv a(B_q)$, $q = d, s$, defined in (1.65) to zero. In order to study CP violation in mixing we must keep terms of order a_q . The corresponding “wrong-sign” CP asymmetry is measured in flavor-specific decays $B_q \rightarrow f$ and equals

$$a_{\text{fs}}^q = \frac{\Gamma(\bar{B}_q^0(t) \rightarrow f) - \Gamma(B_q^0(t) \rightarrow \bar{f})}{\Gamma(\bar{B}_q^0(t) \rightarrow f) + \Gamma(B_q^0(t) \rightarrow \bar{f})} = \text{Im} \frac{\Gamma_{12}^q}{M_{12}^q} = a_q, \quad \text{for } \bar{A}_f = 0 \text{ and } |A_f| = |\bar{A}_{\bar{f}}|. \quad (8.135)$$

A special case of a_{fs}^q is the semileptonic asymmetry, where $f = X\ell^+\nu$, introduced in Sect. 1.4.1. A determination of a_q gives additional information on the three rephasing-invariant quantities $|M_{12}^q|$, $|\Gamma_{12}^q|$ and ϕ_q characterizing $B^0 - \bar{B}^0$ mixing.

Observe that a_{fs}^q in (8.135) is time-independent. While both numerator and denominator depend on t , this dependence drops out from the ratio. The “right-sign” asymmetry, vanishes:

$$\Gamma(B_q^0(t) \rightarrow f) - \Gamma(\bar{B}_q^0(t) \rightarrow \bar{f}) = 0, \quad \text{for } \bar{A}_f = 0 \text{ and } |A_f| = |\bar{A}_{\bar{f}}|. \quad (8.136)$$

This implies that one can measure a_{fs}^q from *untagged* decays [46,53]. It is easily verified from the sum of (1.73) and (1.74) that to order a_q the time evolution of untagged decays exhibits oscillations governed by Δm_q . Since a is small, a small production asymmetry $\epsilon = N_{\bar{B}}/N_B - 1$, which also leads to oscillations in the untagged sample, could introduce an

experimental bias. To first order in the small parameters a_q , and ϵ one finds

$$a_{\text{fs}}^{q, \text{unt}} = \frac{\Gamma[f, t] - \Gamma[\bar{f}, t]}{\Gamma[f, t] + \Gamma[\bar{f}, t]} = \frac{a_q}{2} - \frac{a_q + \epsilon}{2} \frac{\cos(\Delta m_q t)}{\cosh(\Delta \Gamma_q t/2)}, \quad \text{for } \bar{A}_f = 0 \text{ and } |A_f| = |\bar{A}_{\bar{f}}|. \quad (8.137)$$

Note that the production asymmetry between B_q^0 and \bar{B}_q^0 cannot completely fake the effect of a non-zero a_q in (8.137): while both $a_q \neq 0$ and $\epsilon \neq 0$ lead to oscillations, the offset from the constant term indicates $a_q \neq 0$.

The Standard Model predictions for a_d and a_s are

$$\begin{aligned} a_d &\approx -\frac{\bar{\eta}}{R_t^2} \frac{4\pi (K_1 + K_2) m_c^2}{M_W^2 \eta_B b_B S(m_t^2/M_W^2)} \approx -8 \times 10^{-4} \\ a_s &\approx \bar{\eta} \lambda^2 \frac{4\pi (K_1 + K_2) m_c^2}{M_W^2 \eta_B b_B S(m_t^2/M_W^2)} \approx 5 \times 10^{-5}. \end{aligned} \quad (8.138)$$

The huge GIM suppression factor $m_b^2/M_W^2 \sin \phi_d \propto m_c^2/M_W^2$ leads to these tiny predictions for CP violation in mixing. a_d plays a preeminent role in the search for new physics :

- its sensitivity to new physics is enormous, it can be enhanced by two orders of magnitude,
- it is affected by a wide range of possible new physics effects: new CP violating effects in ϕ_d relax the GIM-suppression $\propto m_b^2/M_W^2 \sin \phi_d$, because ϕ_d is no more proportional to $z = m_c^2/m_b^2$. New physics contributions to *any* of the CKM-suppressed decay modes $b \rightarrow \bar{c}cd$, $b \rightarrow \bar{u}cd$ or $b \rightarrow \bar{u}ud$ can significantly enhance $|\Gamma_{12}^d|$ and thereby a_d .

Of course new physics contributions to $\arg M_{12}^d$ will not only affect ϕ_d , but also the CP asymmetry in $B_d^0 \rightarrow \psi K_S$. But from this measurement alone one cannot extract the new physics contribution, because one will know the true value of $\beta = \arg(-\xi_t^{d*}/\xi_c^{d*})$ only poorly, once new physics affects the standard analysis of the unitarity triangle. For the discussion of new physics it helps to write

$$a_q = \frac{2|\Gamma_{12}^q|}{\Delta m_q} \sin \phi_q = \frac{|\Delta \Gamma_q|}{\Delta m_q} \frac{\sin \phi_q}{|\cos \phi_q|}. \quad (8.139)$$

If both $|\Delta \Gamma_d|$ and a_d are measured, one can determine both $|\Gamma_{12}^d|$ and $\sin \phi_d$.

a_s is less interesting than a_d , because Γ_{12}^s stems from CKM-favored decays and is not very sensitive to new physics. The ratio $\Delta \Gamma_{\text{CP}}^s/\Gamma_s \leq 0.2$ from (8.86) and the current experimental limit $\Delta m_s \geq 14.9 \text{ ps}^{-1}$ [33] imply that $|a_s| \leq 0.01$. New physics can affect ϕ_s only through $\arg M_{12}^s$, but this new physics can be detected most easily through CP asymmetries in $B_s \rightarrow \psi\phi$ or $B_s \rightarrow D_s^{(*)+} D_s^{(*)-}$ decays. Since the Standard Model predictions for these asymmetries are essentially zero, there is no problem here to disentangle standard from non-standard physics. Note that the measurement of $\text{sgn} \sin \phi_s$ reduces the four-fold ambiguity in ϕ_s from the measurement of $|\cos \phi_s|$ to a two-fold one. The unambiguous determination of ϕ_s is discussed in detail in [46].

8.3.4 Angular analysis to separate the CP components[†]

8.3.5 CP -odd and CP -even components in $B_s \rightarrow J/\psi\phi$

The most general amplitude for $B_s \rightarrow J/\psi\phi$ can be written in terms of the polarization states of the two vector mesons as [55,56]

$$A(B_s(t) \rightarrow J/\psi\phi) = \frac{A_0(t)}{x} \epsilon_{J/\psi}^{*L} \epsilon_\phi^{*L} - A_{||}(t) \epsilon_{J/\psi}^{*T} \cdot \epsilon_\phi^{*T} / \sqrt{2} - i A_\perp(t) \epsilon_{J/\psi}^* \times \epsilon_\phi^* \cdot \hat{\mathbf{p}}_\phi / \sqrt{2}, \quad (8.140)$$

where $x \equiv p_{J/\psi} \cdot p_\phi / (m_{J/\psi} m_\phi)$ and $\hat{\mathbf{p}}_\phi$ is the unit vector along the direction of motion of ϕ in the rest frame of J/ψ .

Since the “ CP violation in decay” of $B_s \rightarrow J/\psi\phi$ is vanishing,

$$\bar{A}_0(0) = A_0(0), \quad \bar{A}_{||}(0) = A_{||}(0), \quad \bar{A}_\perp(0) = -A_\perp(0). \quad (8.141)$$

The final state is thus an admixture of different CP eigenstates: A_0 and $A_{||}$ are CP -even amplitudes whereas A_\perp is CP -odd. The decay rate is given by

$$\Gamma(t) \propto |A_0(t)|^2 + |A_{||}(t)|^2 + |A_\perp(t)|^2, \quad (8.142)$$

where the time evolutions of the individual terms are [57]

$$\begin{aligned} |A_{0,||}(t)|^2 &= |A_{0,||}(0)|^2 \left[e^{-\Gamma_L t} - e^{-\bar{\Gamma} t} \sin(\Delta m_s t) \delta\phi \right], \\ |A_\perp(t)|^2 &= |A_\perp(0)|^2 \left[e^{-\Gamma_H t} + e^{-\bar{\Gamma} t} \sin(\Delta m_s t) \delta\phi \right]. \end{aligned} \quad (8.143)$$

Here, $\bar{\Gamma} \equiv \Gamma_s = (\Gamma_L + \Gamma_H)/2$. Note that this is *not* the average lifetime of B_s as measured through its semileptonic decays [58].

The value of

$$\delta\phi \equiv 2\beta_s \approx 2\lambda^2 \eta \approx 0.03 \quad (8.144)$$

is small in the standard model⁷, so that the terms proportional to $\delta\phi$ in (8.143) can be neglected in the first approximation. The time evolution of (8.142) is then a sum of two exponential decays with lifetimes $1/\Gamma_H$ and $1/\Gamma_L$.

In principle, a fit to the time dependence of the total decay rate (8.142) can give the values of Γ_H and Γ_L separately, but $\Delta\Gamma_s/\bar{\Gamma}$ is expected to be less than 20%, and it is not easy to separate two closely spaced lifetimes. The inclusion of angular information will increase the accuracy in the measurement of $\Delta\Gamma_s$ multi-fold, as we'll see in the section 8.3.6 below.

[†]Author: Amol Dighe

⁷Generalizations of the formulae to the case of new physics can be found in [46].

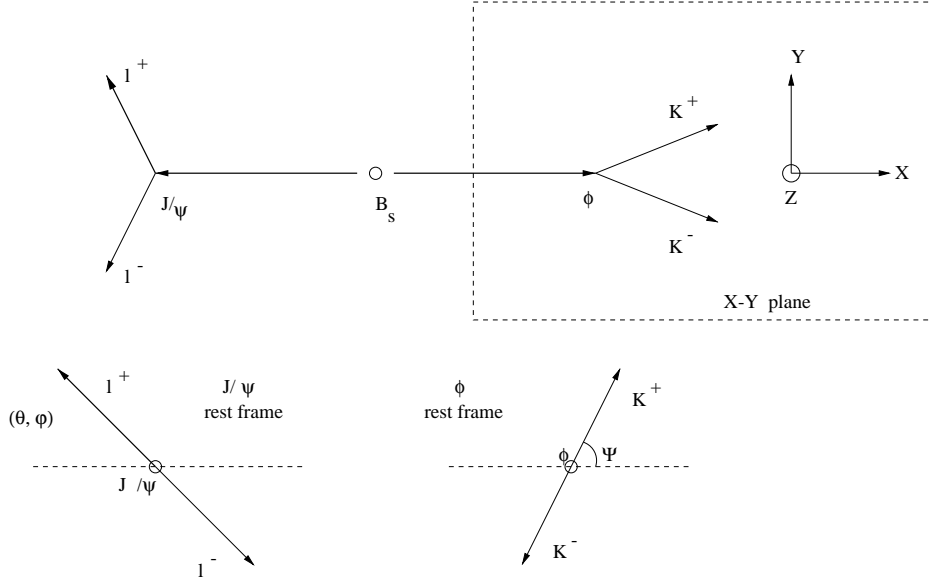


Figure 8.4: The definitions of angles θ, φ, ψ . Here θ is the “transversity” angle.

8.3.6 The transversity angle distribution

Since there are four particles in the final state, the directions of their momenta can define three independent physical angles. Our convention for the definitions of angles [56,57] is as shown in Fig. 8.4. The x -axis is the direction of ϕ in the J/ψ rest frame, the z axis is perpendicular to the decay plane of $\phi \rightarrow K^+ K^-$, and $p_y(K^+) \geq 0$. The coordinates (θ, φ) describe the direction of l^+ in the J/ψ rest frame and ψ is the angle made by $\vec{p}(K^+)$ with the x axis in the ϕ rest frame. With this convention,

$$\begin{aligned} \mathbf{x} &= \mathbf{p}_\phi, & \mathbf{y} &= \frac{\mathbf{p}_{K^+} - \mathbf{p}_\phi(\mathbf{p}_\phi \cdot \mathbf{p}_{K^+})}{|\mathbf{p}_{K^+} - \mathbf{p}_\phi(\mathbf{p}_\phi \cdot \mathbf{p}_{K^+})|}, & \mathbf{z} &= \mathbf{x} \times \mathbf{y}, \\ \sin \theta \cos \varphi &= \mathbf{p}_{l^+} \cdot \mathbf{x}, & \sin \theta \sin \varphi &= \mathbf{p}_{l^+} \cdot \mathbf{y}, & \cos \theta &= \mathbf{p}_{l^+} \cdot \mathbf{z}. \end{aligned} \quad (8.145)$$

Here, the bold-face characters represent *unit* 3-vectors and everything is measured in the rest frame of J/ψ . Also

$$\cos \psi = -\mathbf{p}'_{K^+} \cdot \mathbf{p}'_{J/\psi}, \quad (8.146)$$

where the primed quantities are *unit vectors* measured in the rest frame of ϕ .

The θ defined here is the *transversity* angle [59], which separates out the CP -even and CP -odd components. The angular distribution in terms of θ is given by [56]:

$$\frac{d\Gamma(t)}{d\cos\theta} \propto (|A_0(t)|^2 + |A_{\parallel}(t)|^2) \frac{3}{8} (1 + \cos^2 \theta) + |A_{\perp}(t)|^2 \frac{3}{4} \sin^2 \theta, \quad (8.147)$$

where the time evolutions of the terms are as given in (8.143).

The CP -even and CP -odd components are now separated by not only their different lifetimes (which are very close) but also by their decay angular distributions (which are

distinctly different). The study of information content about the value of $\Delta\Gamma_s$ in the time and angular measurements [60] suggests that, in order to get the same degree of accuracy in $\Delta\Gamma_s$ with only time measurements, one would need about two orders of magnitude more number of events than if both the time and angular measurements were used (see Fig. 3 in [60]). This indicates that the strategy of selecting one decay mode (*e.g.* $J/\psi\phi$) and studying its angular distribution will turn out to be more fruitful than trying to combine all CP eigenstate decay modes and determine Γ_H and Γ_L solely from their time evolutions. Note that, in the limiting case of $\Gamma_H = \Gamma_L$, the time evolution by itself *cannot* separate the CP even and odd components, whereas the angular measurements can.

A fit to the transversity angle distribution (8.147) with its complete time evolution (8.143) also gives the value of $\delta\phi$ and Δm_s , though a better measurement of the latter may be obtained through other decay channels.

The transversity angle distribution (8.147) is valid for any $B_s \rightarrow J/\psi(\rightarrow \ell^+\ell^-)C_1C_2$ decay, where C_1 and C_2 are (a) self-conjugate particles, or (b) scalars and CP conjugates of each other [59]. The particles C_1 and C_2 need not be the products of any resonance, and their total angular momentum is irrelevant. So the time and transversity angle measurements from all the resonant and non-resonant decays of this form may be combined to gain statistics. Here the values of $(|A_0(0)|^2 + |A_{\parallel}(0)|^2)$ and $|A_{\perp}(0)|^2$ are just some *effective* average values, but the decay widths Γ_H and Γ_L are the same for all such decay modes, and hence for the whole data sample.

8.3.7 Three-angle distribution in $B_s \rightarrow J/\psi(\rightarrow l^+l^-)\phi(\rightarrow K^+K^-)$

While the one-angle distribution (8.147) is in principle sufficient to determine the values of Γ_H , Γ_L , $\delta\phi$ and Δm_s , using the information present in all the angles (θ, ϕ, ψ) will improve the measurements. In addition, one also gets access to the magnitudes of all the three amplitudes $A_0(0)$, $A_{\parallel}(0)$, $A_{\perp}(0)$ and the strong phases between them, which was not possible with the one-angle distribution [57]. A method to combine the three-angle distributions of $B_s \rightarrow J/\psi\phi$ and $B_d \rightarrow J/\psi K^*$ to resolve a discrete ambiguity in the CKM angle β has also been proposed [61].

The three angle distribution of an initially present (i.e. tagged) B_s meson is [56,57]

$$\begin{aligned} \frac{d^3\Gamma[B_s(t) \rightarrow J/\psi(\rightarrow l^+l^-)\phi(\rightarrow K^+K^-)]}{d\cos\theta d\varphi d\cos\psi} &\propto \frac{9}{32\pi} \left\{ 2|A_0(t)|^2 \cos^2\psi (1 - \sin^2\theta \cos^2\varphi) \right. \\ &+ \sin^2\psi \left[|A_{\parallel}(t)|^2 (1 - \sin^2\theta \sin^2\varphi) + |A_{\perp}(t)|^2 \sin^2\theta - \text{Im}(A_{\parallel}^*(t)A_{\perp}(t)) \sin 2\theta \sin\varphi \right] \\ &\left. + \frac{1}{\sqrt{2}} \sin 2\psi \left[\text{Re}(A_0^*(t)A_{\parallel}(t)) \sin^2\theta \sin 2\varphi + \text{Im}(A_0^*(t)A_{\perp}(t)) \sin 2\theta \cos\varphi \right] \right\}. \quad (8.148) \end{aligned}$$

Note that the same angular distribution (8.148) is also valid for $B_d \rightarrow J/\psi(\rightarrow \ell^+\ell^-)K^*(\rightarrow K^{\pm}\pi^{\mp})$. The angular distribution for the CP conjugate decay is obtained simply by replacing all A 's by \bar{A} 's [57].

The time evolution of the observables in the angular distribution (the coefficients of the angular terms in (8.148) and its CP conjugate mode) are given in Table 8.2 and 8.3

Observable	Time evolution
$ A_0(t) ^2$	$ A_0(0) ^2 \left[e^{-\Gamma_L t} - e^{-\bar{\Gamma} t} \sin(\Delta m_s t) \delta\phi \right]$
$ A_{\parallel}(t) ^2$	$ A_{\parallel}(0) ^2 \left[e^{-\Gamma_L t} - e^{-\bar{\Gamma} t} \sin(\Delta m_s t) \delta\phi \right]$
$ A_{\perp}(t) ^2$	$ A_{\perp}(0) ^2 \left[e^{-\Gamma_H t} + e^{-\bar{\Gamma} t} \sin(\Delta m_s t) \delta\phi \right]$
$\text{Re}(A_0^*(t)A_{\parallel}(t))$	$ A_0(0) A_{\parallel}(0) \cos(\delta_2 - \delta_1) \left[e^{-\Gamma_L t} - e^{-\bar{\Gamma} t} \sin(\Delta m_s t) \delta\phi \right]$
$\text{Im}(A_{\parallel}^*(t)A_{\perp}(t))$	$ A_{\parallel}(0) A_{\perp}(0) \left[e^{-\bar{\Gamma} t} \sin(\delta_1 - \Delta m_s t) + \frac{1}{2} \left(e^{-\Gamma_H t} - e^{-\Gamma_L t} \right) \cos(\delta_1) \delta\phi \right]$
$\text{Im}(A_0^*(t)A_{\perp}(t))$	$ A_0(0) A_{\perp}(0) \left[e^{-\bar{\Gamma} t} \sin(\delta_2 - \Delta m_s t) + \frac{1}{2} \left(e^{-\Gamma_H t} - e^{-\Gamma_L t} \right) \cos(\delta_2) \delta\phi \right]$

Table 8.2: Time evolution of the decay $B_s \rightarrow J/\psi(\rightarrow l^+l^-)\phi(\rightarrow K^+K^-)$ of an initially (i.e. at $t=0$) pure B_s meson. Here $\bar{\Gamma} \equiv (\Gamma_H + \Gamma_L)/2$.

Observable	Time evolution
$ \bar{A}_0(t) ^2$	$ A_0(0) ^2 \left[e^{-\Gamma_L t} + e^{-\bar{\Gamma} t} \sin(\Delta m_s t) \delta\phi \right]$
$ \bar{A}_{\parallel}(t) ^2$	$ A_{\parallel}(0) ^2 \left[e^{-\Gamma_L t} + e^{-\bar{\Gamma} t} \sin(\Delta m_s t) \delta\phi \right]$
$ \bar{A}_{\perp}(t) ^2$	$ A_{\perp}(0) ^2 \left[e^{-\Gamma_H t} - e^{-\bar{\Gamma} t} \sin(\Delta m_s t) \delta\phi \right]$
$\text{Re}(\bar{A}_0^*(t)\bar{A}_{\parallel}(t))$	$ A_0(0) A_{\parallel}(0) \cos(\delta_2 - \delta_1) \left[e^{-\Gamma_L t} + e^{-\bar{\Gamma} t} \sin(\Delta m_s t) \delta\phi \right]$
$\text{Im}(\bar{A}_{\parallel}^*(t)\bar{A}_{\perp}(t))$	$- A_{\parallel}(0) A_{\perp}(0) \left[e^{-\bar{\Gamma} t} \sin(\delta_1 - \Delta m_s t) - \frac{1}{2} \left(e^{-\Gamma_H t} - e^{-\Gamma_L t} \right) \cos(\delta_1) \delta\phi \right]$
$\text{Im}(\bar{A}_0^*(t)\bar{A}_{\perp}(t))$	$- A_0(0) A_{\perp}(0) \left[e^{-\bar{\Gamma} t} \sin(\delta_2 - \Delta m_s t) - \frac{1}{2} \left(e^{-\Gamma_H t} - e^{-\Gamma_L t} \right) \cos(\delta_2) \delta\phi \right]$

Table 8.3: Time evolution of the decay $\bar{B}_s \rightarrow J/\psi(\rightarrow l^+l^-)\phi(\rightarrow K^+K^-)$ of an initially (i.e. at $t=0$) pure \bar{B}_s meson. Here $\bar{\Gamma} \equiv (\Gamma_H + \Gamma_L)/2$.

respectively. Here $\delta_1 \equiv \text{Arg}(A_{\perp}^* A_{\parallel})$ and $\delta_2 \equiv \text{Arg}(A_0^* A_{\parallel})$. A finite lifetime difference $\Delta\Gamma$ implies that the CP violating terms proportional to

$$\left(e^{-\Gamma_H t} - e^{-\Gamma_L t} \right) \cos(\delta_{1(2)}) \delta\phi \quad (8.149)$$

survive even when the B_s is untagged [57,62]. An experimental feasibility study for extracting the parameters from the time dependent three angle distribution has been performed for the LHC in [63].

8.3.8 Angular moments method

The likelihood fit to the complete angular distribution (8.148) – including the time evolution of the observables (Tables 8.2 and 8.3) – is a difficult task due to the large number of parameters involved. The method of angular moments proposed in [57] can disentangle the angular dependences and split up the likelihood fit into a number of likelihood fits with a smaller number of parameters.

The angular distributions ((8.147) or (8.148)) are of the form

$$f(\Theta, \mathcal{P}; t) = \sum b^{(k)}(\mathcal{P}; t) g^{(k)}(\Theta), \quad (8.150)$$

where \mathcal{P} represents the parameters, and Θ denotes the angles. If we can find *weighting functions* $w^{(i)}$ such that

$$\int [\mathcal{D}\Theta] w^{(i)}(\Theta) g^{(k)}(\Theta) = \delta_{ik}, \quad (8.151)$$

then

$$b^{(i)} \approx \sum_{\text{events}} w^{(i)}(\Theta), \quad (8.152)$$

and the observables are determined directly from the data. It can be shown [57] that such a set of weighting functions exists for any angular distribution of the form (8.150) and such a set can be determined without any *a priori* knowledge of the values of the observables $b^{(i)}$. A likelihood fit can then be performed on each observable $b^{(i)}$ independently in order to determine the parameters.

The angular moments (AM) method is more transparent and easier to implement than the complete likelihood fit method. Although the AM method in its naive form involves some loss of information, the extent of this loss of information in the case of the transversity angle distribution has been found to be less than 10% in the parameter range of interest (see Fig. 5 of [60]). In its full form, the AM method can determine the values of parameters almost as well as the likelihood fit method (see, *e.g.* [64]).

To conclude, the angular analysis of $B_s \rightarrow J/\psi\phi$ decays can separate the CP even and odd components in the final state, and it is perhaps the best way to determine the lifetime difference between B_s^H and B_s^L . As a byproduct, it also helps the measurement of CP odd and even components and their relative strong phases, and with enough statistics, the determination of Δm_s and $\delta\phi$. The angular analysis, possibly employing the angular moments method if the likelihood fit is inadequate, is highly recommended.

8.3.9 $D^0 - \bar{D}^0$ mixing[†]

We define the mass eigenstates in $D^0 - \bar{D}^0$ mixing as

$$\begin{aligned} |D_1\rangle &= p|D^0\rangle + q|\bar{D}^0\rangle, \\ |D_2\rangle &= p|D^0\rangle - q|\bar{D}^0\rangle, \quad \text{with } |p|^2 + |q|^2 = 1. \end{aligned} \quad (8.153)$$

q and p are obtained from the solution of the eigenvalue problem for $M - i\Gamma/2$. In (1.61c) q/p is determined in terms of M_{12} and Γ_{12} . We define

$$\Delta m_D = m_2 - m_1, \quad \Delta\Gamma_D = \Gamma_1 - \Gamma_2 \quad (8.154)$$

$$x_D = \frac{\Delta m_D}{\Gamma} \quad y_D = -\frac{\Delta\Gamma_D}{2\Gamma} = \frac{\Gamma_2 - \Gamma_1}{2\Gamma}. \quad (8.155)$$

The definitions in (8.153) and (8.154) comply with the conventions of Sect. 1.3 for $B^0 - \bar{B}^0$ mixing. In particular the time evolution formulae of (1.58) - (1.60) are also valid for $D^0 - \bar{D}^0$ mixing with the replacement $B^0 \rightarrow D^0$. Unlike in the case of $B^0 - \bar{B}^0$ mixing we cannot

[†]Author: Ulrich Nierste

expand in $\Delta\Gamma_D/\Delta m_D$. We also refrain from expanding in a defined in (1.65). Then (1.73) - (1.77) can be used for D^0 mesons, if $1+a$ in (1.74) is replaced by $|p/q|^2$ and $1-a$ in (1.76) is replaced by $|q/p|^2$. Note that the definition of y_D in (8.155) is opposite in sign to the one of y in the B meson system in (1.93). In (8.155) we have used the sign convention which is usually used in $D^0 - \bar{D}^0$ mixing. Since $D^0 - \bar{D}^0$ mixing is very small, one can expand in $\Delta m_D t$ and $\Delta\Gamma_D t$. Using x_D and y_D from (8.155) the small t expansion of (1.73) - (1.77) gives

$$\Gamma(D^0(t) \rightarrow f) = \mathcal{N}_f |A_f|^2 e^{-\Gamma_D t} \left[1 + (-\text{Im } \lambda_f x_D + \text{Re } \lambda_f y_D) \Gamma_D t + \left(\frac{|\lambda_f|^2 + 1}{4} y_D^2 + \frac{|\lambda_f|^2 - 1}{4} x_D^2 \right) (\Gamma_D t)^2 \right], \quad (8.156)$$

$$\Gamma(\bar{D}^0(t) \rightarrow f) = \mathcal{N}_f |A_f|^2 e^{-\Gamma_D t} \left| \frac{p}{q} \right|^2 \left[|\lambda_f|^2 + (\text{Im } \lambda_f x_D + \text{Re } \lambda_f y_D) \Gamma_D t + \left(\frac{|\lambda_f|^2 + 1}{4} y_D^2 - \frac{|\lambda_f|^2 - 1}{4} x_D^2 \right) (\Gamma_D t)^2 \right], \quad (8.157)$$

$$\Gamma(D^0(t) \rightarrow \bar{f}) = \mathcal{N}_f |\bar{A}_{\bar{f}}|^2 e^{-\Gamma_D t} \left| \frac{q}{p} \right|^2 \left[|\lambda_{\bar{f}}|^{-2} + \left(\text{Im } \frac{1}{\lambda_{\bar{f}}} x_D + \text{Re } \frac{1}{\lambda_{\bar{f}}} y_D \right) \Gamma_D t + \left(\frac{|\lambda_{\bar{f}}|^{-2} + 1}{4} y_D^2 - \frac{|\lambda_{\bar{f}}|^{-2} - 1}{4} x_D^2 \right) (\Gamma_D t)^2 \right], \quad (8.158)$$

$$\Gamma(\bar{D}^0(t) \rightarrow \bar{f}) = \mathcal{N}_f |\bar{A}_{\bar{f}}|^2 e^{-\Gamma_D t} \left[1 + \left(-\text{Im } \frac{1}{\lambda_{\bar{f}}} x_D + \text{Re } \frac{1}{\lambda_{\bar{f}}} y_D \right) \Gamma_D t + \left(\frac{|\lambda_{\bar{f}}|^{-2} + 1}{4} y_D^2 + \frac{|\lambda_{\bar{f}}|^{-2} - 1}{4} x_D^2 \right) (\Gamma_D t)^2 \right], \quad (8.159)$$

with $\Gamma_D = (\Gamma_1 + \Gamma_2)/2$. Δm_D and $\Delta\Gamma_D$ are very small, because they are GIM-suppressed by a factor of m_s^2/M_W^2 . For this reason they are also difficult to calculate, because at scales of order m_s non-perturbative effects become important. A recent calculation, which incorporates non-perturbative effects with the help of the quark condensate, can be found in [54].

8.3.10 New Physics Effects in Meson Mixing[†]

The existence of new physics may modify the low-energy effective Hamiltonian governing B and D physics in several ways: (i) via contributions to the Wilson coefficients of the Standard Model operators, (ii) by generating new operators, or (iii) through the presence of new CP violating phases. These effects may originate from new interactions in tree-level meson decays or from the virtual exchange of new physics in loop-mediated processes. The

[†] Author: JoAnne Hewett

scale of new physics is expected to be large compared to M_W , and hence it is generally anticipated that additional tree-level contributions to meson decays are suppressed [65]. However, large new contributions may be present in loop processes, making meson mixing a fertile ground to reveal the influence of new interactions. All three above classes of new physics contributions may play a role in meson mixing. Such effects may be discovered in observables which are suppressed in the Standard Model, such as the asymmetry a_{fs}^q measuring CP violation in $B_{d,s}$ mixing or in D^0 meson mixing, they may modify the mixing-induced CP asymmetries in $B \rightarrow \psi K_S$ and $B \rightarrow \pi\pi$ decays, or they may alter the precisely calculated SM value of the ratio of B_s to B_d mixing. We will discuss each of these observables in this section. The effects of new physics on meson width differences is described in Sect. 8.3.2.2.

8.3.10.1 B_d Mixing

It is well-known that new physics can play a large role in B_d mixing. One important consequence of this is that the constraints in the $\rho - \eta$ plane from Δm_d can be altered, resulting in a significant shift [66] of the allowed region in this plane from its Standard Model range. This in turn modifies the expected values for $\sin 2\beta$ and $\sin 2\alpha$, even if new sources of CP violation are not present. In fact, this comprises the most significant effect from new physics on the CP asymmetries in $B \rightarrow \psi K_S$ and $B \rightarrow \pi\pi$ decays in a large class of models.

A model independent determination of such effects has been presented in Ref. [67]. New physics contributions to B_d mixing can be parameterized in a model independent fashion by considering the ratio

$$\frac{\langle B_d^0 | \mathcal{H}^{\text{full}} | \bar{B}_d^0 \rangle}{\langle B_d^0 | \mathcal{H}^{\text{SM}} | \bar{B}_d^0 \rangle} = \left(r_d e^{i\theta_d} \right)^2, \quad (8.160)$$

where $\mathcal{H}^{\text{full(SM)}}$ represents the Hamiltonian responsible for B_d mixing in the case of the Standard Model plus new physics (just Standard Model), and $r_d(\theta_d)$ represents the new physics contribution to the magnitude (phase) of B_d mixing. In the Standard Model, the unitarity triangle is constrained by measurements of $\sin 2\beta$, $\sin 2\alpha$, the ratio of semileptonic decays $\Gamma(b \rightarrow u\ell\nu)/\Gamma(b \rightarrow c\ell\nu)$, and $x_d = C_t R_t^2$, where R_t is defined in Section 8.3.1. These quantities are then modified in the presence of new interactions via $a_{\psi K_S} = \sin(2\beta + 2\theta_d)$, $a_{\pi\pi} = \sin(2\alpha - 2\theta_d)$, and $x_d = C_t R_t^2 r_d^2$. Note that the new phase contributions in $a_{\psi K_S}$ and $a_{\pi\pi}$ conspire to cancel in the triangle constraint and the relation $\alpha + \beta + \gamma = \pi$ is retained. Measurement of these four quantities allows one to disentangle the new physics effects and fully reconstruct the true unitarity triangle (*i.e.*, find the true values of α , β , and R_t) as well as determine the values of r_d and θ_d in a geometrical fashion. This is depicted in Fig. 8.5. While this technique is effective in principle, in practice it is limited by theoretical uncertainties in x_d , α , and the ratio of semileptonic decays, as well as discrete ambiguities.

Model independent bounds on new physics contributions to B_d mixing can also be directly placed from measurements of Δm_d and $\sin 2\beta$. In the class of models which respect 3×3 CKM unitarity, where tree-level B decays (in particular their phase) are dominated

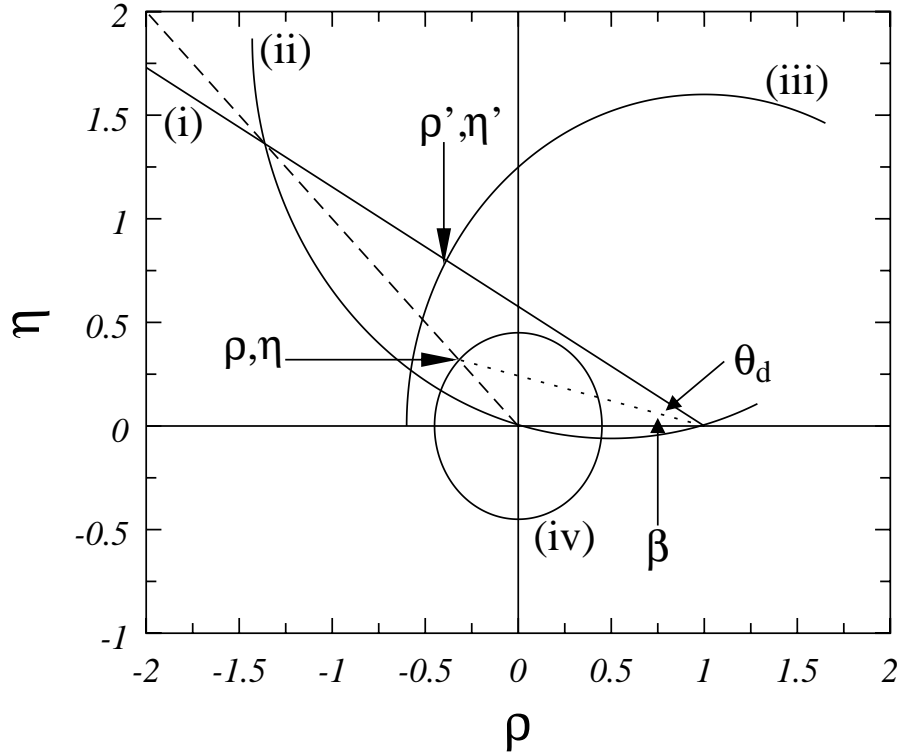


Figure 8.5: The model independent analysis in the $\rho - \eta$ plane: (i) the $a_{\psi K_S}$ ray, (ii) the $a_{\pi\pi}$ circle, (iii) the x_d circle, (iv) the semileptonic decay ratio circle. The γ ray is given by the dashed line and the true β ray corresponds to the dotted line. The true vertex of the unitarity triangle is at (ρ, η) , while the point (ρ', η') serves to determine r_d and θ_d .

by the SM, and where $\Gamma_{12} \simeq \Gamma_{12}^{\text{SM}}$, the new physics effects in B_d mixing can be isolated. The modification to M_{12} can then be described as above in terms of r_d, θ_d . The direct determination of Δm_d provides a bound on the magnitude of new physics contributions, r_d , while measurement of $\sin 2\beta$ constrains the new phase θ_d . Taking into account the uncertainties on the values of the relevant CKM factors and the hadronic matrix elements, present data constrains $0.5 \leq r_d \leq 1.8$ and $\sin 2\theta_d \geq -0.53$ at 95% C.L. It is clear that large contributions to B_d mixing from new interactions are still allowed, and may hence admit for an exciting discovery as future measurements improve.

We note that another useful parameterization of new physics contributions which is common in the literature is given by

$$M_{12}^{\text{NP}} = h e^{i\sigma} M_{12}^{\text{SM}}, \quad (8.161)$$

where these variables are related to the previous ones via

$$r_d^2 e^{2i\theta_d} = 1 + h e^{i\sigma}. \quad (8.162)$$

Constraints on this set of parameters from current data is presented in [68] in various classes of models.

These parameters can be related to new physics contributions in other observables. For instance, the CP asymmetry in flavor-specific B_d decays (see Sect. 8.3.3), which is given by

$$a_{\text{fs}}^d = \text{Im} \frac{\Gamma_{12}^d}{M_{12}^d}, \quad (8.163)$$

and has a value of -8×10^{-4} in the Standard Model (see (8.138)), provides a good opportunity to probe the existence of new interactions. Since Γ_{12}^d/M_{12}^d is essentially real in the Standard Model, the contributions of new interactions to the flavor-specific CP asymmetry can be written as

$$a_{\text{fs}}^d = - \left(\frac{\Gamma_{12}^d}{M_{12}^d} \right)_{\text{SM}} \frac{\sin 2\theta_d}{r_d^2}. \quad (8.164)$$

The above bounds from present data on the new physics contributions to B_d mixing restrict

$$-2.1 \leq \frac{a_{\text{fs}}^d}{(\Gamma_{12}^d/M_{12}^d)_{\text{SM}}} \leq 4.0. \quad (8.165)$$

It is important to note that a_{fs}^d can lie outside this range, if new new physics enhances Γ_{12}^d , which is composed of CKM-suppressed decay modes.

There are a plethora of new physics scenarios which can yield substantial contributions to B_d mixing; some examples are briefly cataloged here. Models which respect the structure of the 3×3 CKM matrix contribute simply to the Wilson coefficient of the Standard Model operator. This is best illustrated by the virtual exchange in the box diagram of charged Higgs bosons which are present in flavor conserving two-Higgs-doublet models [69] and by the contributions of supersymmetric particles [70] when a Standard Model-like super-CKM structure is assumed. If the super-CKM angles (\tilde{V}) are allowed to be arbitrary, the structure of the Wilson coefficients are altered. In this case, the supersymmetric amplitude relative to that of the Standard Model is roughly given by $\sim (M_W/\tilde{m})^n (\tilde{V}_{td}\tilde{V}_{tb}/V_{td}V_{tb})$ and can constitute a flavor problem for Supersymmetry if the sparticle masses, \tilde{m} , are near the weak scale. The existence of a fourth generation would also modify the CKM structure of the Wilson coefficients. New $|\Delta B| = 2$ operators are generated in scenarios [71] such as Left-Right Symmetric models, theories of strong dynamics, as well as in Supersymmetry. Tree-level contributions [72] are manifest in flavor changing two-Higgs-doublet models, in scenarios with a flavor changing extra neutral gauge boson, and in Supersymmetry with R-parity violation. Most of these examples also contain new phases which may be present in B_d mixing. It is interesting to note that various forms of Supersymmetry may affect B_d mixing in all possible manners!

While it is possible to obtain large effects in B_d mixing in all of these scenarios, it is difficult to use Δm_d at present to tightly restrict these contributions and constrain the parameter space in the models, due to the current sizable errors on the Standard Model theoretical prediction arising from the imprecisely determined values of the CKM factors and the hadronic matrix elements. Frequently, other flavor changing neutral current processes, such as $b \rightarrow s\gamma$, provide more stringent constraints.

8.3.10.2 B_s Mixing

A similar analysis as employed above may be used to constrain new physics contributions to B_s mixing. In the class of models which respect the 3×3 CKM unitarity and where tree-level decays are dominated by the Standard Model contributions, we can again parameterize potential new contributions to Δm_s via $M_{12} = (r_s e^{i\theta_s})^2 M_{12}^{\text{SM}}$. This gives

$$\frac{\Delta m_d}{\Delta m_s} = \frac{\lambda^2 R_t^2}{\xi^2} \frac{m_{B_d}}{m_{B_s}} \frac{r_d^2}{r_s^2}, \quad (8.166)$$

which reduces to the Standard Model expression when $r_d = r_s$. The parameter θ_s can be constrained once CP asymmetries in the B_s system are measured or, if θ_s is large, from measurements of $\Delta\Gamma_s$ as described in Sect. 8.3.2.2.

As discussed above, the ratio $\Delta m_d/\Delta m_s$ yields a good determination of the CKM ratio $|V_{td}/V_{ts}|$ within the Standard Model, since the ratio of hadronic matrix elements is accurately calculated in lattice gauge theory. Remarkably, this remains true in many scenarios beyond the Standard Model. In a large class of models which retain the 3×3 CKM structure, the virtual exchange of new particles in the box diagram alters the Inami-Lim function, but not the remaining factors in the expression for $\Delta m_{d,s}$. The effects of new physics thus cancel in the ratio. As an explicit example, consider charged Higgs exchange in the box diagram within the context of two-Higgs-doublet models. The expression for the mass difference in B_s mixing in this case is

$$\begin{aligned} \Delta m_s &= \frac{G_F^2 M_W^2}{6\pi^2} f_{B_s}^2 B_{B_s} \eta_{B_s} m_{B_s} |V_{tb} V_{ts}^*|^2 \left[S(m_t^2/M_W^2) + F(m_t^2/m_{H^\pm}^2, \tan \beta) \right] \\ &= \Delta m_d \xi^2 \frac{m_{B_s}}{m_{B_d}} \frac{|V_{ts}|^2}{|V_{td}|^2}, \end{aligned} \quad (8.167)$$

where m_{H^\pm} represents the charge Higgs mass and $\tan \beta$ is the ratio of vevs. Here, we see that the charged Higgs contribution is the same for B_d and B_s mixing (neglecting d - and s -quark masses) and thus cancels exactly in the ratio. This cancellation also occurs in several other classes of models, including minimal Supersymmetry with flavor conservation. Notable exceptions to this are found in models which (i) change the structure of the CKM matrix, such as the addition of a fourth generation, or extra singlet quarks, or in Left-Right symmetric models, (ii) have sizable Yukawa couplings to the light fermions, such as leptoquarks or Higgs models with flavor changing couplings, or (iii) have generational dependent couplings, including supersymmetry with R-parity violation.

8.3.10.3 Mixing in the Charm Sector

The short distance Standard Model contribution to Δm_D proceeds through a W box diagram with internal d, s, b -quarks. In this case the external momentum, which is of order m_c , is communicated to the light quarks in the loop and can not be neglected. The effective Hamiltonian is

$$\mathcal{H}_{eff}^{\Delta c=2} = \frac{G_F \alpha}{8\sqrt{2}x_w} \left[|V_{cs} V_{us}^*|^2 (I_1^s \mathcal{O} - m_c^2 I_2^s \mathcal{O}') + |V_{cb}^* V_{ub}|^2 (I_3^b \mathcal{O} - m_c^2 I_4^b \mathcal{O}') \right], \quad (8.168)$$

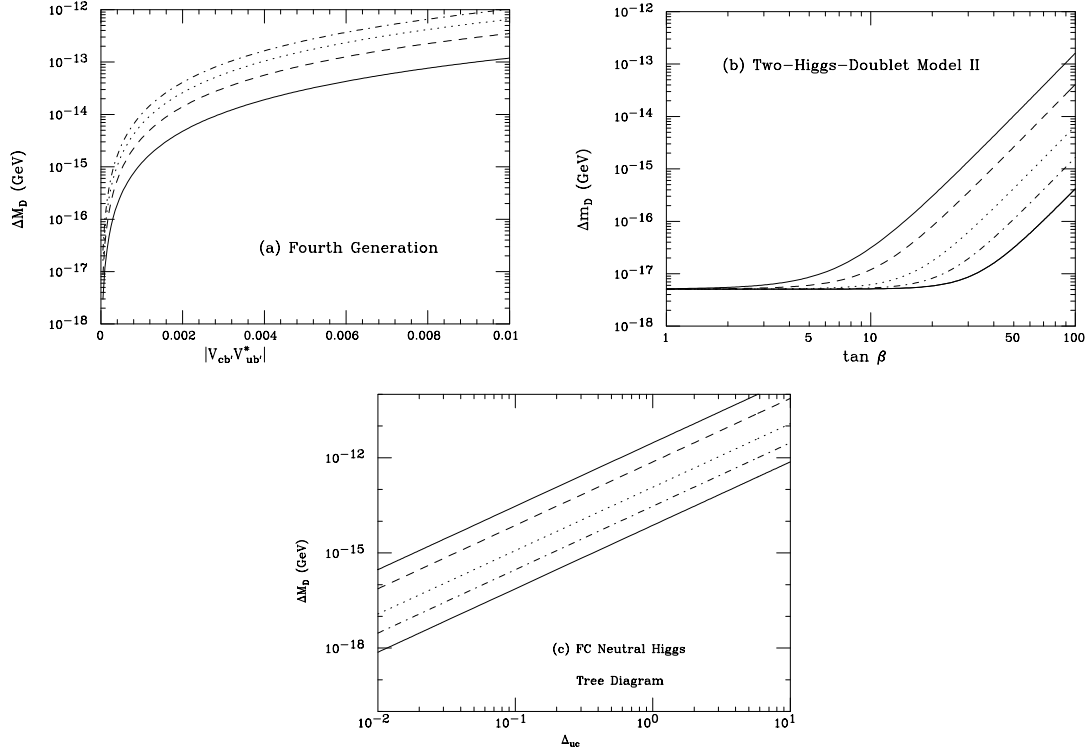


Figure 8.6: Δm_D in (a) the four generation Standard Model as a function of the appropriate 4×4 CKM elements, taking the b' -quark mass to be 100, 200, 300, 400 GeV from top to bottom, (b) the two-Higgs-doublet model II as a function of $\tan \beta = v_2/v_1$ with $m_{H^\pm} = 50, 100, 250, 500, 1000$ GeV from top to bottom, and (c) the flavor-changing Higgs model with tree-level contributions as a function of the mixing factor, with $m_{h^0} = 50, 100, 250, 500, 1000$ GeV from top to bottom.

where the I_j^q represent integrals [73] that are functions of m_q^2/M_W^2 and m_q^2/m_c^2 , and $\mathcal{O} = [\bar{u}\gamma_\mu(1-\gamma_5)c]^2$ is the usual mixing operator, while $\mathcal{O}' = [\bar{u}\gamma_\mu(1+\gamma_5)c]^2$ arises in the case of non-vanishing external momentum. The numerical value of the short distance contribution is $\Delta m_D \sim 5 \times 10^{-18}$ GeV (taking $f_D = 200$ MeV). The long distance contributions have been computed via an intermediate state dispersive approach and in heavy quark effective theory, yielding values [74] in the range $\Delta m_D \sim 10^{-17} - 10^{-16}$ GeV. The Standard Model predictions are clearly quite small and allow for a large window for the observation of new physics effects.

Since the Standard Model expectation is so small, large enhancements in Δm_D are naturally induced by new interactions. A compilation of such effects in various models and list of references can be found in [75]. This article shows that the present experimental bound on D -mixing already constrains the parameter space in many scenarios, and an order of magnitude improvement would exclude (or discover) some models. Here, for purposes of illustration, we present the potential enhancements that can occur in three scenarios [66]. We examine (i) the case of a fourth generation to demonstrate the effect of heavy fermions participating in the box diagram, (ii) the contributions from charged Higgs exchange in flavor conserving two-Higgs-doublet models, which is often used as a benchmark in studying

new physics, and (iii) the tree-level contributions in flavor-changing Higgs models, where the flavor changing couplings are taken to be $\lambda_{h^0 f_i f_j} \sim (\sqrt{2}G_F)^{1/2} \sqrt{m_i m_j} \Delta_{ij}$ with Δ_{ij} being a combination of mixing angles. The mass difference as a function of the model parameters is shown in Fig. 8.6 for each case. We see that in each case the parameter space is already restricted by the current experimental value, and that an improvement in the bound would provide a sensitive probe of these models.

8.4 Interesting decay modes[†]

In this section we list the decay modes which are useful for the determination of Δm_q , $\Delta \Gamma_q$ and B meson lifetimes. Flavor-specific decay modes are summarized in Table 8.4, CKM-favored decays into CP eigenstates are listed in Table 8.5 and decays which are neither flavor-specific nor CP -specific can be found in Table 8.6.

quark decay	hadronic decay	remarks
$\bar{b} \rightarrow \bar{c} \ell^+ \nu_\ell$	$B_{d,s} \rightarrow D_{(s)}^- \ell^+ \nu_\ell$ $B_{d,s} \rightarrow X \ell^+ \nu_\ell$	
$\bar{b} \rightarrow \bar{c} u d$	$B_d \rightarrow D^{(*)-} \pi^+$ $B_d \rightarrow D^{(*)-} \pi^+ \pi^+ \pi^-$ $B_d \rightarrow D^{*-} \pi^+ \pi^+ \pi^- \pi^0$ $B_d \rightarrow \bar{D}^{(*)0} \rho^0$ [$\rightarrow K^+ \pi^-$ or $K^+ \pi^+ \pi^- \pi^-$ or $K^{(*)+} \ell^- \bar{\nu}_\ell$ etc.] $B_s \rightarrow D_s^{(*)-} \pi^+$ $B_s \rightarrow D_s^{(*)-} \pi^+ \pi^+ \pi^-$ $B_s \rightarrow D_s^{*-} \pi^+ \pi^+ \pi^- \pi^0$ $B_s \rightarrow \bar{D}^{(*)0} K_S$ [$\rightarrow K^+ \pi^-$ or $K^+ \pi^+ \pi^- \pi^-$ or $K^{(*)+} \ell^- \bar{\nu}_\ell$ etc.]	$\text{BR}(\rho^0 \rightarrow \pi^+ \pi^-) \approx 100\%$. The $\bar{D}^{(*)0}$ must be detected in a final state f such that $D^{(*)0} \rightarrow f$ is forbidden or suppressed.
$\bar{b} \rightarrow \bar{c} c \bar{s}$	$B_d \rightarrow \psi K^+ \pi^-$ $B_d \rightarrow D^{(*)+} D_s^{(*)-}$	mainly $B_d \rightarrow \psi K^{(*)}$ [$\rightarrow K^+ \pi^-$]
$\bar{b} \rightarrow \bar{c} d \bar{d}$	$B_s \rightarrow \psi K^- \pi^+$ $B_s \rightarrow D_s^{(*)-} D^{(*)+}$	mainly $B_s \rightarrow \psi \bar{K}^{(*)}$ [$\rightarrow K^- \pi^+$]
$\bar{b} \rightarrow \bar{c} X$	$B_d \rightarrow D^{(*)-} X$	small contamination from $\bar{b} \rightarrow \bar{c} d \bar{d}$

Table 8.4: Interesting flavor-specific decays.

[†] Author: Ulrich Nierste

quark decay	hadronic decay	remarks
$\bar{b} \rightarrow \bar{c}u\bar{d}$	$B_d \rightarrow \bar{D}^{(*)0} \rho^0 [\rightarrow \rho_0 K_S \text{ or } K\bar{K} \text{ or } \pi^+\pi^-]$	The $\bar{D}^{(*)0}$ must be detected in a CP -specific final state f (hence $D^{(*)0} \rightarrow f$ is equally allowed).
	$B_d \rightarrow \bar{D}^{(*)0} \pi^+\pi^- [\rightarrow \rho_0 K_S \text{ or } K\bar{K} \text{ or } \pi^+\pi^-]$	This decay mode has color-unsuppressed contributions.
	$B_s \rightarrow \bar{D}^{(*)0} K_S [\rightarrow \rho_0 K_S \text{ or } K\bar{K} \text{ or } \pi^+\pi^-]$	
$\bar{b} \rightarrow \bar{c}c\bar{s}$	$B_d \rightarrow \psi K_S$	The \bar{B}_d can decay into the same final state $K_S \rho^0$. Angular analysis separates CP -eigenstates.
	$B_d \rightarrow \psi K_S \rho^0$	
	$B_d \rightarrow \psi \phi K_S \text{ or } \psi K_S \rho^0$	Angular analysis required.
	$B_d \rightarrow \psi \phi K^* [\rightarrow K_S \pi^0]$	Angular analysis required, π^0 is problematic.
	$B_d \rightarrow D_s^{(*)+} D_s^{(*)-} K_S$	Angular analysis required.
	$B_s \rightarrow \psi \phi$	Angular analysis required.
	$B_s \rightarrow \psi K\bar{K} \text{ or } \psi K^* \bar{K}^*$	Same remark
	$B_s \rightarrow \psi \phi \phi$	Same remark.
	$B_s \rightarrow \psi \eta$	
	$B_s \rightarrow \psi \eta'$	
	$B_s \rightarrow D_s^+ D_s^-$	Angular analysis required.
	$B_s \rightarrow D_s^{*+} D_s^{*-}$	Non-spectator decays.
	$B_s \rightarrow D^{(*)+} D^{(*)-} \text{ or } D^{(*)0} \bar{D}^{(*)0}$	CP -odd final state.
	$B_s \rightarrow \psi f_0$	CP -odd final state.
	$B_s \rightarrow \chi_{c0} \phi$	
$\bar{b} \rightarrow \bar{c}cd$	$B_d \rightarrow D^+ D^-$	CP -even final state.
	$B_d \rightarrow D^{*+} D^{*-}$	
	$B_d \rightarrow \psi \rho^0$	
	$B_s \rightarrow \psi K_S$	
	$B_s \rightarrow \psi K_S \pi^0$	
		Mainly $B_s \rightarrow \psi \bar{K}^{(*)} [\rightarrow K_S \pi^0]$.

Table 8.5: Interesting CKM-favored decays into CP -eigenstates.

quark decay	hadronic decay	remarks
$\bar{b} \rightarrow \bar{c}c\bar{s}$	$B_s \rightarrow \psi K\bar{K}^*$ combined with $\psi K^* \bar{K}$	angular analysis plus analysis analogous to $B_s \rightarrow D_s^\pm K^\mp$ required.

Table 8.6: Interesting CKM-favored decays into CP non-eigenstates accessible to B and \bar{B} .

8.5 Introduction and Physics Input for CDF

This section summarizes technical issues and physics inputs that are relevant to mixing and lifetime measurements at CDF. The CDF detector improvements that are critical for these measurements are the following :

1. The Level-1 and Level-2 trigger systems have been upgraded to allow triggers on high momentum tracks at Level-1, using the central drift chamber (“XFT”), and on large impact parameter tracks at Level-2, using the silicon vertex detector (“SVT”). This in turn allows CDF to trigger on all-hadronic decays of b hadrons, such as $B_s \rightarrow D_s \pi$. Extensive simulations, together with run I data, have been used to estimate trigger rates and event yields for the analyses discussed below.
2. The silicon vertex detector has been upgraded for improved silicon tracking and extended fiducial coverage. This upgrade is most relevant to analyses which depend critically on vertex position resolution, in particular the measurement of B_s mixing.
3. The CDF muon system has been upgraded to allow extended fiducial coverage and lower trigger thresholds. The increase of the fiducial volume is treated as a simple scale factor for all analyses using muons; the change in trigger threshold applies to the analysis of central di-muons only.

The basic information needed to make projections for Tevatron Run II is the event yield for the b hadron decay channels in question. Projections are relatively simple for channels obtained from lepton triggers using extrapolations from the Run I data. An example of this scaling is given in 6.2.2. The projections for channels which are triggered by the newly implemented displaced track trigger system, often referred to as the hadronic trigger, are more difficult and are based primarily on simulations.

The CDF trigger system is organized in three levels of which only the first two are simulated for the following studies, since the third level should not reject good signal events. In addition to the trigger simulation, physics inputs are needed for the total B cross sections and production and branching fractions. Both the physics inputs and the description of the trigger simulation are given below. Some of the issues are already partially covered in the CP violation chapter in Section 6.2.2. Here the emphasis is mostly on the hadronic trigger.

8.5.1 Physics Input

The Monte Carlo program Bgenerator [76] is used to generate b hadrons; it parameterizes the p_T and y distributions for b quarks according to next-to-leading-order calculations [77]. The b quarks are fragmented into b hadrons using the Peterson [78] function with a fragmentation parameter value of $\epsilon_b = 0.006$. The CLEO Monte Carlo Program QQ [79] is used to decay the b hadrons. Events generated with Bgenerator contain particles only from the decay of the b hadrons, and do not include particles produced in the b quark fragmentation or the underlying event from the $p\bar{p}$ collision.

Quantity	Value	Reference
$B(D_s^+ \rightarrow \phi\pi^+)$	$(3.6 \pm 0.9) \times 10^{-2}$	[82]
$B(D_s^+ \rightarrow K^+\bar{K}^{*0})$	$(3.3 \pm 0.9) \times 10^{-2}$	[82]
$B(D_s^+ \rightarrow \pi^+\pi^+\pi^-)$	$(1.0 \pm 0.4) \times 10^{-2}$	[82]
$B(D^0 \rightarrow K^-\pi^+)$	$(3.85 \pm 0.09) \times 10^{-2}$	[82]
$B(D^0 \rightarrow K^-\pi^+\pi^+\pi^-)$	$(7.6 \pm 0.4) \times 10^{-2}$	[82]
$B(\Lambda_c^+ \rightarrow pK^-\pi^+)$	$(5.0 \pm 1.3) \times 10^{-2}$	[82]
$B(\Lambda_c^+ \rightarrow \Lambda\pi^+\pi^-\pi^+)$	$(3.3 \pm 1.0) \times 10^{-2}$	[82]
$B(\Lambda \rightarrow p\pi^-)$	$(63.9 \pm 0.5) \times 10^{-2}$	[82]
$B(\phi(1020) \rightarrow K^+K^-)$	$(49.1 \pm 0.8) \times 10^{-2}$	[82]
$B(K^*(892) \rightarrow K\pi)$	1	[82]
f_{Λ_b}	$(0.116 \pm 0.020) \times 10^{-2}$	[82]
$f_s/(f_u + f_d)$	$(0.213 \pm 0.038) \times 10^{-2}$	[81]
$\sigma_B^0(p_T(B^0) > 6 \text{ GeV}; y < 1)$	$(3.52 \pm 0.61)\mu b$	[80]

Table 8.7: Physics input used for event yield estimates.

Quantity	Value	Reference
$B(B_s \rightarrow D_s\pi)$	$(3.0 \pm 0.4) \times 10^{-3}$	from B^0 [82]
$B(B_s \rightarrow D_s\pi\pi\pi)$	$(8.0 \pm 2.5) \times 10^{-3}$	from B^0 [82]
$B(B_s \rightarrow D_sD_s)$	$(8.0 \pm 3.0) \times 10^{-3}$	from B^0 [82]
$B(B_s \rightarrow D_s^*D_s)$	$(2.0 \pm 0.6) \times 10^{-2}$	from B^0 [82]
$B(B_s \rightarrow D_s^*D_s^*)$	$(2.0 \pm 0.7) \times 10^{-2}$	from B^0 [82]

Table 8.8: Branching fraction estimates for B_s decays.

The overall production cross section is normalized using the CDF measurement for B^0 production with $p_T > 6 \text{ GeV}$, $|y| < 1$ [80]. The B_s and Λ_b production fractions in $p\bar{p}$ collisions are based on the CDF measurement of $f_s/(f_u + f_d)$ [81] and the world average value for f_{Λ_b} , respectively. Assuming the b hadron production spectra follow the distributions from [77], and using the CDF measurement from Reference [80], a total production cross section for B^0 mesons of $50.1 \mu b$ is obtained. Table 8.7 lists the measured rates and production fractions assumed in the CDF analyses, together with the relevant hadronic decay branching fractions that are known. In addition, we have estimated the branching fractions for b -hadron decays that have not been measured directly, using various symmetry assumptions as described below.

Branching Fraction Estimates Since many of the hadronic decay channels have so far not been measured or even observed, certain branching ratios have to be estimated. This is relatively simple for B_s decays, using related B^0 decay modes. These estimates are summarized in Table 8.8. The related uncertainties should be small, on the order of roughly 10% in the form factors or 20% in the event yields.

For Λ_b baryons the situation is more complicated. Several patterns arise when comparing bottom and charm branching fractions, as well as meson and baryon branching fractions.

The most important is the fact that the branching fractions of B mesons are often quite small compared to those of the corresponding D decays. For instance

$$\begin{aligned}\mathcal{B}(B^0 \rightarrow D^- \pi^+) &= (3.0 \pm 0.4) \times 10^{-3}, \\ \mathcal{B}(D^0 \rightarrow K^- \pi^+) &= (3.83 \pm 0.09) \times 10^{-2}.\end{aligned}\tag{8.169}$$

Comparing the two gives a B to D ratio of 0.08. One might suppose, neglecting that $c \rightarrow s$ involves a light quark, that the widths of these modes would be similar, but the total widths reflected in the mean lifetimes are different. Moreover, the b sector involves considerably more decay channels. The semileptonic decays, however, remain qualitatively different, and do not scale in the same way.

A similar pattern for the hadronic decay modes may reasonably be expected for baryons. Indeed, in the one hadronic branching fraction measured for the Λ_b , we have:

$$\begin{aligned}\mathcal{B}(\Lambda_b \rightarrow J/\psi \Lambda) &= (4.7 \pm 2.8) \times 10^{-4}, \\ \mathcal{B}(\Lambda_c^+ \rightarrow p K^{*0}) &= (1.6 \pm 0.5) \times 10^{-2}, \\ \mathcal{B}(\Lambda_c^+ \rightarrow p \phi) &= (1.2 \pm 0.5) \times 10^{-3}.\end{aligned}\tag{8.170}$$

In comparing the Λ_c^+ branching fraction to the Λ_b branching fraction, it is assumed that virtual $W^- \rightarrow \bar{c}s$ occurs about as frequently as $W^- \rightarrow \bar{u}d$. The Λ_b to Λ_c^+ ratio is about 0.03 when comparing to $\Lambda_c^+ \rightarrow p K^{*0}$. A similar comparison can be made with the second Λ_c^+ decay mode, which, aside from the $|V_{us}/V_{ud}|^2$ factor, is most similar to $\Lambda_b \rightarrow J/\psi \Lambda$; the ratio is about 0.02. However, since applying this factor to a color-suppressed mode is problematic, the first ratio is preferred

$$g_{bc} = 0.03\tag{8.171}$$

to multiply Λ_c^+ hadronic branching fractions to obtain estimates of corresponding Λ_b fractions.

Another difference between charm and bottom decays is that the bottom hadrons can avail themselves of the virtual $W^- \rightarrow \bar{c}s$ transition which is disallowed for charm decays. The ratio of branching fractions for an external $W^- \rightarrow \bar{c}s$ to $W^- \rightarrow \bar{u}d$ is similar to the ratio of the square of the decay constants

$$g_{D_s}^2 = \left(\frac{f_{D_s^+}}{f_{\pi^+}} \right)^2 = \left(\frac{280 \text{ MeV}}{130.7 \text{ MeV}} \right)^2 = 4.58,\tag{8.172}$$

the effect of which is seen in comparing branching fractions of $B^0 \rightarrow D^- D_s^+$ and $D^- \pi^+$, with the usual caveats.

Adding a $\pi^+ \pi^-$ to the final state of a decay mode tends to result in a larger branching fraction. This effect is observed in the mesons, but the ratio calculated among Λ_c^+ modes is preferred because of the different baryon structure:

$$g_{\pi\pi} = \frac{\mathcal{B}(\Lambda_c^+ \rightarrow \Lambda \pi^+ \pi^+ \pi^-)}{\mathcal{B}(\Lambda_c^+ \rightarrow \Lambda \pi^+)} = \frac{3.3}{0.9} = 3.7.\tag{8.173}$$

Λ_b decay	Λ_c decay	$\mathcal{B}(\Lambda_c^+)$	estimate	$\mathcal{B}(\Lambda_b)$ estimate
$\Lambda_c^+ \pi^-$	$\Lambda \pi^+$	$b_1 = (9.0 \pm 2.8) \times 10^{-3}$	$b_1 g_{bc}$	2.6×10^{-4}
$\Lambda_c^+ \pi^- \pi^+ \pi^-$	$\Lambda \pi^+ \pi^- \pi^+$	$b_2 = (3.3 \pm 1.0) \times 10^{-2}$	$b_2 g_{bc}$	9.7×10^{-4}
$p D^0 \pi^-$ (nr)	$p K^- \pi^+$ (nr)	$b_3 = (2.8 \pm 0.8) \times 10^{-2}$	$b_3 g_{bc}$	8.2×10^{-4}
$p K^-$			$b_1 g_{bc} g_{bu} g_{\pi K}$	8.1×10^{-6}
$p \pi^-$			$b_1 g_{bc} g_{bu}$	2.0×10^{-6}
$p \pi^- \pi^+ \pi^-$			$b_2 g_{bc} g_{bu}$	7.4×10^{-6}

Table 8.9: Branching ratio estimates for Λ_b decays using scale factors described in the text.

Another factor is used to estimate the branching fractions where the external W yields a D_s^{*+} rather than a D_s^+ . Here the B^0 branching fractions are used

$$g_* = \frac{\mathcal{B}(B^0 \rightarrow D^{(*)-} D_s^{*+})}{\mathcal{B}(B^0 \rightarrow D^{(*)-} D_s^+)} = \frac{1.0 + 2.0}{0.80 + 0.96} = 1.7. \quad (8.174)$$

A similar factor is obtained when comparing analogous decays with ρ^+ and π^+ final states of B^0 decays. Decay modes such as $\Lambda_c^+ \rightarrow \Lambda \rho^+$ have not been observed.

Once certain $b \rightarrow c$ branching fractions have been estimated, they are scaled by

$$g_{bu} = |V_{ub}/V_{cb}|^2 \sim 0.0077 \quad (8.175)$$

to obtain estimates for corresponding $b \rightarrow u$ transitions. Finally, the recently measured branching fractions

$$\begin{aligned} \mathcal{B}(B^0 \rightarrow \pi^+ \pi^-) &= (4.3 \pm 1.6) \times 10^{-6}, \\ \mathcal{B}(B^0 \rightarrow K^+ \pi^-) &= (17.2 \pm 2.8) \times 10^{-6}, \end{aligned} \quad (8.176)$$

are used to estimate $\Lambda_b \rightarrow p K^-$ from $\Lambda_b \rightarrow p \pi^-$:

$$g_{\pi K} = \frac{17.2}{4.3} = 4. \quad (8.177)$$

The resulting branching ratio estimates for the different Λ_b decay modes are summarized in Table 8.9.

8.5.2 Detector Simulation

Hadronic Trigger Only The Level-1 track trigger is based on a set of kinematic cuts originally developed for two-body decays of neutral B mesons. The Level-1 triggering algorithm is therefore based on pairs of XFT trigger tracks. To reduce the background of inelastic collisions relative to B hadron production, only track pairs in which both tracks have transverse momentum p_T greater than a specified value are considered. Because of the time that would be spent on combinatorics, an event with more than six such tracks passes Level-1 automatically. For real B^0 and B_s^0 decays of interest, the two highest p_T tracks are correlated in angle and generally have opposite charge; consequently, the Level-1 requirements are chosen as follows:

B_s decay	ϵ_{L1}	ϵ_{L2Bs}	ϵ_{L2Bd}	ϵ_{L2Tot}	ϵ_{fid}	N_{RunII}
$B_s \rightarrow D_s \pi$	0.025	0.0045	0.0029	0.0050	0.0027	36900
$B_s \rightarrow D_s \pi \pi \pi$	0.018	0.0032	0.0018	0.0033	0.0011	38300
$B_s \rightarrow D_s D_s$	0.019	0.0035	0.0015	0.0037	0.0014	2500
$B_s \rightarrow D_s^* D_s$	0.016	0.0031	0.0011	0.0032	0.0013	5700
$B_s \rightarrow D_s^* D_s^*$	0.014	0.0030	0.0011	0.0031	0.0012	5200

Table 8.10: Event yields for hadronic B_s decays relevant for CP violation and $\Delta\Gamma_s$ measurements. Only the feasible D_s decays to $\phi\pi$, K^*K and $\pi\pi\pi$ are considered.

Λ_b (sub)decay	ϵ_{L1}	ϵ_{L2Bs}	ϵ_{L2Bd}	ϵ_{L2Tot}	ϵ_{fid}	N_{RunII}
$\Lambda_b \rightarrow \Lambda_c^+ \pi^- (\Lambda_c^+ \rightarrow p K^- \pi^+)$	0.026	0.0040	0.0029	0.0045	0.0031	2400
$\Lambda_b \rightarrow \Lambda_c^+ \pi^- \pi^+ \pi^- (\Lambda_c^+ \rightarrow p K^- \pi^+)$	0.017	0.0024	0.0014	0.0026	0.0012	3400
$\Lambda_b \rightarrow p D^0 \pi^- (D^0 \rightarrow K^- \pi^+)$	0.029	0.0043	0.0036	0.0048	0.0032	6100
$\Lambda_b \rightarrow p D^0 \pi^- (D^0 \rightarrow K^- \pi^+ \pi^- \pi^+)$	0.020	0.0028	0.0018	0.0030	0.0012	4300
$\Lambda_b \rightarrow p \pi^-$	0.056	0.0054	0.011	0.011	0.011	1300
$\Lambda_b \rightarrow p \pi^- \pi^+ \pi^-$	0.030	0.0041	0.0032	0.0046	0.0030	1300
$\Lambda_b \rightarrow p K^-$	0.056	0.0053	0.011	0.011	0.011	5400

Table 8.11: Event yields for most sizeable hadronic Λ_b decays.

- two tracks having opposite charge
- individual track $p_T > 2.0$ GeV/ c
- $p_T, 1 + p_T, 2 > 5.5$ GeV/ c
- $\delta\phi < 135$ deg

The Level-2 trigger is based on tracking information provided by the SVT [83,84]. One application for the hadronic b trigger is the decay $B^0 \rightarrow \pi^+ \pi^-$, where the two pions give oppositely-charged tracks with high transverse momenta and large impact parameters. The trigger is also used to select other multibody hadronic b decays, but due to the different kinematics of these decays, the Level-2 selection criteria are modified to optimize the efficiencies [84]. An event passes the Level-2 track trigger if it satisfies either option A) or option B)

A) Multi hadronic B trigger

- $120\mu\text{m} < |d_0| < 1\text{mm}$
- $2\text{ deg} < \delta\phi < 90\text{ deg}$
- $p_T \cdot X_v > 0$

B) Hadronic pair trigger

- $100\mu\text{m} < |d_0| < 1\text{mm}$
- $20\text{ deg} < \delta\phi < 135\text{ deg}$
- $p_T \cdot X_v > 0$
- $d_{0,B} < 140\mu\text{m}$

For an event to be useful in offline analysis after it passes the trigger, all the b hadron decay products have to be reconstructible in the detector. The requirement for a b hadron to be considered reconstructible in this simulation is that all its stable, charged daughter particles are within $|\eta| < 1$ and have transverse momenta greater than 400 MeV/ c . These requirements are probably conservative in two ways: first, track reconstruction in

Run II will be possible over a larger η range; stand-alone silicon tracking will probably be possible up to $|\eta| < 2$. Second, the reconstruction efficiency for the COT will be similar to that for the CTC during Run I. The efficiency for track reconstruction in the CTC extended down to $p_T \simeq 200$ MeV/ c and rose over the transverse momentum range $200 \text{ MeV}/c < p_T < 400 \text{ MeV}/c$, reaching about 93% for tracks with $p_T > 400 \text{ MeV}/c$.

Applying the trigger to various B_s and Λ_b decays, we estimate the event yields at the two trigger levels. A summary of these estimates is given in Tables 8.10 and 8.11 for B_s and Λ_b , respectively.

Hadronic Trigger Combined with Lepton Apart from the purely hadronic trigger there is the possibility of using the hadronic trigger in conjunction with the lepton triggers. Therefore, a single lepton requirement is combined with the requirement of a displaced track in the SVT. This trigger option is studied for the semi-inclusive $B_s \rightarrow \nu \ell D_s X$ sample.

The additional requirement of a displaced track allows a lower threshold for the lepton momentum, while keeping the trigger rate at a reasonable level. The trigger cross section for an 8 GeV inclusive electron trigger would need to be prescaled in Run II. However, it is possible to lower the cross section for a 4 GeV electron trigger below 100 nb by adding the displaced track found by SVT with $p_T > 2 \text{ GeV}/c$ and $d_0 > 120 \mu\text{m}$.

Since Run I data are considered to be most reliable for predictions, the signal yield for Run II CDF is obtained by scaling the Run I analysis results with the ratio of the acceptances between Run I and Run II. The acceptance ratio between Run I and Run II is obtained using a Monte Carlo sample of semileptonic B_s decays containing a D_s . The SVT tracking efficiency is assumed to be $\sim 75\%$ per track, or 56% for 2-tracks.

The $\ell + D_s$ sample composition is assumed to be,

- $eD_s : \mu D_s = 50\% : 50\%$
- $B_s \rightarrow \ell \nu D_s^* : \ell \nu D_s^* : \ell \nu D_s^{**} = 2 : 5 : 0$; D_s^{**} usually decays to $D^{0,\pm}$

The E_T and SVT d_0 resolutions are taken to be of $14\%/\sqrt{E_T}$ and $35 \mu\text{m}$, respectively. All tracks (ℓ , K , and π) are required to have $p_T > 400 \text{ MeV}/c$, and to be in the fiducial volume of the tracking detector. The silicon vertex detector coverage is $|z| < 30 \text{ cm}$ in Run I and $|z| < 45 \text{ cm}$ in Run II. The standard analysis Run I cuts are applied to the final state particles, namely $p_T(K) > 1.2 \text{ GeV}/c$, $p_T(\pi) > 0.8 \text{ GeV}/c$, and $3 \text{ GeV}/c^2 < M(\ell D_s) < 5 \text{ GeV}/c^2$.

The event yields for different lepton p_T values are summarized in Table 8.12, which shows signal yields per 2 fb^{-1} . Choosing a value of $3 \text{ GeV}/c$ lepton p_T , roughly 40k semileptonic B_s decay are obtained in 2 fb^{-1} of integrated luminosity.

Rate Estimates – Hadronic Trigger Because the trigger rates depend on the way in which the Tevatron is operated in Run II, different XFT trigger cuts were considered for three different running scenarios. Scenario A corresponds to a luminosity of less than $1 \times 10^{32} \text{ cm}^{-2}\text{s}^{-1}$ with collisions every 396 ns, while scenarios B and C correspond to luminosities of $1 - 2 \times 10^{32} \text{ cm}^{-2}\text{s}^{-1}$ with collisions every 132 ns and 396 ns, respectively.

Trigger	Run II/Run I	$N_{\text{Run II}}$
8 GeV ℓ	1.0	14000
2 GeV ℓ + SVT	5.9	64000
3 GeV ℓ + SVT	4.0	43000
4 GeV ℓ + SVT	2.7	30000
5 GeV ℓ + SVT	1.9	21000

Table 8.12: Event yields corresponding to 2 fb^{-1} for semileptonic B_s decays ($B_s \rightarrow \nu \ell D_s X$) for different lepton p_T trigger thresholds.

	Scenario A	Scenario B	Scenario C
\mathcal{L}	$< 1 \times 10^{32} \text{ cm}^{-1}\text{s}^{-1}$	$1\text{-}2 \times 10^{32} \text{ cm}^{-1}\text{s}^{-1}$	$1\text{-}2 \times 10^{32} \text{ cm}^{-1}\text{s}^{-1}$
BX interval	396 ns	132 ns	396 ns
$p_T^{(1)}, p_T^{(2)}$	$> 2 \text{ GeV}/c$	$> 2.25 \text{ GeV}/c$	$> 2.5 \text{ GeV}/c$
$p_T^{(1)} + p_T^{(2)}$	$> 5.5 \text{ GeV}/c$	$> 6 \text{ GeV}/c$	$> 6.5 \text{ GeV}/c$
$\delta\phi$	$< 135^\circ$	$< 135^\circ$	$< 135^\circ$
cross section	$252 \pm 18 \mu\text{b}$	$152 \pm 14 \mu\text{b}$	$163 \pm 16 \mu\text{b}$

Table 8.13: Level-1 XFT trigger cuts and cross sections for the three Tevatron operating scenarios considered.

The cuts considered for each scenario are listed in Table 8.13 along with the total cross section. These expectations were derived using tracks recorded in Run I with additional hit occupancy close to the beam axis generated using the MBR [85] Monte Carlo program. The trigger cuts provide trigger rates which are compatible with the total Level-1 bandwidth of approximately 50 kHz.

At Level-2, the impact parameter information associated with the tracks is available, and the cuts described above are used to select b hadron decays. The requirements are that the impact parameters of both tracks satisfy $120 \mu\text{m} < |d| < 1 \text{ mm}$, that their point of intersection occurs with a positive decay length, and that their opening angle is further restricted to $\delta\phi < 90^\circ$. The trigger cross sections are reduced to approximately 489, 386 and 283 nb for scenarios A, B and C, respectively, and produce Level-2 trigger rates between 38 Hz and 67 Hz. This is well within the available Level-2 bandwidth of 300 Hz.

For efficiency estimates in the sections below, scenario A has been chosen. When implementing trigger option B the numbers of expected events do not vary significantly compared with the uncertainties quoted above. The trigger scenario C is not likely to be implemented, assuming that the Tevatron will be upgraded to 132 ns bunch spacing.

8.6 Projections for Δm

8.6.1 B_s mixing measurement at CDF[†]

The probability that a B_s meson decays at proper time t in the same state, or has mixed to the \bar{B}_s state is given by

$$\begin{aligned} P_{\text{unmix}}(t) &= \frac{1}{2} (1 + \cos \Delta m_s t) , \\ P_{\text{mix}}(t) &= \frac{1}{2} (1 - \cos \Delta m_s t) , \end{aligned} \quad (8.178)$$

where the mixing frequency, Δm_s , is the mass difference between the heavy and light CP eigenstates.

The canonical B_s mixing analysis, in which oscillations are observed and the mixing frequency, Δm_s , is measured, proceeds as follows. The B_s meson flavor at the time of its decay is determined by reconstructing a flavor specific final state. The proper time, $t = m_{B_s^0} L / pc$, at which the decay occurred is determined by measuring the decay length, L , and the B_s momentum, p . Finally, the production flavor must be tagged in order to classify the event as being mixed or unmixed at the time of its decay. Oscillations manifest in a time dependence of, for example, the mixed asymmetry:

$$A_{\text{mix}}(t) = \frac{N_{\text{mixed}}(t) - N_{\text{unmixed}}(t)}{N_{\text{mixed}}(t) + N_{\text{unmixed}}(t)}. \quad (8.179)$$

In practice, the production flavor will be correctly tagged with a probability \mathcal{P}_{tag} which is significantly smaller than unity. The functional form of the mixed asymmetry follows

$$A_{\text{mix}}(t) = -D \cos \Delta m_s t \quad (8.180)$$

with the dilution, D , related to \mathcal{P}_{tag} by $D = 2\mathcal{P}_{\text{tag}} - 1$. The mixing frequency is determined for example by fitting the measured asymmetry to a function of this form.

So far, B_s oscillations have not been observed experimentally, and the lower limit on x_s is above 15. This means that B_s mesons oscillate much more rapidly than B^0 mesons. The rapidity of the B_s oscillation implies a significant difference in the experimental requirements for the B^0 and B_s analyses. The limiting factor in B^0 mixing analyses is solely the effective tagging efficiency, which is equivalent to the effective statistics. In B_s mixing measurements the resolution of the proper time becomes another very critical issue. To determine the proper time, not only the positions of primary and secondary vertices have to be measured precisely, but also the measurement of the B_s momentum is crucial. Therefore, it is desirable to have fully exclusive final states such as $B_s \rightarrow D_s \pi (D_s \rightarrow \phi \pi, \phi \rightarrow KK)$. Semileptonic B_s decays have the intrinsic disadvantage that the neutrino momentum is undetected.

In Run I CDF reconstructed 220 and 125 B_s semileptonic decay events with fully reconstructed $D_s \rightarrow \phi \pi$ and $D_s \rightarrow K^* K$ channels, respectively, in low p_T ($> 8 \text{ GeV}/c$) inclusive

[†]Authors: M. Jones, Ch. Paus, M. Tanaka.

lepton (e and μ) trigger samples [89]. An additional 600 semileptonic B_s decays were used, reconstructed in the $D_s \rightarrow \phi X + \text{track}$ channel. Those events were part of the dilepton ($\mu\mu$ and $e\mu$) trigger samples, where the second lepton was used for the B flavor tag. The best limit on x_s was given by the dilepton trigger dataset [90].

In Run II much more statistics will be available using the lepton trigger, the lepton trigger plus one secondary vertex track and the all hadronic trigger. From the event yield estimates in Tables 8.12 and 8.10, we expect 40k events in the lepton plus displaced track and 75k events in the all hadronic trigger.

In the following four sections the measurements of B_s mixing using semileptonic or hadronic decays are discussed. Since the flavor tagging and the sensitivity estimates are very similar for the semileptonic and hadronic B_s decay samples, they will be discussed first.

8.6.1.1 Projections for Sensitivity to x_s

The mixing frequency can be determined by calculating, for example, a maximum likelihood function derived from the measured and expected asymmetries and minimizing this function with respect to Δm_s . The significance of an observation of mixing is quantified in terms of the depth of this minimum compared with the second deepest minimum or some asymptotic value at large Δm_s . To a good approximation, the *average* significance is given as

$$\text{Sig}(\Delta m_s) = \sqrt{\frac{N\epsilon D^2}{2}} e^{-(\Delta m_s \sigma_t)^2/2} \sqrt{\frac{S}{S+B}} \quad (8.181)$$

where $N = S$ is the number of reconstructed B_s signal events, S/B is the signal-to-background ratio, ϵ is the efficiency for applying the flavor tag with associated dilution D , and σ_t is the average resolution with which the proper time is measured. This definition is essentially the same as what would be used to define $n\sigma$ confidence intervals for a Gaussian probability density function.

Given estimates for these parameters, the limit of sensitivity is defined as the maximal value of Δm_s for which the significance is above a specified value. The studies described here use the canonical 5 standard deviations to define an unambiguous observation of mixing. In the following sections the estimates for N , ϵD^2 , σ_t and S/B are described.

8.6.1.2 Flavor Tagging Efficiency

In Run II, a Time-of-Flight detector will provide CDF with the ability to distinguish kaons from pions at the 2σ level below a momentum of about 1.6 GeV/ c . This allows two new flavor tags to be implemented which rely on the charge of kaons identified in the event to tag the production flavor of the B_s . As a summary, in Table 8.14 the tagging efficiency for $B_s \rightarrow D_s \pi$ expected for Run II is compared to equivalent numbers obtained in Run I. We compare the standard figure of merit for each tagger, namely ϵD^2 . The two additional kaon taggers are briefly explained below.

Method	Run I – ϵD^2	Run II – ϵD^2
SLT	1.7%	1.7%
JQT	3.0%	3.0%
SST(kaon)	1.0%	4.2%
OSK	—	2.4%
Total	5.7%	11.3%

Table 8.14: Comparison of the various flavor taggers in terms of the ϵD^2 parameter between Run I and expectations for Run II. The most significant differences are the kaon taggers based on the new Time-of-Flight detector.

Opposite Side Kaon Tag Due to the $b \rightarrow c \rightarrow s$ weak decays, B -mesons containing a b quark will be more likely to contain a K^- in the final state than a K^+ . As for all the other opposite side taggers the determination of the quark flavor on the opposite side determines the flavor on the vertexing side, since $b\bar{b}$ quarks are produced in pairs.

For the opposite side kaon tagging, kaon candidates are selected that are well separated from the reconstructed B_s decay. Kaon candidates coming from a b hadron decay are separated from prompt kaons by requiring a large impact parameter. These requirements are implemented by imposing an isolation cut of

$$\Delta R_{\eta\phi} = \sqrt{\Delta\eta^2 + \Delta\phi^2} > 1 \quad (8.182)$$

and a cut on the combined transverse and longitudinal impact parameters of

$$\chi_{d_0 z_0}^2 = \frac{d_0^2}{\sigma_{d_0}^2} + \frac{z_0^2}{\sigma_{z_0}^2} > 9. \quad (8.183)$$

Tagging the production flavor of the B_s using the charge of the kaon selected in this way gives a contribution to the tagging efficiency of

$$\epsilon D^2 = (2.4 \pm 0.2)\%. \quad (8.184)$$

Same Side Kaon Tag Same side kaon tagging in B_s decays is the equivalent of same side pion tagging in B^0 decays. In the hadronization process, when a B_s meson is produced, an $s\bar{s}$ pair must be popped from the vacuum during fragmentation. The remaining s or \bar{s} quark is likely to join with a \bar{u} or u quark to form a charged kaon. The charge of the kaon thus depends on the flavor of the B_s meson at production.

To estimate the ϵD^2 of the same side kaon tagging algorithm the same side pion tagging algorithm is extended with particle identification using Time-of-Flight information. It should be noted that ϵD^2 for this algorithm is strongly dependent on the momentum spectrum of the B_s meson. Therefore, a rough simulation of the Level-1 and Level-2 triggers are applied to the Monte Carlo sample. The B_s p_T spectrum of this event sample peaks at around 10 GeV/ c , and ϵD^2 is estimated to be

$$\epsilon D^2 = (4.2 \pm 0.3)\%. \quad (8.185)$$

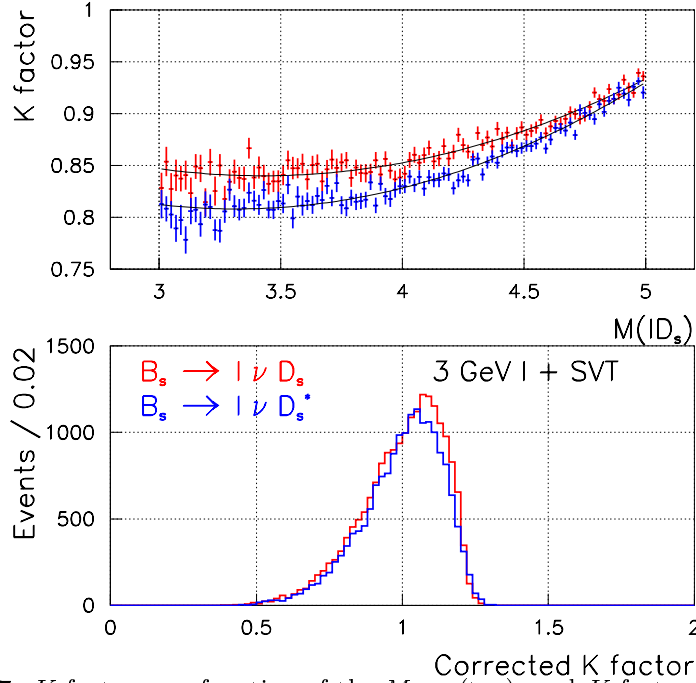


Figure 8.7: K factor as a function of the $M_{\ell D_s}$ (top), and K factor distribution after the $M_{\ell D_s}$ correction (bottom).

8.6.1.3 B_s Mixing with Semileptonic Decays

As discussed in the introduction the key issue for semileptonic B_s decays is the resolution of the proper time measurement. Including the estimates for flavor-tagged event yields, the x_s sensitivity determination is straightforward.

Proper Time Resolution The proper decay time in semileptonic decays is derived as follows

$$ct = \frac{L_T(B_s)M(B_s)}{p_T(B_s)} = \frac{L_T(B_s)M(B_s)}{p_T(\ell D_s)} \cdot K, \quad K = \frac{p_T(\ell D_s)}{p_T(B_s)}, \quad (8.186)$$

where the transverse decay length, $L_T(B_s)$, and transverse momentum, $p_T(\ell D_s)$, are measured from data. The K factor which is used as an average correction for the incomplete B_s reconstruction is obtained from Monte Carlo samples, and $M(B_s)$ is the B_s mass [82]. The proper time resolution is given as

$$\sigma_t = \sigma_{t_0} \oplus t \cdot \frac{\sigma K}{K}, \quad (8.187)$$

where the constant term ($\sigma_{t_0} \sim 60$ fs) is due to the beam spot and the vertex detector resolution, and the K factor resolution ($\sigma K/K \sim 14\%$) is due to the momentum spectrum of the undetected particles, namely the neutrino in the B_s decay or the photon/ π^0 in the subsequent D_s^* decay.

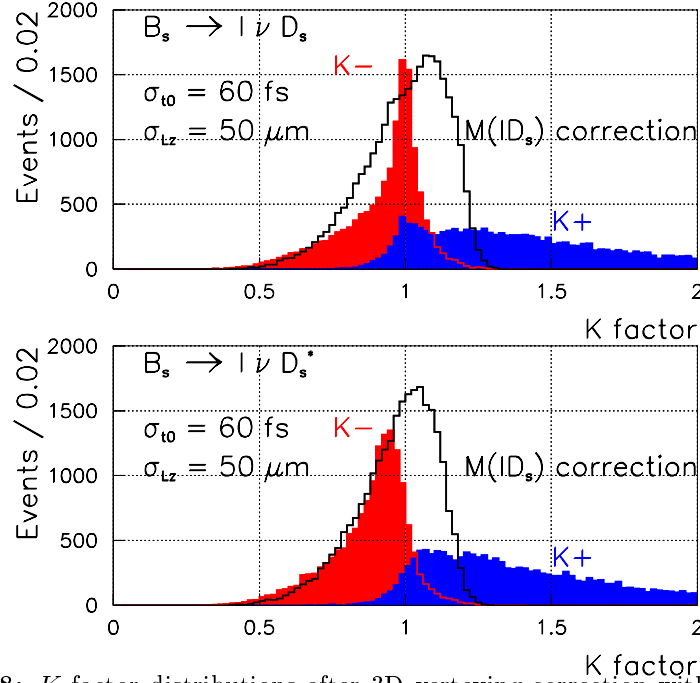


Figure 8.8: K factor distributions after 3D vertexing correction with vertex detector resolutions of $\sigma_{t_0} = 60$ fs and $\sigma_{L_z} = 50$ μm .

The K factor depends strongly on the lepton + D_s invariant mass, $M(\ell D_s)$; this dependence is shown in Figure 8.7 for the D_s and D_s^* channels. Since the invariant lepton + D_s mass is measured, this dependence is corrected for on an event-by-event basis to improve the K factor resolution.

For the $B_s \rightarrow \ell D_s X$, $X = \nu + x$ channel, the following energy and momentum conservation rules are given

$$\begin{aligned} E_{B_s} &= E_{\mu D_s} + E_X, \\ p_X^2 &= |\vec{p}_X|^2 = |\vec{p}_{B_s} - \vec{p}_{\mu D_s}|^2 = p_{B_s}^2 + p_{\mu D_s}^2 - 2p_{B_s}p_{\mu D_s} \cos \Theta, \end{aligned} \quad (8.188)$$

where Θ is the angle in the laboratory frame between the B_s and $\ell + D_s$ directions, which are obtained using the 3D vertex information of the Run II SVX. By assuming $M_X = 0$ the quadratic equation can be solved exactly. Notice that the equation gives generally two solutions, $K^- < K^+$. The equation sometimes has nevertheless no physical solutions due to the finite detector resolution. Furthermore, the equation does not give the correct answer for the $B_s \rightarrow \ell \nu D_s^*$ channel because of the missing photon, $M_X = M_{\nu\gamma} > 0$.

The K factor distributions after all the trigger and offline selection cuts are shown in Figure 8.8. A vertex resolution of $\sigma_{t_0} = 60$ fs and $\sigma_{L_z} = 50$ μm has been assumed. The D_s and the D_s^* channels are displayed in the upper and lower plots, respectively. The probability for the quadratic equation to have a real solution is approximately 50 percent. However, the correction still improves the K factor resolution if there is a physical solution.

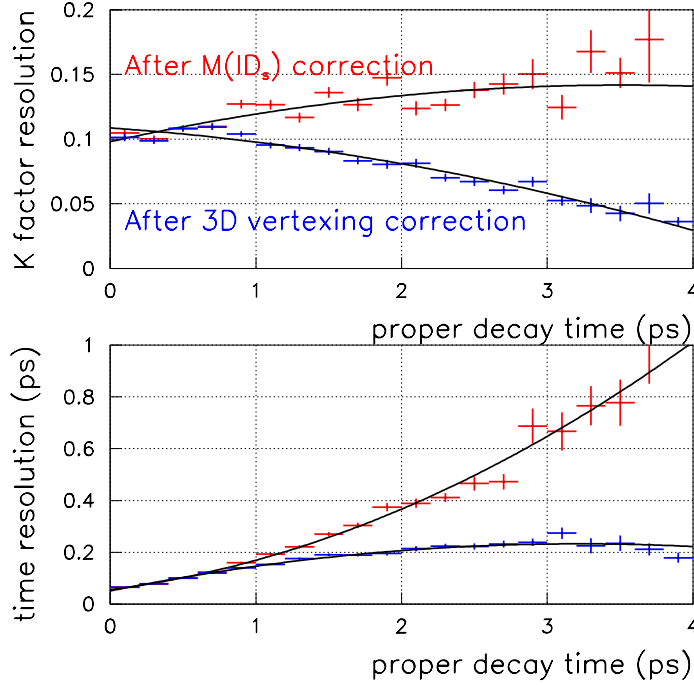


Figure 8.9: K factor and time resolution for $B_s \rightarrow \ell \nu D_s$ decays.

Since the 3D vertexing correction strongly depends on the Θ resolution, it improves for longer B_s decay lengths. In Figure 8.9 the K factor and time resolutions are shown as functions of the proper decay time for the D_s channel after the $M_{\ell D_s}$ correction and 3D vertexing correction.

To perform the 3D vertexing correction, it is assumed that the correct solution, K^- or K^+ , is known, and that the $M(\ell D_s)$ corrected K factor is used if there are no physical solutions. The K factor resolution is significantly improved for the longer decay time events. Both channels D_s and D_s^* show similar results. Unfortunately, the improved K factor resolution is not sufficient to greatly improve the sensitivity to x_s ; practically all of the sensitivity comes from the very short decay length events.

Backgrounds In Run I the signal to background ratio in B_s reconstruction in the semileptonic channels was typically 1:1. Since the kinematics of the Run II event sample will be somewhat different, a conservative signal to background ratio of 1:2 is assumed in the following.

Projected Sensitivity The parameters which influence the projected B_s mixing sensitivity, calculated using equation 8.181, are summarized as follows:

$$N(B_s) : 43k \text{ see Table 8.12}$$

$$\epsilon D^2 : 11.3\% \text{ see Table 8.14}$$

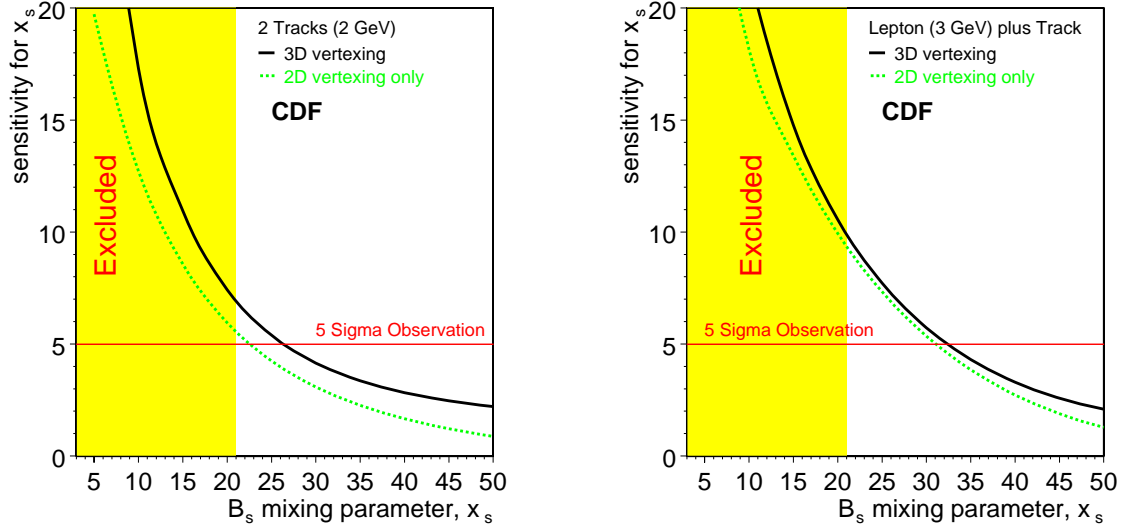


Figure 8.10: Sensitivity for measuring x_s using B_s semileptonic decays for the hadronic two track trigger (left) and the lepton plus displaced track trigger (right). The dashed lines show the significance after $M_{\ell D_s}$ correction, the solid lines after further applying the 3D vertex correction.

σ_t : see Figure 8.9

S/B : 1 : 2 as explained above

The analysis described above for the 3 GeV/ c lepton plus displaced track triggers can easily be extended to the hadronic two-track triggers defined in Table 8.13, where the trigger path is satisfied by a semileptonic decay; given the large ($\sim 20\%$) semileptonic combined branching ratio, the hadronic trigger turns out to be highly efficient for semileptonic decay modes. The significances for measuring x_s for the two-track trigger (left) and the lepton plus displaced track (right) are shown in Figure 8.10. The dashed lines show the significance after the $M_{\ell D_s}$ correction, and the solid lines after the additional 3D vertexing correction. The x_s reach of the semileptonic decay sample is estimated to be about 30 for an observation with five standard deviations. This is significantly less than that for the fully reconstructed hadronic channels, which are discussed below, but it does provide an independent trigger path.

8.6.1.4 B_s Mixing with Hadronic Decays

The fully hadronic event sample is particularly important for B_s mixing analyses since the fully reconstructed decays $B_s \rightarrow D_s^- \pi^+$ and $B_s \rightarrow D_s^- \pi^+ \pi^- \pi^+$ have excellent proper time resolution, much smaller than the expected period of oscillation.

Proper Time Resolution The proper time of a B_s decay is calculated from the measured decay length, and the reconstructed B_s momentum. The uncertainty on the proper time is then given by

$$\sigma_t = t \sqrt{\left(\frac{\sigma_L}{L}\right)^2 + \left(\frac{\sigma_P}{P}\right)^2}. \quad (8.189)$$

To resolve the rapid oscillations of the B_s it is generally required that this resolution not be significantly larger than the period of oscillation. For partially reconstructed semileptonic B_s decays, the uncertainty in the momentum is the limiting factor in the mixing analyses. However, for the fully reconstructed B_s decays obtained using the XFT+SVT triggers, the momentum uncertainty will be less than 0.4%. This does not contribute significantly to the overall proper time resolution and has been ignored in the projections described below.

Backgrounds To date, no hadron collider experiment has operated with a displaced track based trigger. Hence, the level of backgrounds to be expected in the B_s sample is uncertain. Data recorded by CDF in Run I based on the single lepton triggers are used to study the purity of the B_s signal after imposing the XFT and SVT trigger cuts on the opposite side b hadron decays.

It has been observed that even a modest decay length cut suppresses the light flavor contribution significantly. Therefore, the main concern is that the signal is not overwhelmed by background from events containing real b - and c -quarks.

Because of the small branching ratios of the $B_s \rightarrow D_s^+ \pi^-, D_s^+ \pi^+ \pi^- \pi^-$ decays, few, if any, such decays are expected to be present in the Run I data after imposing the XFT and SVT trigger cuts. A similar set of cuts with higher efficiency was used to search for the hadronic B^0 and B^+ decays in the $D\pi$ final states. As a result of those studies it is concluded that a signal to background ratio of 1:1 should be achievable. To see the dependence of the significance on this parameter, this ratio is varied between 1:2 and 2:1 in the following projections.

Projected Sensitivity The parameters which influence the projected B_s mixing sensitivity, calculated using equation 8.181, are summarized as follows:

$$\begin{aligned} N(B_s) &= 75k \text{ see Table 8.12} \\ \epsilon D^2 &= 11.3\% \text{ see Table 8.14} \\ \sigma_t &= 0.045 \text{ ps} \\ S/B &= 1 : 2 - 2 : 1 \text{ as explained above} \end{aligned}$$

The results are again presented in terms of the dimensionless mixing parameter $x_s = \Delta m_s \tau_{B_s}$ where the B_s lifetime of 1.54 ps [86] is used. In addition to the analytic expression for the sensitivity, Equation 8.181, an alternative analysis has been performed using a series of simulated Monte Carlo experiments. The lifetime distributions of mixed and unmixed decays are generated and the mixed asymmetry is fitted to Equation 8.180. An example

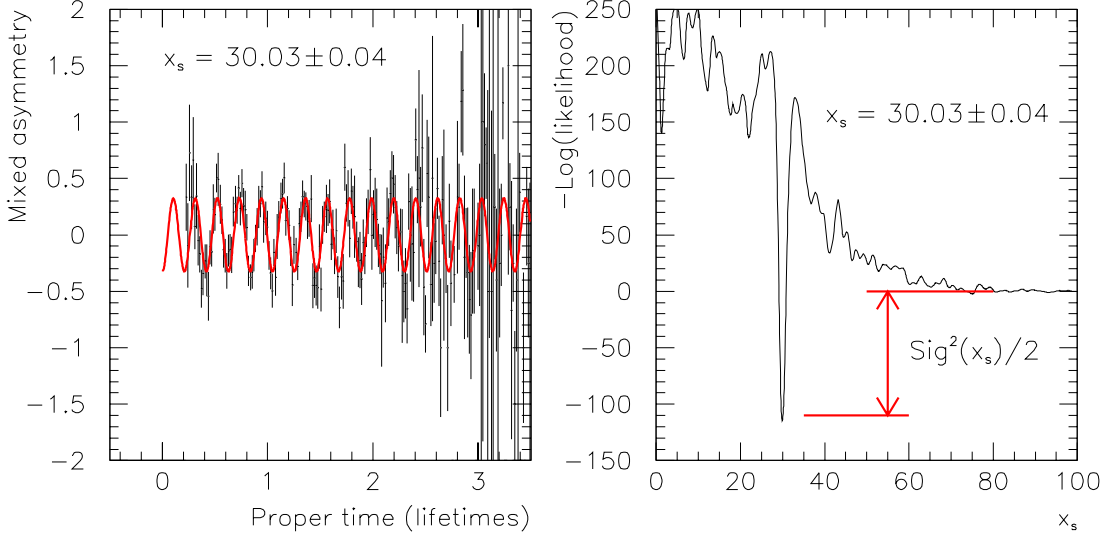


Figure 8.11: Example of a single toy Monte Carlo experiment: the mixed asymmetry distribution (left) and negative log-likelihood from the fit as a function of x_s (right)

of the mixed asymmetry distribution and the negative log-likelihood curve is shown in Figure 8.11. The negative log-likelihood curve is shown as a function of x_s , obtained from one of these Monte Carlo experiments. The comparison of the analytic expression with the averages of many Monte Carlo simulations indicates that the analytic approximation is very good.

The average significance for B_s oscillation measurements is shown in Figure 8.12. Various event yields and signal-to-background scenarios are considered. As stated above, the default event yield is 75k events and the signal-to-background fraction is 1:1.

From the analytic expression, equation 8.181, the following 5 standard deviation sensitivity limits are derived:

$$\begin{aligned} \text{Maximum: 75k events } x_s &= \begin{cases} 74 & \text{for } S/B = 2 : 1 \\ 69 & \text{for } S/B = 1 : 2 \end{cases} \\ \text{Maximum: S:B = 1:1 } x_s &= \begin{cases} 73 & \text{for 125k events} \\ 59 & \text{for 25k events} \end{cases} \end{aligned}$$

The Monte Carlo samples give very similar results as indicated above. It is concluded that even in the worst case the reach is $x_s \sim 60$.

Fits to various experimental results which assume the Standard Model indicate that $22.0 < x_s < 30.8$ at the 95% confidence level [87]. If mixing occurs near the frequency expected in the Standard Model, it should be easily observable by CDF in Run II. Figure 8.13 (left) shows the luminosity required to achieve an observation with an average significance of 5 standard deviations as a function of x_s . The figure indicates that if mixing occurs

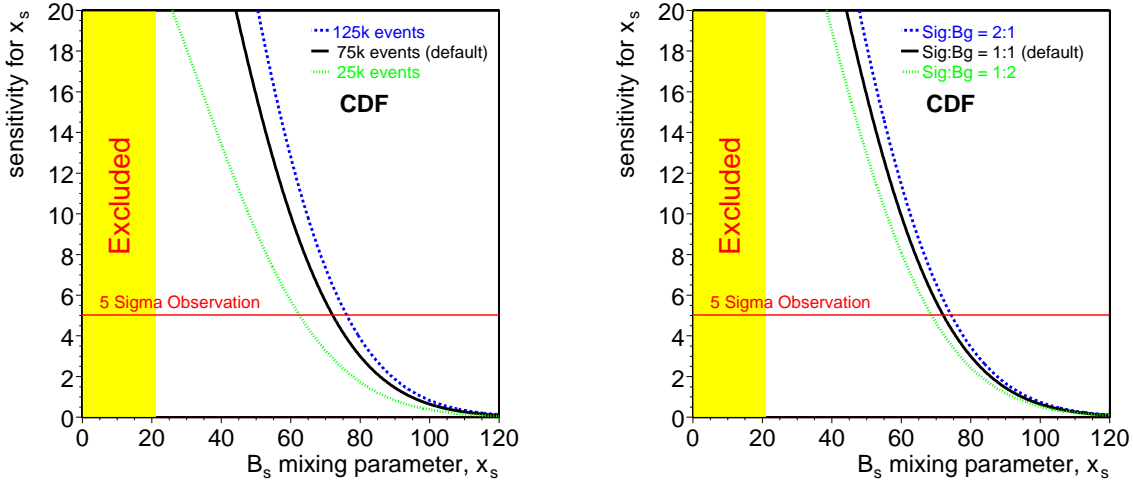


Figure 8.12: Average significance of mixing measurements expected as a function of the mixing parameter x_s for various event yields (left) and signal-to-background ratios (right). The default is 75k events at a signal-to-background ratio of 1:1. The shaded area is excluded by the combined world lower limit on x_s .

within the context of the Standard Model, then it should be observed with a small fraction of 2 fb^{-1} , with CDF in a fully operational state.

While the significance of an observation of mixing is determined from the depth of the minimum in the negative log-likelihood curve, the uncertainty on the measured value of x_s is determined by how sharp this minimum is. In the case of rapid oscillations, many periods will be reconstructed over a few B_s lifetimes and the minimum is expected to be very sharp leading to a small uncertainty.

The average uncertainty is described approximately by the analytic expression

$$\frac{1}{\sigma_{x_s}} = \sqrt{N\epsilon D^2} e^{-(x_s \sigma_t / \tau)^2 / 2} \sqrt{\frac{S}{S+B}}. \quad (8.190)$$

The expected uncertainty from the analytic formula versus the mixing parameter, x_s , is shown in Figure 8.13 (right). This formula is confirmed using a series of Monte Carlo samples.

8.6.2 B_s mixing measurement at $D\bar{O}$ [†]

The expected luminosity of the Tevatron, $2 \times 10^{32} \text{ cm}^{-2}\text{s}^{-1}$, in Run II will lead to a huge rate for $b\bar{b}$ production, $\sim 10^{11}$ events/year. These enormous statistics combined with the upgraded detector will allow us to search for B_s mixing. The resulting measurement of Δm_s , when used to determine the ratio $\Delta m_d / \Delta m_s$ using the well-measured value for Δm_d ,

[†]Authors: N. Cason, R. Jesik, and N. Xuan.

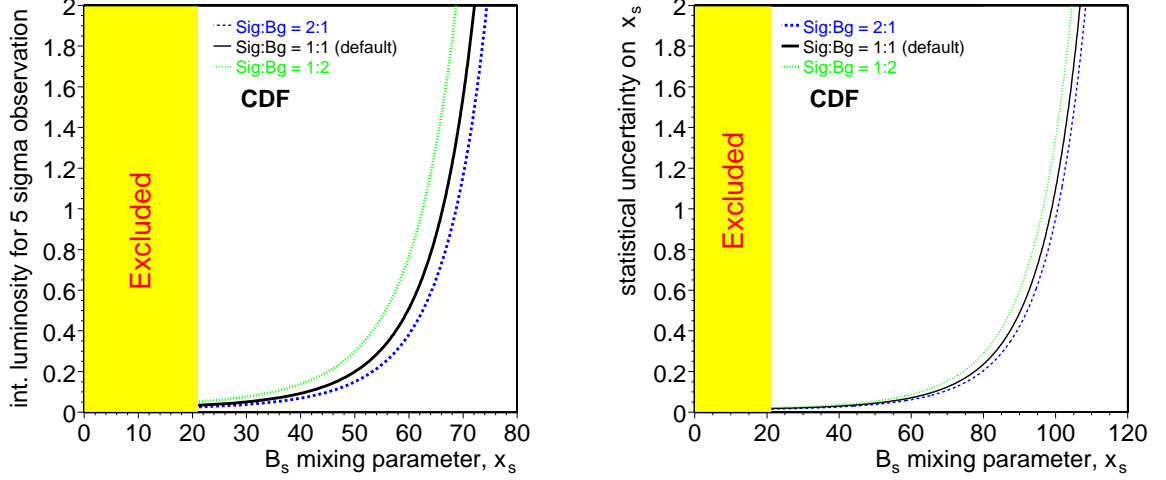


Figure 8.13: Luminosity required to achieve a 5 standard deviation observation of mixing (left) and the statistical uncertainty as a function of the mixing parameter, x_s (right). The curves on the right are calculated using Equation 8.190.

gives a theoretically clean measurement of $|V_{td}|^2/|V_{ts}|^2$. This puts a precise constraint on the CKM parameters ρ and η .

For B_s^0 mesons, existing data exclude small values of the mixing parameter $x_s = \Delta m_s/\Gamma_s$, requiring $x_s > 19.0$ at the 95% CL [82]. Consequently the mass difference Δm_s is much larger than Δm_d , and the $B_s^0 - \overline{B}_s^0$ oscillation frequency will therefore be much higher than that for the B_d^0 . Excellent decay length and momentum resolutions are thus essential in order to observe the rapid oscillations as a function of proper time.

Various decay modes of B_s^0 mesons are under investigation by the DØ collaboration. Among them are:

$$\begin{aligned}
 B_s^0 &\rightarrow D_s^-(K^- K^+ \pi^-) \pi^+, & (\text{BR} = 1.1 \times 10^{-4}), \\
 B_s^0 &\rightarrow D_s^-(K^- K^+ \pi^-) 3\pi, & (\text{BR} = 2.8 \times 10^{-4}), \\
 B_s^0 &\rightarrow J/\psi(\mu^+ \mu^-, e^+ e^-) K^*(K^\pm \pi^\mp), & (\text{BR} = 5.1 \times 10^{-6}), \\
 B_s^0 &\rightarrow D_s^-(K^- K^+ \pi^-) \ell^+ \nu, & (\text{BR} = 1.1 \times 10^{-4}).
 \end{aligned} \tag{8.191}$$

Taking advantage of the good SMT resolution, we can select B_s decays by using displaced secondary vertices or using tracks with large impact parameters. The B_s final states will be flavor tagged by the charge of the lepton, the charge of the reconstructed charm meson or the charge of the kaon as appropriate.

The actual measurement strategy for x_s will depend on the frequency of the oscillation. For smaller oscillation frequencies, semileptonic B_s decays can be used. The lepton in the final state provides an easy trigger, giving a large statistics sample. If nature cooperates, a measurement in this range will come very early in Run II.

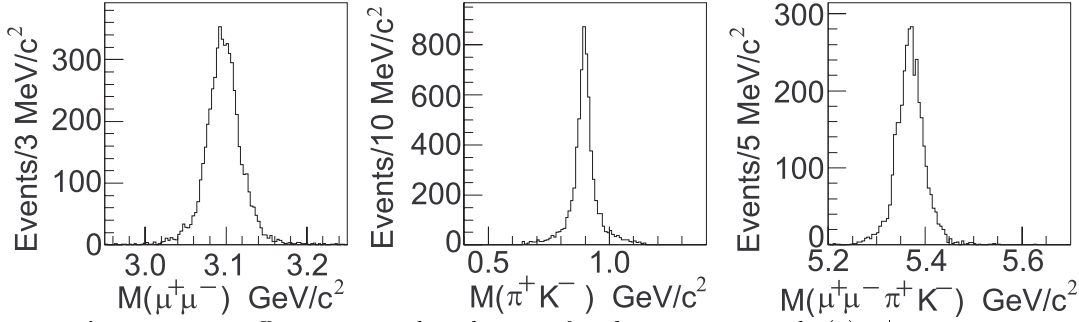


Figure 8.14: Effective mass distributions for the reconstructed: (a) $\mu^+\mu^-$ system, (b) π^+K^- system, and (c) $\mu^+\mu^-\pi^+K^-$ system. These distributions are prior to using vertex and mass constraints.

For higher oscillation frequencies, the measurement becomes more difficult. Exclusive decays must be used in order to achieve the necessary momentum (and therefore proper time) resolution. Decays which DØ has focused on include: $B_s \rightarrow D_s^- \pi^+ (\pi^- \pi^+)$, where the D_s^- decays to $\phi \pi^-$ or $K^{*-} K^0 / K^- K^{*0}$; and $B_s \rightarrow J/\psi \bar{K}^{*0}$ followed by $J/\psi \rightarrow e^+ e^-$ or $\mu^+ \mu^-$ and $\bar{K}^{*0} \rightarrow K^- \pi^+$. We can only trigger on B_s decays into fully hadronic final states when the other B in the event decays semileptonically. Using single lepton triggers, we expect to be able to collect about a thousand reconstructed exclusive B_s decays in each mode in the first two years, allowing us to measure x_s values up to $\sim 20 - 30$. We are presently investigating better trigger scenarios, such as lowering the p_T threshold of the lepton and requiring another moderately high p_T track (or tracks), which would increase our Δm_s reach.

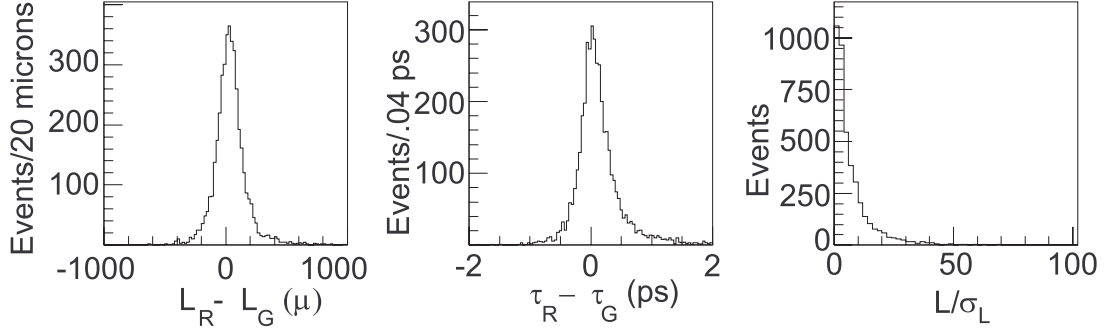
A Monte Carlo study of the $B_s \rightarrow J/\psi \bar{K}^{*0}$ decay has been carried out in order to estimate the number of events which will be in a data sample based on a 2 fb^{-1} exposure. We have analyzed 20,000 events using the MCFAST program. The events were generated using Pythia and a simulation of the upgraded DØ detector. Each event had a $B_s \rightarrow J/\psi \bar{K}^{*0}$ decay as well as a generic \bar{B} decay. The J/ψ decayed to $\mu^+ \mu^-$ (83% of the time) or $\mu^+ \mu^- \gamma$ (17% of the time). (The radiative decays are not discussed further here.) The \bar{K}^{*0} decayed to $\pi^+ K^-$.

Event reconstruction efficiency was estimated using the geometric acceptance of the silicon vertex detector and of the fiber tracker. (Tracking inefficiencies are not yet included.) We find that 21% of the events have all four charged tracks reconstructed.

Shown in Fig. 8.14 are the reconstructed $\mu^+ \mu^-$, $\pi^+ K^-$, and $\mu^+ \mu^- \pi^+ K^-$ effective mass distributions for the reconstructed tracks. The mass resolution of the B_s improves by more than a factor of two when vertex and J/ψ mass constraints are imposed. Effective mass resolutions are given in Table 8.15.

Resolutions of vertex position, decay length, and proper time were estimated using the nominal silicon vertex detector and fiber tracker resolutions. Shown in Fig. 8.15 are distributions of the fitted minus measured decay length of the B_s , the fitted minus measured proper decay time of the B_s , and the ratio of the decay length to the error in the decay length (L/σ_L). We summarize the resolutions in vertex positions, decay length and proper

Quantity	Level	σ (MeV/c^2)
$M(B_s)$	Reconstruction	37
$M(B_s)$	J/ψ mass fit	15
$M(\mu^+\mu^-)$	Reconstruction	29

Table 8.15: Mass Resolutions**Figure 8.15:** Distributions of: (a) the reconstructed B_s decay length minus the generated B_s decay length; (b) the reconstructed B_s proper time minus the generated B_s proper time; and (c) the reconstructed B_s decay length divided by its error.

time in Table 8.16.

In order to get a realistic estimate of the number of events which would be available for analysis, additional cuts were placed on the sample. The muons were required to have $p_T > 1.5$ GeV/c and to have $|\eta| < 2$. A total of 24% of the reconstructed events satisfied these cuts. Combined with the reconstruction efficiency of 21%, we are left with a sample of 5.0% of the generated events for further analysis.

For most purposes, additional cuts will be required to obtain a sample of events with a good signal-to-noise ratio. To estimate the sample size after such cuts, we impose a cut on the variable L/σ_L . Of the 5.0% of the events satisfying all the previous cuts, 83% have $L/\sigma_L > 2.0$, 73% have $L/\sigma_L > 3.0$, and 63% have $L/\sigma_L > 4.0$. The required cut value will not be known until the data is in hand, but we use the $L/\sigma_L > 3.0$ cut for further estimates. Hence the overall combined efficiency which we use below is $(.050)*0.73=0.036$.

In order to do mixing studies, it is necessary to tag the flavor of the B_s (or \overline{B}_s). This can be tagged if we identify the sign of the charged kaon in the K^* . Although $D\overline{O}$ does

Quantity	σ
Production vertex (x,y, and z) (μm)	34, 34, 80
Decay vertex (x,y, and z) (μm)	50, 50, 140
B_s decay length (μm)	140
Proper time (ps)	0.40

Table 8.16: Resolutions

not have particle identification in the traditional sense, it is possible in this event sample to determine whether the positive or negative particle from the K^* decay is the charged kaon by calculating the effective mass under the two assumptions ($K^+\pi^-$ and $K^-\pi^+$) and taking as correct that combination which gives an effective mass closest to the nominal K^* mass ($0.890 \text{ GeV}/c^2$). We find that we are correct using this assignment 67% of the time. Flavor tagging of the other b quark will have the efficiency and dilution summarized previously in Table 6.3.

Using estimates of the $b\bar{b}$ production cross section ($158 \text{ } \mu\text{b}$); the fraction of this cross section producing B_s (0.167); the $B_s \rightarrow J/\psi \bar{K}^{*0}$ branching ratio (5.1×10^{-6}); the $J/\psi \rightarrow \mu^+\mu^-$ branching ratio (0.06); the luminosity (2 fb^{-1}); and the overall combined efficiency from above (.036), we obtain a signal of 1000 events. We would expect a similar sample will be obtained using the $J/\psi \rightarrow e^+e^-$ mode.

8.6.3 Measurement of B_s Mixing in BTeV[†]

In this section, the x_s reach of BTeV will be demonstrated using $B_s \rightarrow D_s^- \pi^+$ and $B_s \rightarrow J/\psi \bar{K}^{*0}$. This study was carried out in several steps, the first step being a simulation of the BTeV detector response to signal events. The output of this step was treated as real data and passed through a physics analysis program to determine the yield, the time resolution and the signal-to-background ratio in each mode. This information was then passed to a separate program which computed the x_s reach; this program is discussed in section 8.6.3.2. A separate background study was performed.

8.6.3.1 Yields, Resolutions and Signal-to-Background Ratios

The mode for which BTeV has the most sensitivity to x_s is $B_s \rightarrow D_s^- \pi^+$, where the D_s^- decays either by $D_s^- \rightarrow \phi \pi^-$, $\phi \rightarrow K^+ K^-$, or by $D_s^- \rightarrow K^{*0} K^-$, $K^{*0} \rightarrow K^+ \pi^-$. Both of these D_s^- modes have narrow intermediate states and characteristic angular distributions, both of which can be used to improve the signal-to-background ratio.

For this study, Monte Carlo events were generated using Pythia and QQ and the detector response was simulated using BTeVGeant. The simulated events were analyzed as real data. For the $D_s \rightarrow \phi \pi$ decay mode the following cuts were used:

- All tracks were required to have at least 3 hits in the silicon pixel detector.
- Each of the tracks in the B_s candidate were required to have an impact parameter with respect to the primary vertex of $> 3\sigma$.
- To reduce the background due to tracks that really come from other interactions it was required that all 4 tracks have an impact parameter with respect to the primary vertex of less than 0.2 cm.

[†]Author: R. Kutschke.

- At least one of the kaons from the ϕ decay was required to be strongly identified as a kaon by the RICH detector. The second kaon was only required to be loosely identified. No particle ID requirements were placed on the pion candidates.
- The ϕ and D_s candidates were required to be within $\pm 2.5\sigma$ of their nominal masses.
- It was required that the distance between the primary vertex and D_s decay vertex be $L < 8.0$ cm and the D_s decay vertex have a decay length significance of $L/\sigma_L(D_s) > 10.0$.
- It was required that the B_s have decay length significance of $L/\sigma_L(B_s) > 4.0$.
- The B_s candidate was required to point back to the primary vertex: the transverse momentum of the B_s with respect to its line of flight from the primary vertex was required to be less than 1.0 GeV/c and the impact parameter of the B_s with respect to the primary vertex was required to be less than 3σ .

The combined geometric acceptance and reconstruction efficiency was found to be 2.7%. Of the events that passed these analysis cuts, 74% passed the level 1 trigger. For the $D_s \rightarrow K^* K$ mode we used the same cuts except that both kaons from the D_s decay were required to be identified in the RICH. There was also a broader cut on the intermediate K^* mass. The combined reconstruction efficiency and geometric acceptance for the $D_s \rightarrow K^* K$ mode was found to be 2.3%, and the level 1 trigger efficiency for the events passing the analysis cuts was 74%. For both modes the resolution on the mass of the B was found to be 18 MeV/ c^2 and the mean resolution on the proper decay time was found to be 43 fs. The nominal acceptance of the BTeV level 2 trigger for the accepted events is 90% of the events which remain after the level 1 trigger. The nominal flavor tagging power of BTeV was estimated in chapter 5 to be $\epsilon D^2 = 0.1$ which arises from $\epsilon = 0.70$ and $D = 0.37$.

It is believed that the dominant source of backgrounds will be events of the form $X_b \rightarrow D_s^- X$, where X_b may be any b flavored hadron. The background combinations arise when a true D_s^- combination is combined with some other track in the event. An MC-Fast based study of 1 million $B \rightarrow D_s^- X$ events was performed using an older version of the detector geometry, the one used for the BTeV Preliminary Technical Design Report (PTDR) [91]. Comparisons between BTeVGeant and MC-Fast, and comparisons between the old and new detector geometries, show that these background studies remain valid. When the 1 million $B \rightarrow D_s^- X$ events were passed through MC-Fast and analyzed as real data, 8 entries remained in a mass window 6 times larger than the mass window used to select signal B_s candidates. From this it is estimated that the signal-to-background ratio in this channel is 8.4:1. This study was performed without the proper treatment of multiple interactions in one beam crossing. To account for this, the signal-to-background ratio used in the estimate of the x_s reach is 3:1.

The background from direct charm production has not yet been investigated. While direct charm production has a cross-section about 10 times higher than that for production of charm via B decay, it is triggered much less efficiently. Moreover the requirement of two, distinct detached vertices greatly reduces the background from direct charm. In the end it is expected that the background from $B \rightarrow D_s^- X$ will dominate.

Quantity	Value	Yield (Events/year)
Luminosity:	$2 \times 10^{32} \text{ cm}^{-2}\text{s}^{-1}$	
One Year:	10^7 s	
$\sigma_{b\bar{b}}$:	$100 \text{ } \mu\text{b}$	
$\mathcal{B}(B_s \rightarrow D_s^- \pi^+)$:	3.0×10^{-3}	
$\mathcal{B}(D_s^- \rightarrow \phi \pi^-)$:	0.030	
$\mathcal{B}(D_s^- \rightarrow K^{*0} K^-)$:	0.036	
$\mathcal{B}(\phi \rightarrow K^+ K^-)$:	0.49	
$\mathcal{B}(K^{*0} \rightarrow K^+ \pi^-)$:	0.67	
$\mathcal{B}(\bar{b} \rightarrow B_s)$	0.13	6,210,000
$\epsilon(\text{Geometry} + \text{cuts} : \phi \pi^-)$	0.027	
$\epsilon(\text{Geometry} + \text{cuts} : K^{*0} K^-)$	0.023	
$\epsilon(\text{Trigger}) \text{ Level 1}$	0.74	
$\epsilon(\text{Trigger}) \text{ Level 2}$	0.90	
$\epsilon(\text{Tag})$	0.70	72,000
Tagging Dilution	0.37	
S/B	3:1	
$\sigma(\text{Proper Decay time})$	43 fs	

Table 8.17: Projected yield for $B_s \rightarrow D_s^- \pi^+$ in one year of BTeV running. The numbers in the third column give the expected yield when all of the factors down to and including that line have been considered. The branching fraction $\mathcal{B}(B_s \rightarrow D_s^- \pi^+)$ was estimated to be the same as $\mathcal{B}(B_d \rightarrow D^- \pi^+)$.

Table 8.17 gives a summary of the preceding results and discusses a list of all assumptions which went into the computation of the yield. The value for $\mathcal{B}(\bar{b} \rightarrow B_s)$ is obtained from Reference [92]. In one year it is expected that 72,000 events will trigger, survive all analysis cuts and have their birth flavor tagged.

Another mode with good x_s sensitivity is $B_s \rightarrow J/\psi \bar{K}^{*0}$, $J/\psi \rightarrow \mu^+ \mu^-$, $\bar{K}^{*0} \rightarrow K^- \pi^+$. Although this mode is Cabibbo suppressed, other factors are in its favor: the final state consists of a single detached vertex and the state is triggerable with several independent strategies, including impact parameter triggers, secondary vertex triggers and dimuon triggers [93]. While this mode does not have the x_s reach of $D_s^- \pi^+$ it does cover much of the expected range and it provides a powerful check with partly independent systematics.

For reasons of time limitations, the simulation of the $J/\psi \bar{K}^{*0}$ mode used MCFast, not BTeVGeant. The analysis of this mode proceeded as follows. To be considered as part of a signal candidate, a track was required to have at least 20 total hits and at least 4 pixel hits. The only further requirement placed on π^\pm candidates was that they have a momentum greater than 0.5 GeV/c. In order to be considered a muon candidate, a track was required to have a momentum $p > 5$ GeV/c, to penetrate the hadron filter and to leave hits in the most downstream muon chambers. Kaon candidates were required to satisfy a simplified model of the RICH system: the track was required to have a momentum in the range $3 < p < 70$ GeV/c and was required to have hits in the tracking station downstream

of the RICH mirror. True kaons which satisfied this criteria were identified as kaons with an efficiency of 90%; other hadrons which satisfied this criteria were (mis)identified as kaons 3% of the time.

A $\mu^+\mu^-K^-\pi^+$ combination was accepted as a B_s candidate if the confidence level of fitting all four tracks to a single vertex was greater than 0.005. It was also required that the resonant substructure requirements be satisfied. Combinations were considered for further analysis provided the decay length of the B_s candidate, L , satisfied $L/\sigma_L > 10$ and the impact parameter of the B_s candidate with the primary vertex, d , satisfied $d < 3\sigma_d$. Each of the four B_s granddaughters were required to have an impact parameter with the primary vertex, d , of $d > 2\sigma_d$. Candidates with poor time resolution were rejected by demanding $\sigma_t \leq 0.09$ ps. Also the mass of the J/ψ was constrained to its PDG value. The above procedure found that the efficiency for the 4 tracks to be within the fiducial volume of the tracking system was $14.2 \pm 0.3\%$ and the efficiency for the remaining candidates to pass the analysis cuts was 0.29 ± 0.01 . The resolution on the mass of the B_s was found to be 8.6 ± 0.3 MeV/ c^2 and the mean resolution on the proper decay time was found to be 36 fs.

The BTeV Level 1 trigger simulation was run on the $J/\psi\bar{K}^{*0}$ sample and, of the candidates which passed all analysis cuts, $68 \pm 2\%$ also passed the trigger; the error is statistical only. However, this mode can also be triggered by the dimuon trigger. Section 8.3, of the BTeV proposal [94], which describes the algorithms and performance of the muon trigger, estimates a trigger efficiency of 50% for this decay mode. There is, as yet, no calculation of the total Level 1 trigger efficiency which takes into account the correlations between the two triggers. For this proposal it will be estimated that the combined Level 1 trigger efficiency is 85%. As for the $D_s\pi$ final state, the Level 2 trigger is expected to have an efficiency of about 90%.

By far the dominant background is expected to come from decays of the form $X_b \rightarrow J/\psi X$, $J/\psi \rightarrow \mu^+\mu^-$, where X_b is any b flavored hadron. An MCFast based simulation of 500,000 such decays was performed and the signal-to-background level was estimated to be about 2:1. Some sources of background that one might, at first, think to be important turn out not to be a problem. First, the more copious $B_s \rightarrow J/\psi \phi$ final state is not a significant source of background because of the excellent particle ID provided by the RICH system. Second, the mass resolution is sufficient to separate the decay $B_d \rightarrow J/\psi\bar{K}^{*0}$.

Finally, the expected yield can be increased by at least 50% by using the decay mode $J/\psi \rightarrow e^+e^-$. This mode will have an efficiency for secondary vertex triggers which is comparable to that for $J/\psi \rightarrow \mu^+\mu^-$ but the acceptance of the ECAL is smaller than that of the muon detectors. The smaller acceptance of the ECAL is somewhat offset by also using the RICH for electron identification.

The information reported here is summarized in Table 8.18 and is used in the mini-Monte Carlo described in the next section. The estimate for $\mathcal{B}(B_s \rightarrow J/\psi\bar{K}^{*0})$ is obtained from Reference [93] and that for $\mathcal{B}(\bar{b} \rightarrow B_s)$ is obtained from Reference [92].

Quantity	Value	Yield (Events/year)
Luminosity:	$2 \times 10^{32} \text{ cm}^{-2} \text{ s}^{-1}$	
One Year:	10^7 s	
$\sigma_{b\bar{b}}$:	$100 \text{ } \mu\text{b}$	
$\mathcal{B}(B_s \rightarrow J/\psi \bar{K}^{*0})$:	8.5×10^{-5}	
$\mathcal{B}(J/\psi \rightarrow \mu^+ \mu^-)$:	0.061	
$\mathcal{B}(\bar{K}^{*0} \rightarrow K^- \pi^+)$:	0.667	
$\mathcal{B}(\bar{b} \rightarrow B_s)$	0.13	180000
$\epsilon(\text{Geometric})$	0.142	
$\epsilon(\text{Analysis cuts})$	0.26	6600
$\epsilon(\text{Trigger})$ Level 1 Tracking only	0.60	
$\epsilon(\text{Trigger})$ Level 1 Total	0.85	
$\epsilon(\text{Trigger})$ Level 2	0.90	5100
$\epsilon(\text{Tag})$	0.70	3600
Include $J/\psi \rightarrow e^+ e^-$	1.5	5300
Tagging Dilution	0.37	
S/B	2:1	
$\sigma(\text{Proper Decay time})$	36 fs	

Table 8.18: Projected yield for $B_s \rightarrow J/\psi \bar{K}^{*0}$ in one year of BTeV running. The numbers in the third column give the expected yield when all of the factors down to and including that line have been considered. The trigger efficiency is quoted as a fraction of those events which pass the analysis cuts.

8.6.3.2 Computation of the x_s Reach

The final step in the study was to use a mini-Monte Carlo to study the x_s reach of BTeV. This mini-Monte Carlo generates two lifetime distributions, one for mixed events and one for unmixed events, smears the distributions and then extracts a measured value of x_s from a simultaneous fit of the two distributions. The time smearing is a Gaussian of fixed width, using the mean time resolutions determined above. The model includes the effects of mistagging, background under the signal, and the minimum time cut which is implied by the L/σ_L cut. It is assumed that the lifetime distribution of the background is an exponential with the same mean lifetime as that of the B_s .

Figures 8.16 a) and b) show the proper time distributions which result from one run of the mini-Monte Carlo for a generated value of $x_s = 40$. The simulation is for the decay mode $B_s \rightarrow D_s^- \pi^+$ for one month of BTeV running. Part a) shows the proper time distribution for unmixed decays while part b) shows the distribution for mixed decays. Part c) of the figure shows, as a function of x_s , the value of the unbinned negative log likelihood function computed from the simulated events. A clear minimum near the generated value of x_s is observed and the likelihood function determines the fitted value to be $x_s = 39.96 \pm 0.08$. A step of 0.5 in the negative log likelihood function determines the 1σ error bounds and a line is drawn across the figure at the level of the 5σ error bound.

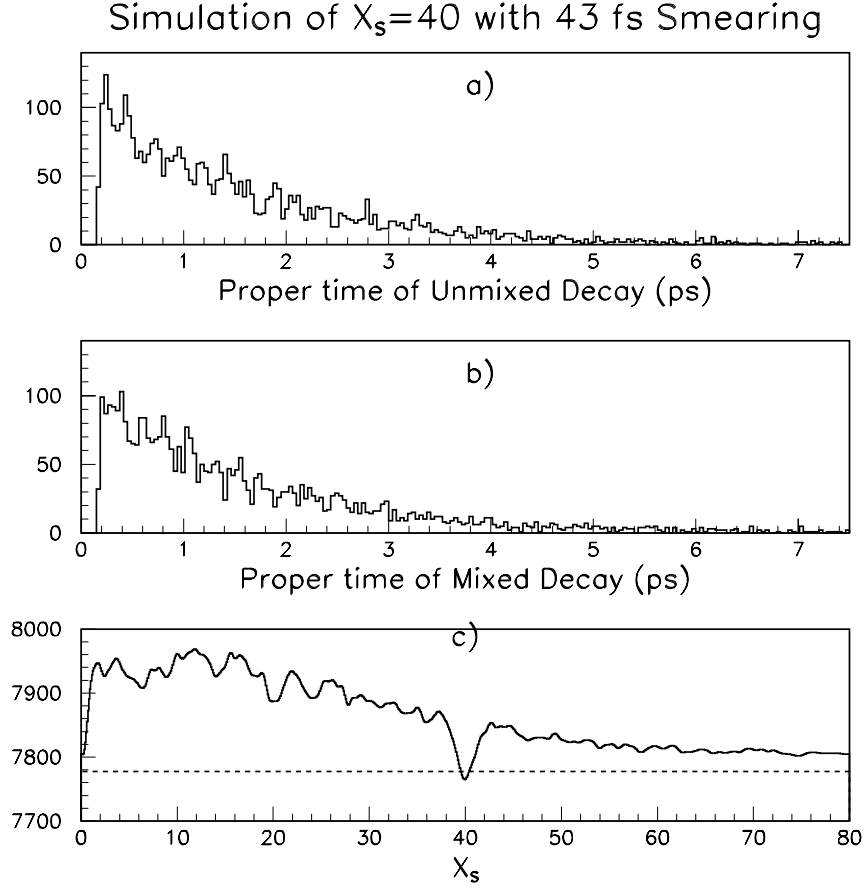


Figure 8.16: Mini Monte Carlo proper lifetime plots of a) unmixed and b) mixed decays for a generated value of $x_s = 40$. The plots simulate the results of the $B_s \rightarrow D_s^- \pi^+$ channel after one month of running. The oscillations are prominent. Part c) shows the negative log likelihood function which was obtained from the entries in parts a) and b). A prominent minimum is seen at the generated value of x_s . The dashed line marks the level above the minimum which corresponds to 5σ significance.

This figure nicely illustrates the distinction between two quantities which are often confused, the significance of the result and the error on x_s . The significance of the signal is determined by how far the depth of the global minimum falls below that of the next most significant minimum. The error on x_s is determined by the curvature of the likelihood function at the global minimum. While these quantities are clearly related, they are distinct; in particular, the significance of the signal is not the relative error on x_s .

The error returned by the fit was checked in two ways. First, an ensemble of mini-Monte Carlo experiments was performed and the errors were found to correctly describe the dispersion of the measured values about the generated ones. Second, the errors returned by the fit were found to be approximately equal to the Cramer-Rao minimum variance bound.

The mini-Monte Carlo was also used to study the level of statistics below which the

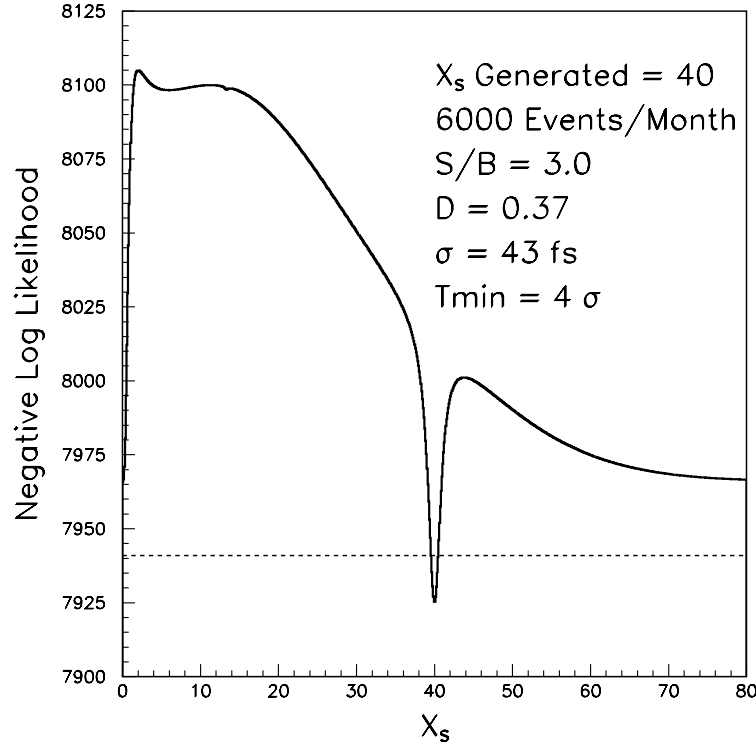


Figure 8.17: The same likelihood function as in part c) of the previous figure but obtained using the integral method described in the text. The overall shape is the same but the statistical fluctuations have been removed. There is also an overall level shift which is related to the goodness of fit in the previous figure.

experiment is unable to measure x_s . As the number of events in a trial is reduced, the negative log likelihood function becomes more and more ragged and the secondary minima become more pronounced. Eventually there are secondary minima which reach depths within 12.5 units of negative log likelihood (5σ) of the global minimum. When this happens in a sufficiently large fraction of the trials, one must conclude that only a lower limit on x_s can be established. In the region of the parameter space which was explored, the absolute error on x_s was approximately 0.1 when this limit was reached. This was independent of the generated value of x_s ; that is, the discovery measurement of x_s will have errors of something like ± 0.1 , even if x_s is large, say 40.

It is awkward to map out the x_s reach of the apparatus by running a large ensemble of mini-Monte Carlo jobs; instead the following automated procedure was used. Following ideas from McDonald [95], the sum over events in the likelihood function was replaced with an integral over the parent distribution. Because the parent distribution does not have any statistical fluctuations, the fluctuations in the likelihood function are removed, leaving only the core information. An example of such a likelihood function is shown in Fig. 8.17.

A likelihood function computed in this way has the property that it scales linearly with the number of events being simulated. This can be stated formally as follows. Let x_0 denote the generated value of x_s and let $\mathcal{L}(x; x_0, N)$ denote the value of the likelihood function,

evaluated at x , for a sample which has a true value of x_0 and which contains N events. Then,

$$\mathcal{L}(x; x_0, N) = N \mathcal{L}(x; x_0, 1). \quad (8.192)$$

Now, one can define the significance of the minimum, n , as,

$$n^2 = 2.0 N [\mathcal{L}(\infty; x_0, 1) - \mathcal{L}(x_0; x_0, 1)]. \quad (8.193)$$

For practical purposes ∞ was chosen to be 160. If one did not have to worry about the missing statistical fluctuations it would be normal to define a significant signal as 5σ , or $n^2 = 25$. Instead, sufficient significance was defined as $n^2 = 31.25$, by adding a somewhat arbitrary safety margin; this allows for the usual 5σ plus a downwards fluctuation of up to 2.5σ anywhere else in the plot. Equation 8.193 was solved for N , which was then converted into the running time required to collect N events. This procedure was repeated for many different values of x_0 to obtain Fig. 8.18. The solid line shows, for the $D_s^- \pi^+$ mode, the number of years needed to obtain a measurement with a significance of 5σ plus the safety margin. The safety margin reduces the x_s reach at 3 years by only 3 or 4 units of x_s . For small values of x_s , the effect of the safety margin is not visible. The dashed line shows the same information but for the $J/\psi \bar{K}^{*0}$ mode; for this mode the effect of the safety margin is similarly small.

Inspection of Fig. 8.18 shows that, using the $D_s^- \pi^+$ mode, BTeV is capable of observing all x_s less than 75 in one year of running, which is equivalent to an integrated luminosity of 2 fb^{-1} .

8.6.4 Summary of Projections for Mixing

The Standard Model expectation for B_s mixing is $22 < x_s < 31$ [87]. All three experiments CDF, DØ and BTeV have shown that they will be able to reconstruct a substantial amount of B_s decays which will allow for mixing studies.

With 2 fb^{-1} CDF and BTeV safely cover the range for mixing as predicted by the Standard Model. The CDF sensitivity for a 5 standard deviation observation reaches from x_s values of 59 to 74 depending on the event yields and the signal-to-background ratios. BTeV's sensitivity comfortably covers x_s values of 75 with even some conservative safety margins included. Due to the large event yields CDF will be able to observe B_s mixing within the first few month of data taking provided that the displaced track trigger and the silicon detector work as advertised.

Once the oscillations are observed the statistical uncertainty on x_s will be small and in conjunction with an accurate B^0 mixing measurement it will constitute a stringent constraint on the unitarity triangle.

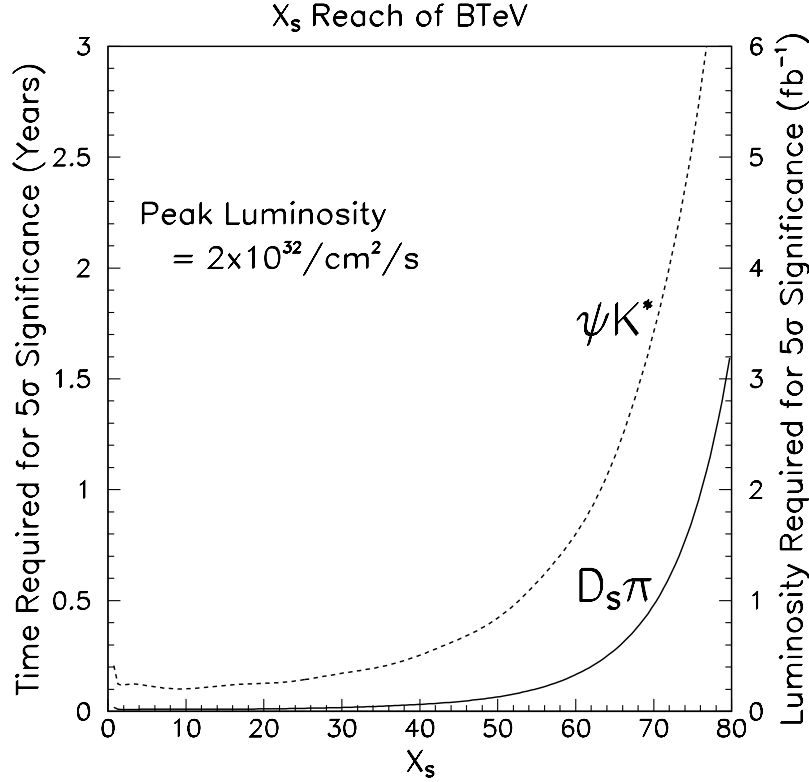


Figure 8.18: The x_s reach of the BTeV detector. The curves indicate the number of years of running which are required to make a measurement of x_s with a statistical significance of 5σ ; a safety margin, discussed in the text, has been included in the definition of 5σ . The curves are for the two different decay modes indicated on the figure.

8.7 Projections for $\Delta\Gamma$

8.7.1 B_s Lifetime Difference in CDF[†]

The promise of large B_s samples in Run II puts in reach the measurement of the width difference between the two weak eigenstates of this meson. With its analysis of semileptonic decays in Run I, CDF has already published a limit of $\Delta\Gamma_s/\Gamma_s < 0.85$ at 95% confidence level [96]. This limit was established by fitting the lifetime distribution of the ℓD_s events with two exponentials.

In Run II, however, it becomes possible to measure the lifetime of samples in which the weak eigenstates are separated: for instance, 2 fb^{-1} of data yield approximately 4000 $B_s \rightarrow J/\psi \phi$ events, which is expected to be dominated by the shorter-lived eigenstate, B_s^H , and for which an angular analysis is used to separate the two components [98]. Further it is expected to yield roughly 75,000 of flavor-specific $B_s \rightarrow D_s \pi$ and $B_s \rightarrow D_s \pi \pi \pi$ decays, which are well-defined mixtures of B_s^H and B_s^L .

[†]Authors: Ch. Paus, J. Tseng

It is straightforward to show that computing the difference between two lifetimes has more statistical power than fitting for two exponentials or fitting for $\Delta\Gamma_s$ in B_s mixing in flavor-specific samples. The leading term in taking the difference between two measured lifetimes is $\Delta\Gamma_s$. On the other hand, the lifetime distribution in a flavor-specific sample is

$$f(t) = \Gamma_H \left[e^{-\Gamma_H t} + e^{-\Gamma_L t} \right] = \Gamma_H e^{-\bar{\Gamma} t} \left[e^{-\Delta\Gamma t/2} + e^{+\Delta\Gamma t/2} \right] = \Gamma_H e^{-\bar{\Gamma} t} \left[1 + \left(\frac{\Delta\Gamma t}{2} \right)^2 + \dots \right], \quad (8.194)$$

where $\Delta\Gamma$ enters as a second-order effect.

The B_s decay to $D_s^+ D_s^-$ is another valuable source of information to determine the lifetime difference of the B_s meson. First of all $D_s^+ D_s^-$ is a pure CP even eigenstate and thus its lifetime is a clean measurement of the CP even lifetime. In addition its branching fraction directly measures $\Delta\Gamma/\Gamma$ under certain theoretical assumptions [99]. The complication in this particular decay mode comes from the associated production of $D_s^{*\pm}$.

8.7.1.1 Lifetime Difference Measurements

$B_s \rightarrow J/\psi \phi$ The decay mode $B_s \rightarrow J/\psi \phi$ has been analyzed at CDF in two Run I analyses, examining its lifetime [106] and angular distributions [98] separately. The basic strategy for Run II is to combine these two analyses into a maximum likelihood fit of the proper decay time, and *transversity angle* of each candidate. In addition to account properly for the background the invariant mass distribution will be simultaneously fitted.

The transversity angle, θ_T , is defined by the angle between the μ^+ and the z axis in the rest frame of the J/ψ decay, where the z axis is orthogonal to the plane defined by the ϕ and the K^+ directions. This angle allows to distinguish CP even and CP odd components: the probability density function for the CP even component is $\frac{3}{8}(1 + \cos^2 \theta_T)$ and for the CP odd component is $\frac{3}{4}\sin^2 \theta_T$. The amplitude of the CP even component sums the squares of the unpolarized and linearly polarized state amplitudes, $|A_0|^2 + |A_{||}|^2$, of the ϕ in the J/ψ rest frame, and the CP odd component the square of the transversely polarized state amplitude, $|A_{\perp}|^2$, of the same. The analysis depends upon the weak eigenstates being also CP eigenstates which is a good approximation for the $B_s \rightarrow J/\psi \phi$ decays.

A toy Monte Carlo study was performed to estimate the uncertainty in $\Delta\Gamma_s$ with 4000 $B_s \rightarrow J/\psi \phi$ decays. The background shapes in mass and proper decay time and the relative fraction of the signal to the background were assumed to be identical to that in the Run I lifetime analysis. The mass resolution was assumed to be the same as in Run I, and all the lifetime distributions were convoluted with the 18 μm resolution projected for Run II. The background was assumed to have a flat transversity angle distribution.

The error on $\Delta\Gamma_s/\Gamma_s$ depends on the CP admixture of the final state. The decay $B_s \rightarrow J/\psi \phi$ is dominated by CP even eigenstates. Therefore the smaller the admixture of CP odd component the larger the sensitivity. Assuming the CP composition as measured in Run I [98] corresponding to a CP even fraction of 0.77 ± 0.19 the expected uncertainty on $\Delta\Gamma_s/\Gamma_s$ is 0.05. This uncertainty varies between 0.08 and 0.035 for CP even fractions of 0.5 and 1.0, respectively.

$B_s \rightarrow D_s^{(*)+} D_s^{(*)-}$ The decay modes $B_s \rightarrow D_s^{(*)+} D_s^{(*)-}$ are also promising for lifetime difference studies, though with smaller sample sizes. These decays are expected to be present among the two-track trigger data. The decay $B_s \rightarrow D_s^+ D_s^-$, in particular, is purely CP even, and requires no angular analysis. Its companion decays, involving D_s^* decays, are expected in the heavy quark limit, and in the absence of CP violation, to be sensitive to CP -even B_s states as well [101]. While these decays are attractive in that they significantly increase the sample size over that of $B_s \rightarrow D_s^+ D_s^-$ alone, their identification is a challenge, since the missing photons from the decay $D_s^{*+} \rightarrow D_s^+ \gamma$ and $D_s^{*+} \rightarrow D_s^+ \pi^0$ considerably broaden the $D_s^+ D_s^-$ invariant mass distribution. On the other hand, the missing mass introduces only about 3% to the proper lifetime resolution.

In a full GEANT based simulation and reconstruction of $B_s \rightarrow D_s^{(*)+} D_s^{(*)-}$ in the CDF detector it is found that the three different cases are separated quite cleanly by using the invariant mass spectrum of the charged decay products. Shifts in the invariant B_s mass are due to the neutral particles which are not reconstructed. PYTHIA has been used to generate $b\bar{b}$ quarks and fragment them to b hadrons. The B_s mesons are decayed using the CLEOMC program according to the branching ratios given in Table 8.8.

In Figure 8.19 the invariant mass spectra of the three different cases are depicted. The spectra are essentially free of combinatoric background since the reconstructions of the resonances at each step allow stringent cuts. For this picture the D_s is always decayed into $K^{*0} K$ which has more combinatorics than the $\phi\pi$ decay mode due to the large width of the K^{*0} .

To estimate the error on the $\Delta\Gamma_s/\Gamma_s$ from this channel several assumptions have to be made since this mode has not been reconstructed in Run I.

In the most conservative estimate only $B_s \rightarrow D_s D_s$ is used which is a clean CP even state. GEANT based Monte Carlo studies indicate that a signal to background fractions of 1:1 - 1:2 are achievable. This is similar to signal to background fraction achieved for the decay mode $B_s \rightarrow \nu\ell D_s$, measured in Run I. The expected error on the lifetime is 0.044 ps is obtained using an event sample of 2.5k events and a signal to background fraction of 1:1.5. This converts into an error on $\Delta\Gamma_s/\Gamma_s$ of 0.06.

Assuming that also the other two decay modes involving D_s^* mesons are clean CP even modes a total of 13k events are available. The estimated error on $\Delta\Gamma_s/\Gamma_s$ is then reduced to 0.025.

8.7.1.2 Related Branching Fractions

The decay modes $B_s \rightarrow D_s^{(*)+} D_s^{(*)-}$ are also interesting because it is expected that they are the largest contribution to the actual difference between the heavy and light widths. Indeed, the other decay modes are estimated to contribute less than 0.01 to the projected ~ 0.15 value of $\Delta\Gamma_s/\Gamma_s$ [102]. The branching fraction to this final state is in the small velocity (SV) limit related to $\Delta\Gamma_s$ by

$$\mathcal{B}(B_s^H \rightarrow D_s^{(*)+} D_s^{(*)-}) = \frac{\Delta\Gamma_s}{\Gamma_s(1 + \frac{\Delta\Gamma_s}{2\Gamma_s})}. \quad (8.195)$$

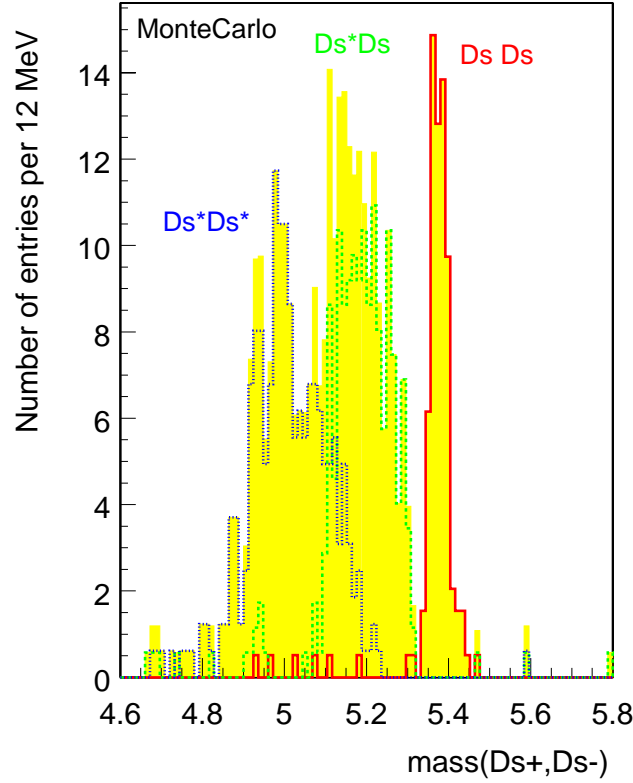


Figure 8.19: D_s^+, D_s^- invariant mass spectra for the three decay modes $B_s \rightarrow D_s D_s$ (solid), $B_s \rightarrow D_s^{(*)} D_s$ (large dashes) and $B_s \rightarrow D_s^{(*)} D_s^{(*)}$ (small dashes). The D_s is always decayed into $K^{*0} K$. The shaded background is the sum of the three decay modes.

This method has been exploited by ALEPH, using $\phi\phi$ correlations, to obtain a value of $\Delta\Gamma_s/\Gamma_s = 0.25_{-0.14}^{+0.21}$ [103]. However the small velocity assumption also referred to a Shifman-Voloshin limit may be very approximative.

The following estimates are made assuming the validity of this limit. Further when measuring branching fractions many systematic effects have to be considered. For example the tracking efficiency for the kinematics of the particular decays has to be determined carefully. Since it is difficult if not impossible to predict those effects only the statistical uncertainties are discussed below.

The statistical error on the branching fraction for 13k events (see Table 8.10) with a signal to background ratio of 1:1 is 0.012. Following Equation 8.195 the turns out to be also the statistic uncertainty on $\Delta\Gamma_s/\Gamma_s$ since the branching ratio is very small. This uncertainty deteriorates to 0.015 when making the signal to background ratio 1:2.

8.7.1.3 Combined CDF Projection

With the analysis possibilities discussed thus far, the lifetime difference method conservatively yields a statistical uncertainty of 0.04 on $\Delta\Gamma_s/\Gamma_s$, utilizing both $J/\psi\phi$ and $D_s^+D_s^-$ decays and just using the lifetime measurements.

If one assumes that the decay modes involving D_s^* are also mostly CP even the sample for the lifetime measurement is extended and the branching ratios can be used in the SV limit. This decreases the statistical uncertainty on $\Delta\Gamma_s/\Gamma_s$ to 0.01.

These numbers refer to the projected Run II luminosity of 2 fb^{-1} and bear all the caveats mentioned in the text.

8.7.2 Estimate of Sensitivity on $\Delta\Gamma$ in BTeV[†]

Since $\Delta\Gamma_{B_s}$ is expected to be much larger than $\Delta\Gamma_{B^0}$, only projections for measurements of $\Delta\Gamma_{B_s}$ have been studied at BTeV for this report. The B_s^0 decay modes studied include CP -even, CP -mixed and flavor specific decay modes and are listed in Table 8.19. The total decay rate for the flavor specific decay $B_s^0 \rightarrow D_s^- \pi^+$ is given by the average of the CP -even and CP -odd rates. The decays $B_s^0 \rightarrow J/\psi\eta$, $J/\psi\eta'$ should be CP -even while the decay to $J/\psi\phi$ is predominantly CP -even.

B_s^0 Decay Mode	CP Mode	Branching Ratio	BR Used
$J/\psi\phi$	Mostly CP -even	$(9.3 \pm 3.3) \times 10^{-4}$	8.9×10^{-4}
$J/\psi\eta$	CP -even	< 0.0038	3.3×10^{-4}
$J/\psi\eta'$	CP -even	< 0.0038	6.7×10^{-4}
$D_s^- \pi^+$	Flavor specific	< 0.13	3.0×10^{-3}

Table 8.19: The B_s^0 decay modes studied for $\Delta\Gamma_{B_s}$ sensitivity studies at BTeV.

CDF has measured the CP -odd fraction of total rate for $J/\psi\phi$ to be $0.229 \pm 0.188(stat) \pm 0.038(syst)$ [104]. The all charged mode decay $B_s^0 \rightarrow K^+K^-$ has a large enough expected branching fraction ($\sim 1 \times 10^{-5}$) and reconstruction efficiency to get high statistics. However although the K^+K^- final state is CP -even, the decay can proceed via both a CP conserving Penguin contribution as well as a CP violating Tree level contribution. Unless the Penguin contribution is completely dominant or the Penguin and Tree level contributions can be exactly calculated it would be difficult to use this mode without significant theoretical errors.

8.7.2.1 Signal yields and backgrounds

Estimation of the signal yields and signal/background ratios were determined using a MC-FAST simulation for the B_s^0 decay mode to $J/\psi\phi$, while all the other modes were simulated using a Geant simulation of BTeV. Although it is easy to simulate the signal to determine

[†]Author: H.W.K. Cheung.

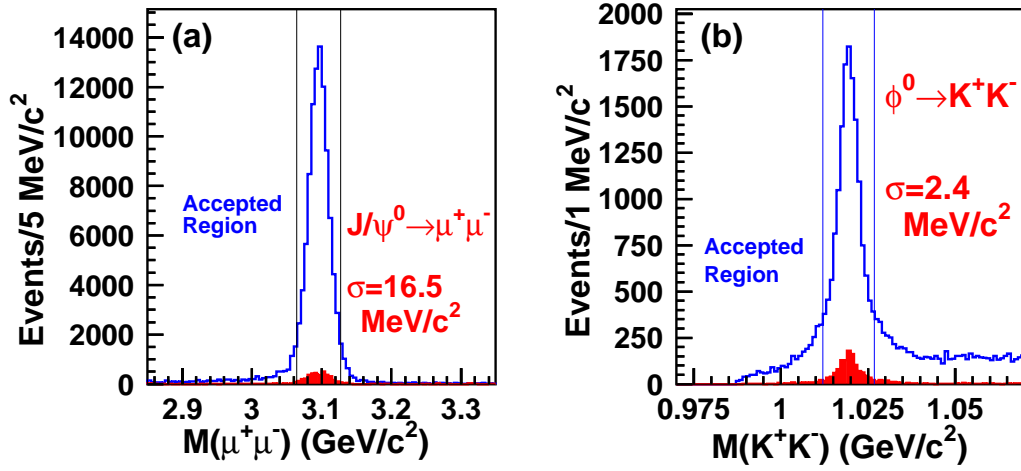


Figure 8.20: (a) The $\mu^+\mu^-$ invariant mass and (b) the K^+K^- invariant mass for a $b\bar{b} \rightarrow J/\psi \phi X$ background sample (open histogram) and for an appropriately normalized $B_s^0 \rightarrow J/\psi \phi$ signal sample (filled histogram).

the reconstruction efficiency, the background simulation can be more troublesome. The signal sample always has an average of two embedded min-bias events. Since it takes too much time to generate enough background one has to determine which backgrounds are dominant for a particular decay.

The decay $B_s^0 \rightarrow J/\psi \phi$ was studied through the decay channels $J/\psi \rightarrow \mu^+\mu^-$ and $\phi \rightarrow K^+K^-$. Studies show that since the $J/\psi \rightarrow \mu^+\mu^-$ is expected to be so clean, the dominant backgrounds come from $b\bar{b} \rightarrow J/\psi X$. For this study only backgrounds from $b\bar{b} \rightarrow J/\psi \phi X$ have been studied. Figure 8.20(a) shows the $\mu^+\mu^-$ invariant mass for a $b\bar{b} \rightarrow J/\psi \phi X$ background sample compared to an appropriately normalized signal sample of $B_s^0 \rightarrow J/\psi \phi$. The two muons were required to form a vertex with a confidence level of greater than 1%. Figure 8.20(b) shows a similar comparison for the K^+K^- invariant mass, again with a vertex requirement of $CL > 1\%$.

Figure 8.21(a) shows the $\mu^+\mu^- K^+K^-$ invariant mass for the $b\bar{b} \rightarrow J/\psi \phi X$ background sample without requiring that the $\mu^+\mu^-$ and K^+K^- masses are consistent with the J/ψ and ϕ masses respectively. The four tracks are required to form a single vertex with a confidence level greater than 1%. This is compared in the plot to an appropriately normalized signal sample. Figure 8.21(b) shows the $J/\psi \phi$ invariant mass plot with vertexing and requirements on the $\mu^+\mu^-$ and K^+K^- masses. The $\mu^+\mu^-$ and K^+K^- masses are required to be within $\pm 2\sigma$ of the true J/ψ and ϕ masses respectively. Both signal and backgrounds are included in the plot and compared to the signal only sample. The signal/background ratio is seen to increase when one applies a primary-to-secondary vertex detachment requirement of $L/\sigma_L > 15$ in Figure 8.21(c). Where L is the 3-dimensional distance between the primary vertex and the B_s^0 decay vertex and σ_L is the error on L calculated for each candidate B_s^0 decay. For $L/\sigma_L > 15$ the reconstruction efficiency is 6.0%, and the signal/background ratio is 47/1 with an error of 32% for the backgrounds considered.

Table 8.20 shows projections for the $B_s^0 \rightarrow J/\psi \phi$ signal yields for 2 fb^{-1} . A total $b\bar{b}$

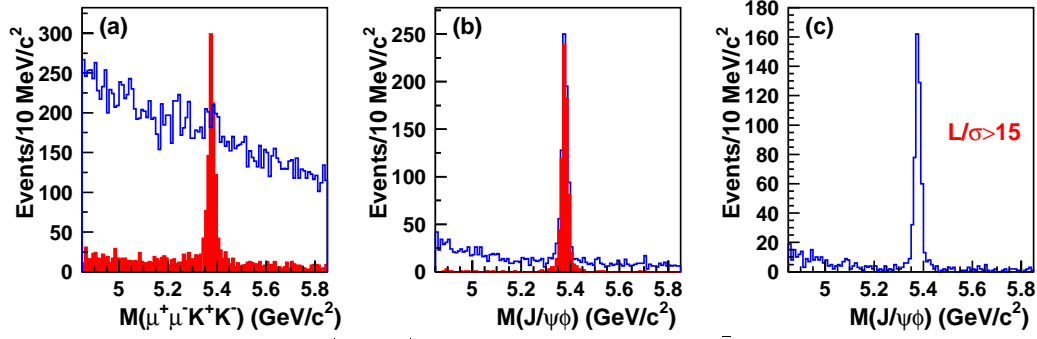


Figure 8.21: (a) The $\mu^+\mu^-K^+K^-$ invariant mass for a $b\bar{b} \rightarrow J/\psi\phi X$ background sample (open histogram) and for a correctly normalized $B_s^0 \rightarrow J/\psi\phi$ signal sample (filled histogram). (b) $J/\psi\phi$ invariant mass for the background plus signal sample (open histogram) compared to just the signal sample (filled histogram). (c) $J/\psi\phi$ mass for $L/\sigma_L > 15$.

production cross-section of $100 \mu\text{b}$ is assumed and we take the fraction of B_s^0/\overline{B}_s^0 per $b\bar{b}$ from Pythia as 1 in 4.3. The branching fraction of $B_s^0 \rightarrow J/\psi\phi$ is taken to be equal to $BR(B_d^0 \rightarrow J/\psi K^0) = 8.9 \times 10^{-4}$. A total of ~ 41400 signal events is expected for 2 fb^{-1} . The expected error on the lifetime for 2 fb^{-1} was determined with a toy Monte Carlo generating 1000 experiments with 41400 signal events and $S/B=47$. The background lifetime distribution was simulated with a short and a long lifetime component as seen in the background studies and is typical of backgrounds seen in fixed target experiments. In the toy MC the short and long components were set to be 0.33 and 1.33 ps respectively. A binned likelihood fit was used to extract the measured lifetime for each of the 1000 experiments, where the lifetime distribution from sidebands is used as a measure of the lifetime distribution in the signal B_s^0 mass region. The method is described in Reference [105]. The expected error is taken to be the *r.m.s.* of the 1000 measured lifetimes and is 0.50%.

Quantity	Value		
Number of $b\bar{b}$	2×10^{11}		
Number of B_s^0/\overline{B}_s^0	4.7×10^{10}		
	$B_s^0 \rightarrow J/\psi\phi$	$B_s^0 \rightarrow D_s^- \pi^+$	
	$J/\psi \rightarrow \mu^+\mu^-$	$D_s^- \rightarrow \phi\pi^-$	$D_s^- \rightarrow K^{*0}K^-$
	$\phi \rightarrow K^+K^-$	$\phi \rightarrow K^+K^-$	$K^{*0} \rightarrow K^+\pi^-$
# of Events	1.2×10^6	2.5×10^6	3.1×10^6
Reconstruction efficiency (%)	6.0	2.7	2.3
S/B	47:1		3:1
L1 Trigger efficiency (%)	70		74
L2 Trigger efficiency (%)	90		90
# of reconstructed decays	41400	91700	

Table 8.20: Projections for yields of B_s^0 decays for 2 fb^{-1} assuming a total $b\bar{b}$ production cross-section of $100 \mu\text{b}$.

Although the $J/\psi\phi$ signal sample can be obtained through the $J/\psi \rightarrow \mu^+\mu^-$ trigger,

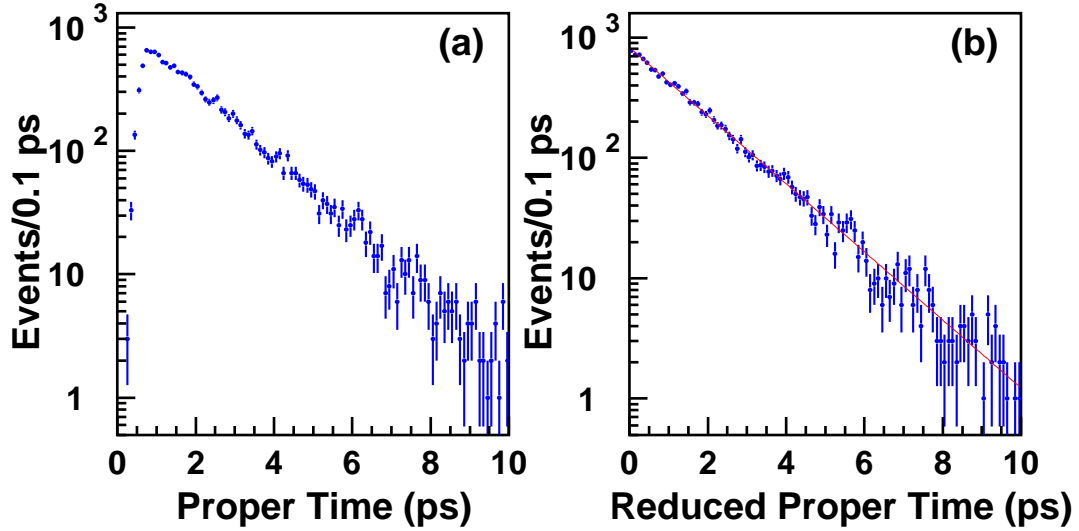


Figure 8.22: (a) Proper time distribution for reconstructed $B_s^0 \rightarrow J/\psi \phi$; (b) Reduced proper time distribution for the same decays, the line is an exponential fit.

the effect of the Level 1 vertex trigger on this mode was studied to determine the effect of the L1 trigger on the lifetime analysis. Figure 8.22(a) shows the proper time ($t = L/\beta\gamma c$) distribution for reconstructed $B_s^0 \rightarrow J/\psi \phi$ signal events for a $L/\sigma_L > 15$ requirement. The loss of short lifetime decays is due to the detachment requirement. One can obtain an exponential distribution if we use the reduced proper time, $t' = t - N\sigma_L/\beta\gamma c$, for a $L/\sigma_L > N$ requirement. This starts the clock at the minimum required decay time for each decay candidate and works because the lifetime follows an exponential distribution irrespective of when the clock is started. Figure 8.22(b) shows the reduced proper time distribution and an exponential fit gives a lifetime of 1.536 ± 0.014 ps, compared to the generated lifetime of 1.551 ps.

Figure 8.23(a) shows the reduced proper time after applying the Level 1 vertex trigger. Short lifetime decays are again lost because the impact parameter requirements of the Level 1 trigger effectively gives a larger minimum required decay time than $N\sigma_L/\beta\gamma c$. The lifetime acceptance function is just the observed reduced proper distribution divided by a pure exponential with the generated lifetime and is given in Figure 8.23(b). In order to extract the correct lifetime from the observed reduced proper time distribution one needs the correct lifetime acceptance function. This is obtained from Monte Carlo and can be checked by using decays modes like $J/\psi \phi$ that can be obtained with the L1 vertex trigger and separately through the L1 $J/\psi \rightarrow \mu^+\mu^-$ dimuon trigger which has no vertexing selection criteria. The L1 trigger lifetime acceptance correction obtained from MC can also be checked by taking samples of prescaled triggers that do not have the L1 trigger requirement.

Note that since the L1 trigger can increase the effective minimum required decay time cut, if one puts on a large impact parameter selection requirement on the B decay daughters, it may be possible to redefine the reduced proper time to take this into account and thereby reduce the lifetime acceptance corrections with some loss of statistics. This still needs to be studied and the details of the L1 trigger may change since one may be able to redesign

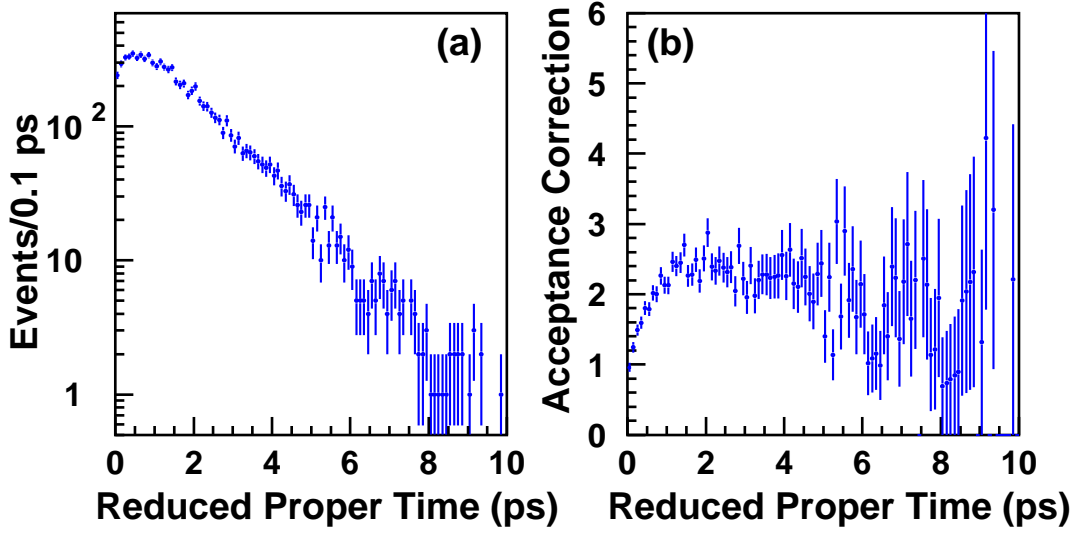


Figure 8.23: (a) Reduced proper time distribution for reconstructed $B_s^0 \rightarrow J/\psi \phi$ decays that pass the Level 1 vertex trigger; (b) Lifetime correction function, obtained by dividing the distribution in (a) by a pure exponential distribution with the generated B_s^0 lifetime.

it to reduced the lifetime acceptance correction.

When an acceptance correction like that given in Figure 8.23(b) is simulated in the toy Monte Carlo, the expected error on the measured lifetime increases to 0.58%, from the previous value of 0.50%. For the decay mode $B_s^0 \rightarrow D_s^- \pi^+$ where the signal to background is smaller the effect is similar, the error increases to 0.44% when adding the acceptance correction effects compared to 0.39%.

Tables 8.21 and 8.20 show the expected signal yields and signal/background ratios for the decays modes $B_s^0 \rightarrow J/\psi \eta$, $B_s^0 \rightarrow J/\psi \eta'$ and $B_s^0 \rightarrow D_s^- \pi^+$. Backgrounds from $b\bar{b} \rightarrow J/\psi X$ were studied for the decay modes $B_s^0 \rightarrow J/\psi \eta^{(\prime)}$, while backgrounds from $b\bar{b} \rightarrow D_s^+ X$ were included in the $B_s^0 \rightarrow D_s^- \pi^+$ analysis. Details of the analyses of these modes can be found in Reference [94]. Expected errors on the lifetimes were determined using toy Monte Carlo simulations as before, where acceptance corrections were also simulated for the $D_s^- \pi^+$ mode. Table 8.22 gives the expected errors on the lifetimes for all modes.

Note that although only backgrounds from $b\bar{b} \rightarrow J/\psi \phi X$ were included in the study of $B_s^0 \rightarrow J/\psi \phi$ to obtain the value of S/B=47/1, the effect of lower values of S/B were studied. If the S/B is decreased to 10/1 which is the expected level for $B_d^0 \rightarrow J/\psi K_s^0$ [94], the expected error on the measured lifetime only increases from 0.50% to 0.51% for 2 fb^{-1} . (For a much lower S/B=3/1 the expected error would be 0.58%.)

8.7.2.2 Results for $\Delta\Gamma/\Gamma_{B_s}$ Sensitivity

With just two lifetime measurements, like τ_{CP+} and τ_{CP-} , which are defined as $\tau_{CP+} = 1/\Gamma(B_s^{\text{even}})$ and $\tau_{CP-} = 1/\Gamma(B_s^{\text{odd}})$, one can determine the error on $\Delta\Gamma_{CP}/\Gamma$ from the errors

Quantity	Value		
Number of $b\bar{b}$	2×10^{11}		
Number of B_s^0/\bar{B}_s^0	4.7×10^{10}		
	$B_s^0 \rightarrow J/\psi\eta$	$B_s^0 \rightarrow J/\psi\eta'$	
	$J/\psi \rightarrow \mu^+\mu^-$		
	$\eta \rightarrow \gamma\gamma$	$\eta' \rightarrow \rho^0\gamma$	$\eta' \rightarrow \pi^+\pi^-\eta$
# of Events	3.5×10^5	5.4×10^5	3.2×10^5
Reconstruction efficiency (%)	0.71	1.2	0.60
S/B	15:1		30:1
L1 Trigger efficiency (%)	75		85
L2 Trigger efficiency (%)	90		90
# of reconstructed decays	1700		6400

Table 8.21: Projections for yields of B_s^0 decays for 2 fb^{-1} assuming a total $b\bar{b}$ production cross-section of $100 \mu\text{b}$.

Decay Mode	Error on Lifetime (%)		
	2 fb^{-1}	10 fb^{-1}	20 fb^{-1}
$J/\psi\phi$	0.50	0.23	0.16
$J/\psi\eta$	2.49	1.19	0.80
$J/\psi\eta'$	1.36	0.55	0.39
$D_s^-\pi^+$	0.44	0.20	0.14

Table 8.22: Projections for statistical errors on lifetimes measured in different modes for 2, 10 and 20 fb^{-1} .

on the two lifetimes:

$$\sigma_{\frac{\Delta\Gamma_{CP}}{\Gamma}} = 4 \frac{\tau_{CP+}\tau_{CP-}}{(\tau_{CP+} + \tau_{CP-})^2} \sqrt{\left(\frac{\sigma_{\tau_{CP+}}}{\tau_{CP+}}\right)^2 + \left(\frac{\sigma_{\tau_{CP-}}}{\tau_{CP-}}\right)^2}, \quad (8.196)$$

where $\Delta\Gamma_{CP} = \Gamma(B_s^{\text{even}}) - \Gamma(B_s^{\text{odd}})$ and $\Gamma = (\Gamma(B_s^{\text{even}}) + \Gamma(B_s^{\text{odd}}))/2$. In the case that one measures τ_{CP+} and τ_{FS} where $\tau_{FS} = 2/(\Gamma(B_s^{\text{even}}) + \Gamma(B_s^{\text{odd}}))$, the error on $\Delta\Gamma_{CP}/\Gamma$ is

$$\sigma_{\frac{\Delta\Gamma_{CP}}{\Gamma}} = 2 \frac{\tau_{FS}}{\tau_{CP+}} \sqrt{\left(\frac{\sigma_{\tau_{CP+}}}{\tau_{CP+}}\right)^2 + \left(\frac{\sigma_{\tau_{FS}}}{\tau_{FS}}\right)^2}. \quad (8.197)$$

It can be seen that for small $\Delta\Gamma_{CP}/\Gamma$, the error is about 2 times larger when one measures with similar errors τ_{CP+} and τ_{FS} compared to measuring τ_{CP+} and τ_{CP-} . Using τ_{CP+} from the $J/\psi\eta^{(\prime)}$ decay modes and τ_{FS} from $D_s^-\pi^+$, we project an error on $\Delta\Gamma_{CP}/\Gamma$ of 0.027 for $\Delta\Gamma_{CP}/\Gamma = 0.15$ for 2 fb^{-1} .

Including the lifetime measurement for the decay mode to $J/\psi\pi$ is more complicated as this is not an equal mixture of CP -even and CP -odd rates. Although a combined lifetime and angular analysis should be done to determine the fraction of CP -odd decay in this mode, and the appropriate error on τ_{CP+} , it was not done for this study. A simpler determination

is made assuming that the fraction of CP -odd has already been determined within some error in a separate analysis or in some other experiment. If the lifetime for this decay mode is defined by $\tau_X = 1/\Gamma_X$ where $\Gamma_X = (1-f)\Gamma(B_s^{even}) + f\Gamma(B_s^{odd})$, then

$$\frac{\Delta\Gamma_{CP}}{\Gamma} = \frac{2(\tau_{FS} - \tau_X)}{(1-2f)\tau_X}, \quad (8.198)$$

$$\sigma_{\frac{\Delta\Gamma_{CP}}{\Gamma}} = \frac{2\tau_{FS}}{(1-2f)\tau_X} \sqrt{\left(\frac{\sigma_{\tau_X}}{\tau_X}\right)^2 + \left(\frac{\sigma_{\tau_{FS}}}{\tau_{FS}}\right)^2 + \left(\frac{\tau_{FS} - \tau_X}{\tau_{FS}}\right)^2 \frac{4f^2}{(1-2f)^2} \left(\frac{\sigma_f}{f}\right)^2}.$$

Setting the value of f to the central valued measured by CDF and assuming the total error can be improved in Run 2 by a factor of $\sqrt{20}$, then for $f = 0.229 \pm 0.043$ and using the $J/\psi \phi$ and $D_s^- \pi^+$ modes only, the projected error on $\Delta\Gamma_{CP}/\Gamma$ is 0.035 for $\Delta\Gamma_{CP}/\Gamma = 0.15$ and 2 fb^{-1} . Although reducing the error on f has only a small effect on the projected error on $\Delta\Gamma_{CP}/\Gamma$, the actual value of f has a huge effect, since as f approaches 0.5 we lose all sensitivity to $\Delta\Gamma_{CP}$ when only comparing to the $D_s^- \pi^+$ mode. It can be seen that even with relatively low statistics, the $J/\psi \eta^{(\prime)}$ decay modes are just as sensitive to $\Delta\Gamma_{CP}$.

Table 8.23 shows the projected errors on $\Delta\Gamma_{CP}/\Gamma$ for different integrated luminosities for the two different combinations of modes used. The error on f is assumed to reduced by \sqrt{R} where R is the ratio of integrated luminosities. The total projected error when all modes are used is also shown. To determine the expected error when all modes are used, a likelihood fit is used where f is constrained by a Gaussian probability likelihood term to be within the 0.043 error of the central value of 0.229. Note that the projected errors have a weak dependence on the value of $\Delta\Gamma_{CP}/\Gamma$ used but a strong dependence on the value of f used. It should also be noted that we are assuming that any systematic errors are insignificant compared to the statistical errors, so that these projected statistical errors are taken as the total error on $\Delta\Gamma_{CP}/\Gamma$. For the range of lifetime errors we are considering this assumption is reasonable since the charm lifetimes can be measured to this level in fixed target experiments with only small systematics. However the lifetime acceptance correction in BTeV may be somewhat larger for the hadronic modes.

Decay Modes Used	Error on $\Delta\Gamma_{CP}/\Gamma$		
	2 fb^{-1}	10 fb^{-1}	20 fb^{-1}
$J/\psi \eta^{(\prime)}, D_s^- \pi^+$	0.0273	0.0135	0.0081
$J/\psi \phi, D_s^- \pi^+$	0.0349	0.0158	0.0082
$J/\psi \eta^{(\prime)}, J/\psi \phi, D_s^- \pi^+$	0.0216	0.0095	0.0067
with $\Delta\Gamma_{CP}/\Gamma = 0.03$	0.0198	0.0088	0.0062
with $f = 0.13$	0.0171	0.0077	0.0054
with $f = 0.33$	0.0258	0.0112	0.0078

Table 8.23: Projections for statistical errors on $\Delta\Gamma_{CP}/\Gamma$ for combining lifetimes from different modes and for using all modes for 2, 10 and 20 fb^{-1} . The values $\Delta\Gamma_{CP}/\Gamma = 0.15$ and $f = 0.229$ are used for the main results and the results for other values of $\Delta\Gamma_{CP}/\Gamma$ and f are also shown for comparison.

The statistical error can be improved by including also the $J/\psi \rightarrow e^+e^-$ decay mode

for the J/ψ reconstruction. The increase in statistics is less than by a factor of 2 since the BTeV ECAL acceptance is smaller than the muon detector and there is no dedicated $J/\psi \rightarrow e^+e^-$ trigger.

It should also be noted that additional measurements of the CP -even rate and especially of the CP -odd rate, even with low statistics, can have a very significant effect on the $\Delta\Gamma_{CP}/\Gamma$ sensitivity. Unfortunately the CP -odd modes look difficult experimentally. For example, two CP -odd modes are $B_s^0 \rightarrow J/\psi f_0(980)$ and $B_s^0 \rightarrow \chi_{c0} \phi$. The $f_0(980)$ is relatively broad compared to the ϕ^0 and decays to $\pi\pi$ or KK and thus will have large backgrounds. The χ_{c0} has small branching fractions, and the dominant decays are to non-resonant states with pions and kaons and thus will also be background challenged. However it will still be worthwhile looking for these CP -odd states.

8.7.3 Summary of Projections for $\Delta\Gamma$

The most sensitive direct measurement of $\Delta\Gamma_{B_s}$ will be from measuring the lifetime differences between decays to CP -specific final states, (*i.e.* to CP -even, CP -odd or CP -mixed modes) and flavor specific decays.

The decay modes to flavor specific final states like $D_s\pi$ will be the most precisely measured. Other decays with larger branching fractions that can be reconstructed with high efficiency and good signal-to-background will be to CP -mixed final states, like $J/\psi \phi$ and $D_s^{(*)+} D_s^{(*)-}$ involving at least one $D_s^{(*)}$. These decays proceed through an unknown admixture of CP -even and CP -odd amplitudes that must be determined experimentally via an angular analysis. The error on $\Delta\Gamma_s/\Gamma_s$ obtained using these modes will be very sensitive to the actual fractions of CP -even and CP -odd, where the sensitivity is poorest for equal mixtures of CP -even and CP -odd.

The decays to purely CP -even or purely CP -odd final states are difficult experimentally, either because the backgrounds are larger and/or the branching fractions are small (*e.g.* for $D_s^+ D_s^-$, $J/\psi K_s$ and $J/\psi f_0(980)$), or they contain difficult to reconstruct neutrals in the final state (*e.g.* like in $J/\psi \eta^{(\prime)}$). However it is important to try to use these decay modes as even with small samples of events they improve the error on the $\Delta\Gamma_s/\Gamma_s$ measurement significantly.

With 2 fb^{-1} CDF should be able to determine $\Delta\Gamma_s/\Gamma_s$ with a statistical error of 0.04 through lifetime measurements, improving to as good as 0.025 if the decay to $D_s^{*+} D_s^{*-}$ proceeds through a 100% CP -even amplitude. CDF can reach a statistical error of 0.01 on a *model dependent* determination of $\Delta\Gamma_s/\Gamma_s$ using just branching ratio measurements.

With a vertex (hadronic) trigger at Level-1 and excellent particle identification and neutral reconstruction, the BTeV experiment should be able to measure the lifetimes of the purely CP -even or purely CP -odd final states well enough to give a model independent determination of $\Delta\Gamma_s/\Gamma_s$ with a statistical error of smaller than 0.02 with 2 fb^{-1} of data. This error is further decreased as low as 0.01 if the decay to $D_s^{*+} D_s^{*-}$ proceeds through a 100% CP -even amplitude. With 20 fb^{-1} of data a statistical error of 0.005 on $\Delta\Gamma_s/\Gamma_s$ should be obtainable. Systematic uncertainties are expected to be under control to a similar level.

8.8 Projections for Lifetimes

8.8.1 b Hadron Lifetimes at CDF[†]

Lifetime measurements have formed an important part of the CDF research program in b physics since the 1992 introduction of the silicon vertex detector with its precision tracking capabilities. This part of the research program has been very successful, producing some of the most precise lifetime measurements with semi-inclusive data samples, but also the most precise measurements with exclusive channels. It is expected that the combination of the Tevatron's large $\bar{b}b$ cross section and precise tracking capabilities will continue to reap benefits in Run II, pushing the comparison between experiment and theoretical calculation to more stringent levels.

A lifetime measurement consists of reconstructing the decay point of a b hadron by tracing back its long-lived charged descendants. For instance, the decay $\bar{B}^0 \rightarrow e^- \bar{\nu}_e D^+ X$ is reconstructed by intersecting the e^- track with the trajectory of the D^+ meson; this trajectory in turn is reconstructed from its own daughters, such as in the decay $D^+ \rightarrow K^- \pi^+ \pi^-$. The distance between the primary interaction vertex and the b decay vertex gives the flight distance of the b hadron. In Run I, this flight distance was measured most precisely in the plane transverse to the beam and the proper time of decay, ct , calculated with the formula

$$ct = \frac{L_{xy} m}{p_T}, \quad (8.199)$$

where L_{xy} is the transverse flight distance, m is the mass of the b hadron, and p_T is the momentum of the b hadron projected in the with respect to the beam direction transverse plane. The transverse momentum is calculated by combining the measured momenta of the charged daughter particles. Unlike the flight distance, this combination requires either the identification and reconstruction of all the daughter particles, as in the analyses of an exclusive hadronic channel, or a correction factor for the particles that are not reconstructed, as in the analyses of much larger semi-inclusive samples. A third possibility, applicable in some special circumstances, allows a constraint to be applied to the momentum of a single particle of known mass; this technique was not applied in Run I but may become more important in Run II with the advent of three-dimensional silicon tracking.

As opposed to the electron-positron machines at the $\Upsilon(4S)$ where only B^+ and B_d^0 mesons are produced, Tevatron produces the full spectrum of b hadrons. Due to this uniqueness in the following particular emphasize is put on lifetime measurements of B_s^0 , B_c^0 and Λ_b .

8.8.1.1 Run I Results at CDF

The Run I CDF lifetime results are summarized in Figure 8.24. They represent a combination of several analyses of different types but have one thing in common: all data samples have been obtained by using the trigger on at least one high-momentum lepton candidate.

[†]Authors: Ch. Paus, J. Tseng.

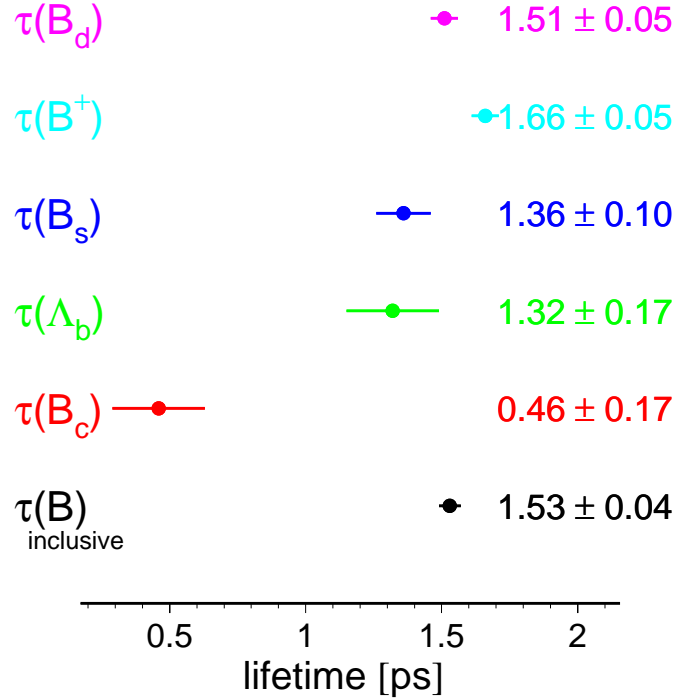


Figure 8.24: Summary of lifetime measurements from CDF during Run I.

Three different types of analyses are performed. There are the exclusive, the semi-exclusive and finally the inclusive analyses. While in the exclusive analyses one or more distinct b hadron decay channels are fully reconstructed, in the semi-inclusive analyses some neutral particle cannot be reconstructed, most typically the neutrino from the semileptonic b hadron decay. In the inclusive analyses the secondary vertex indicates the presence of a b hadron but no attempt is made to reconstruct the mass explicitly.

The features of the different analysis types are complementary. Exclusive analyses usually have small data samples and thus a large statistical uncertainty but the systematic uncertainty is small. Inclusive analyses have usually very large data samples and thus small statistical uncertainties but the systematic errors are large.

The exclusive modes measured also used the J/ψ trigger sample: in Run I, these analyses yield 436 ± 27 decays of the type $B^0 \rightarrow \psi(1S, 2S)K^{(*)0}$, 824 ± 36 of the type $B^+ \rightarrow \psi(1S, 2S)K^{(*)+}$, and 58 ± 12 of the mode $B_s \rightarrow J/\psi \phi$. As will be detailed in the following sections, the B_s lifetime thus measured is expected to mostly reflect the lifetime of the shorter-lived weak eigenstate of the B_s . A small sample of $\Lambda_b \rightarrow J/\psi \Lambda^0$ decays was also reconstructed but was too small for lifetime analysis in light of the large $B^0 \rightarrow J/\psi K_S^0$ backgrounds. The systematic errors are due to background and resolution modeling and detector alignment.

For the semi-exclusive modes the B^0 , B^+ , B_s , and Λ_b hadrons are measured using their semileptonic decays. The charm daughters $D^{(*)}$, D_s , and Λ_c^+ are reconstructed in data.

Since these decays contain neutrinos as well as possible unreconstructed intermediate states such as the D^{**} , they are subject to systematic uncertainties due to production and decay modeling, as well as uncertainties in background and resolution and detector alignment.

An inclusive $b \rightarrow J/\psi X$ lifetime is also measured, where the $J/\psi \rightarrow \mu^+ \mu^-$ is registered on a dilepton trigger, as well as the lifetime of the B_c meson through its decays to $J/\psi \ell X$.

The lifetime measurements have also yielded measurements of the lifetime ratio between charged and neutral B mesons. The measurement of lifetime ratios is particularly interesting since experimental uncertainties and theoretical uncertainties cancel out and thus allow more sensitive tests of some aspects of the theory of heavy quarks. Combining the exclusive and the semileptonic decay modes yields a ratio of 1.09 ± 0.05 in agreement with the world average 1.07 ± 0.02 and both well within the range of the theoretical prediction $1.0 - 1.1$.

The lifetime ratio between B_s and B^0 has not yet been measured with sufficient precision to test the prediction which is within ≈ 1 percent of unity. The experimental value of the lifetime ratio of the Λ_b to the B^0 is of similar precision, but lies well below the current theoretical prediction range of $0.9 - 1.0$. More data is needed to clarify whether there is a discrepancy. From the theoretical point of view baryons are more difficult to calculate and thus the experimental data will hopefully shed some light on this area.

8.8.1.2 Run II Projections for CDF

To derive the expected lifetime uncertainties for the Run II data samples it is assumed that the Run I measurements are statistically limited. This is certainly true for the exclusive decay modes. For the other decay channels it is less clear although experience shows that most systematic errors can be improved when more statistics is available. Therefore in the following only the exclusive measurements are used to estimate the uncertainties on the b hadron lifetime measurements achievable with the Run II data samples. This is a conservative procedure and it is likely that CDF will do better. The increase in statistics for the exclusive decays involving $J/\psi \rightarrow \mu^+ \mu^-$ with respect to Run I is obtained applying simple scale factors as summarized in section 6.2.2.

Leptonic Triggers Considering the lifetime measurement capabilities of CDF in Run II, it is useful as a first step to make a direct extrapolation from the Run I lifetime analyses of exclusive channels. These are shown in Table 8.24, assuming 2 fb^{-1} of J/ψ dimuon triggers with increased muon coverage, lower muon trigger thresholds, and increased silicon tracking cover. The projected uncertainties are only statistical, and, given Run I experience, are likely to be comparable to the levels of systematic uncertainty. Other improvements, not accounted for in the table, include the possibility of a di-electron trigger, which adds approximately 50% more data, and the effect of smaller-radius silicon as well as three-dimensional microstrip tracking, which improves S/N and hence the lifetime measurements.

It is evident from the table that already the projections of only the exclusive decay modes as measured by CDF in Run I improves on the current world-averaged B^-/B^0 lifetime ratio and combined with other experiments, including the B factories, this ratio will be very precisely known.

	Run 1	Run 2	projected
Species	sample size	sample size	$c\tau$ error [ps]
B^-	824	40000	0.01
B^0	436	20000	0.01
B_s	58	3000	0.03
Λ_b	38	2000	0.04

Table 8.24: Run II projections for the Run I exclusive lifetime measurements at CDF corresponding to 2 fb^{-1} .

In the case of the B_s , however, since the $J/\psi \phi$ final state is mostly sensitive to one weak eigenstate, it is useful primarily in measuring $\Delta\Gamma_s$ rather than the average Γ_s which is to be compared with Γ_d . The $\Lambda_b \rightarrow J/\psi \Lambda^0$ lifetime is expected to be known within 0.04 ps — significantly better than the current world average — but depends upon being able to more effectively distinguish the signal from $B^0 \rightarrow J/\psi K_S^0$ decays, which are topologically very similar.

Comparable projections for B_c and Ξ_b exclusive lifetime analyses cannot be made, since their exclusive decays were not observed in Run I data.

Hadronic Triggers Beyond the $J/\psi \rightarrow \ell^+ \ell^-$ trigger samples, there are expected to be large data samples that will be made available by the hadronic displaced-track trigger. Although those samples will also improve on the B^- and B^0 lifetimes most interestingly they will improve on the B_s and Λ_b lifetime measurements. Since the hadronic trigger is a new hardware device all predictions are less certain than the predictions for decay modes originating from the leptonic triggers.

Most branching fractions for the decay modes used below are not measured and have to be estimated. This is particularly difficult for the Λ_b decay modes. Errors of 50 percent for the B_s decays and 100 percent for the Λ_b decays are assumed.

Another principle difficulty in these data samples lies in the understanding of the effect of the trigger on the lifetime distributions. The displaced vertex trigger prefers large lifetime events and introduces a bias in the proper time distribution. In the following it is assumed that it is possible to model the trigger bias and use all of the statistical power of the projected yields.

For the B_s decay modes $D_s \pi$ and $D_s \pi \pi \pi$ there are approximately 75k events projected. This includes the D_s decay modes to $\phi \pi$ and $K^* K$ only, as indicated in Table 8.10. Further it is expected that the signal to background ratios is one, which is rather conservative. This results in an uncertainty of the B_s lifetime of approximately 0.007 ps.

For the lifetime ratio of B_s and B^0 this corresponds to an error of roughly half a percent and is thus in the same order as the theoretical prediction for the deviation from unity.

For the Λ_b decay modes $\Lambda_c \pi$ ($\Lambda_c \rightarrow p K \pi$), $p D^0 \pi$ ($D^0 \rightarrow K \pi$ and $D^0 \rightarrow K \pi \pi \pi$), $p \pi$ and $p K$ there are approximately 24.4k events projected. Again assuming a signal to background ratio of one, a statistical uncertainty of 0.01 ps is obtained. This is more precise than the

expectation from the $J/\psi\Lambda^0$ decay mode. A stringent test will be available for the theoretical predictions of the lifetime ratio of Λ_b to B^0 .

More inclusive strategies, using triggerable combinations of leptons and displaced tracks, will also significantly increase the precision of the lifetime ratios of the rarer b hadrons, such as the B_c and so far by CDF not observed baryons as Ξ_b might be accessible. These strategies have yet to be investigated in detail.

8.8.2 Lifetime measurements at DØ[†]

A rich spectroscopy and lifetime measurement program is planned for both beauty mesons and baryons. We will study any species that has significant decay modes that result in at least one lepton. One of the highlights of this program is a measurement of the Λ_b lifetime in the exclusive decay mode $\Lambda_b \rightarrow J/\psi + \Lambda$. This is particularly interesting since the measured ratio $\tau(\Lambda_b)/\tau(B_d) = 0.78 \pm 0.04$ [107] is significantly different from the naive spectator model prediction of unity. Current theoretical understanding of non-spectator processes such as final-state quark interference and W boson exchange cannot account for such a large deviation. Another important measurement which we will make is a measurement of the B_s lifetime using modes such as $B_s \rightarrow J/\psi\phi$.

Measurements of the Λ_b^0 baryon lifetime have long been hampered by a dearth of statistics. For this reason, the lifetime was measured in the semileptonic decay mode, where the branching fraction is orders of magnitude higher than for any fully reconstructed mode [108–111]. The disadvantage of the semileptonic mode is that the neutrino information is lost. To obtain the true decay length in the absence of neutrino information, the ratio $p_T(\Lambda_c\ell)/p_T(\Lambda_b^0)$ (called the K factor) was obtained from a Monte Carlo calculation and used in the lifetime fit. The limited knowledge of the value of the K factor represented a modest contribution to the uncertainty of this measurement.

In Run II at DØ we can expect to collect 2 fb^{-1} of $p\bar{p}$ collisions or twenty times the statistics of Run I. This provides the opportunity to probe the Λ_b^0 lifetime in a fully reconstructed mode: $\Lambda_b^0 \rightarrow J/\psi\Lambda^0$, where the J/ψ meson decays into two leptons (muon or electron) and the Λ^0 baryon decays into a proton and a pion. Using a fully reconstructed channel avoids the introduction of the K factor and any uncertainty associated with it.

To study this mode, we generated 75 000 Λ_b^0 baryon events using Pythia, simulated the DØ Run II detector using MCFast, and forced the decay mode $\Lambda_b^0 \rightarrow J/\psi\Lambda^0$, followed by $J/\psi \rightarrow \mu^+\mu^-$ and $\Lambda^0 \rightarrow p\pi^-$ with QQ, the CLEO Monte Carlo program. We use this sample to predict the trigger and reconstruction acceptances and to estimate the lifetime resolution. For the purpose of this study, we assume that electrons from J/ψ decays will be reconstructed with a similar efficiency to that of the muons, an assumption which is expected to be approximately true.

The DØ J/ψ trigger identifies events resembling J/ψ decays. The presence of two muon tracks, each with $|\eta| \leq 2.0$ and $p_T \geq 1.5 \text{ GeV}/c$, is sufficient for passing the J/ψ trigger criteria. The trigger acceptance is found to be 16.8% for the muons in these generated

[†] Author: W. Taylor.

Multiplier	Events
$\mathcal{L} = 10^{32} \text{ cm}^{-2}\text{s}^{-1} = 10^{36} \text{ m}^{-2}\text{s}^{-1}$	
$t = 2 \times 10^7 \text{ s}$	
$\sigma_{b\bar{b}} = 158 \mu\text{b} \times 10^{-28} \text{ m}^2/\text{b}$	
$b, \bar{b} = 2$	6.32×10^{11}
$\mathcal{B}(b \rightarrow \Lambda_b^0) = 0.090$	5.7×10^{10}
$\mathcal{B}(\Lambda_b^0 \rightarrow J/\psi \Lambda^0) = 4.7 \times 10^{-4}$	2.7×10^7
$\mathcal{B}(J/\psi \rightarrow \mu\mu, ee) = 2 \times 0.06$	3.2×10^6
$\mathcal{B}(\Lambda^0 \rightarrow p\pi) = 0.639$	2.0×10^6
Detector acceptance = 0.55	1.1×10^6
$\epsilon(\text{trigger}) = 0.168$	1.9×10^5
$\epsilon(\text{track efficiency}) = 0.95^4$	1.5×10^5
$\epsilon(\text{reconstruction}) = 0.096$	14 850

Table 8.25: Event yield determination after 1 year or 2 fb^{-1} .

Monte Carlo events. We introduce by hand an additional acceptance cut of 55% for the holes in the muon detection system not modeled in MCFast.

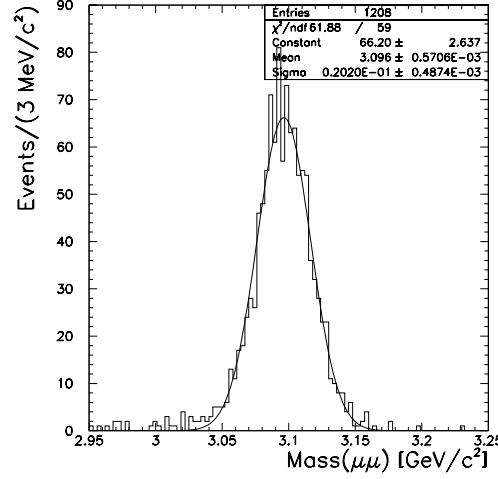
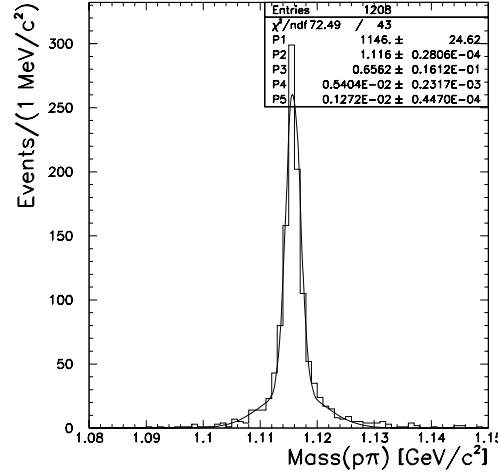
Track quality cuts are applied to all the tracks in the events passing the trigger. The muon tracks from the J/ψ decay are required to have at least four stereo hits in the tracking system (silicon detector and central fiber tracker combined) and at least eight hits (stereo and axial combined) in the silicon detector. For tracks in the central region ($|\eta| \leq 1.7$), at least fourteen hits are required in the central fiber tracker. The transverse momentum is required to be above $400 \text{ MeV}/c$.

The Λ^0 baryon daughters are required to have at least three stereo hits in the tracking system (silicon detector and central fiber tracker combined) and a minimum of eight hits in the central fiber tracker. The transverse momentum is required to be above $400 \text{ MeV}/c$. The long lifetime of the Λ^0 baryon prevents the use of strict silicon hit requirements, as the Λ^0 baryon often decays outside of the fiducial volume of the silicon detector.

The muons are constrained to come from a common vertex in three dimensions as are the Λ^0 daughters. Finally, the location of the Λ_b^0 decay vertex is obtained by extrapolating the Λ^0 baryon momentum direction in three dimensions back to the J/ψ decay vertex. The resulting vertex defines the decay length of the Λ_b^0 baryon.

The acceptance for these selection criteria is 9.6%. We introduce by hand an additional acceptance cut of $(0.95)^4=0.81$ for the tracking efficiency not modeled in MCFast. The final acceptance times efficiency for the trigger and reconstruction criteria is 0.72%. We therefore predict about 15 000 events to be reconstructed in 2 fb^{-1} . Table 8.25 shows the values used to obtain this prediction for the yield.

The mass distributions for the J/ψ and Λ^0 particles are shown in Figures 8.25 and 8.26, respectively. With the application of constraints on both the J/ψ mass and the Λ^0 mass, we predict the Λ_b^0 mass resolution to be $16 \text{ MeV}/c^2$, as indicated in Figure 8.27. The lifetime resolution is found to be 0.11 ps (Figure 8.28).

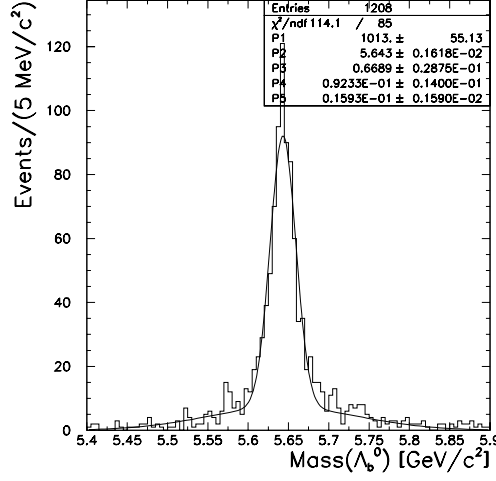
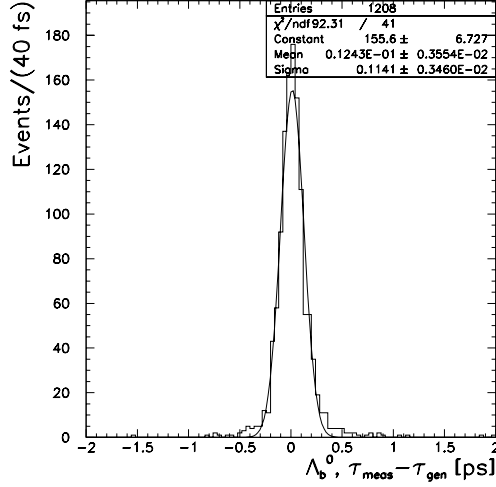
Figure 8.25: J/ψ mass distribution.Figure 8.26: Λ^0 mass distribution.

8.8.3 Summary of Projections for Lifetimes

The exclusive b hadron event samples involving $J/\psi \rightarrow \mu^+\mu^-$ alone will enable CDF and DØ during Run II to push the precision of lifetime measurements to values close to 1 fs. Further inclusion of other hadronic decay modes will decrease the statistical error further below 1 fs.

In particular the lifetime measurements of B_s and Λ_b which cannot be measured by the B factories will achieve a statistical precision of about 0.007 ps and 0.01 ps, respectively. Those measurements determine the ratio of $\tau(B_s)/\tau(B^0)$ to roughly half a percent which allows a first test of the theoretical predictions.

Lifetimes of other interesting b hadrons like the B_c will be improved significantly, and there is a good chance to observe Ξ_b for the first time and measure its lifetime.

Figure 8.27: Λ_b^0 mass distribution.Figure 8.28: $\tau(\Lambda_b^0)_{\text{meas}} - \tau(\Lambda_b^0)_{\text{gen}}$.

8.9 Conclusions

The Tevatron provides a unique testing ground for mixing and lifetime studies. For these measurements it is superior to the B -factories, because the large boosts of the produced hadrons and the higher statistics allow to study the decay distributions more precisely. Moreover, studies of B_s mesons and b -flavored baryons are not possible at current B -factories running at the $\Upsilon(4S)$ resonance. At Run II $B_s^0 - \bar{B}_s^0$ mixing will be discovered and the mass difference Δm_s will be determined very precisely. This measurement is of key importance for the phenomenology of the unitarity triangle. Our knowledge of the lifetime pattern of b -flavored hadrons will significantly improve, the yet undetected width difference $\Delta\Gamma_s$ between the B_s mass eigenstates is within reach of Run II and the Λ_b lifetime puzzle will be addressed.

References

- [1] Particle Data Group, Eur. Phys. J. **C 3** (1998) 1.
- [2] M.A. Shifman and M.B. Voloshin, (1981) unpublished, presented in the review V.A.Khoze and M.A. Shifman, Sov. Phys. Usp. 26 (1983) 387.
- [3] M.A. Shifman and M.B. Voloshin, Sov. J. Nucl. Phys. 41 (1985) 120.
- [4] M.A. Shifman and M.B. Voloshin, Sov. Phys. JETP 64 (1986) 698.
- [5] B. Chibisov, R.D. Dikeman, M.A. Shifman, and N. Uraltsev, Int. J. Mod. Phys. A12 (1997) 2075.
- [6] I. Bigi, M. Shifman, N. Uraltsev, and A. Vainshtein, Phys. Rev. D59 (1999) 054011.
- [7] I.I. Bigi, N.G. Uraltsev, and A.I. Vainshtein, Phys. Lett. B293 (1992) 430; [E: B297 (1993) 477].
- [8] B. Guberina, S. Nussinov, R. Peccei, and R. Rückl, Phys. Lett. B89 (1979) 11.
- [9] N. Bilić, B. Guberina, and J. Trampetić, Nucl. Phys. B248 (1984) 261.
- [10] I. Bigi, B. Blok, M.A. Shifman, and A. Vainshtein, Phys. Lett. B323 (1994) 408.
- [11] G. Altarelli and S. Petrarca, Phys. Lett. B261 (1991) 303.
- [12] E. Bagan, P. Ball, V.M. Braun, and P. Gosdzinsky, Phys. Lett. B342 (1995) 362.
- [13] Q. Hokim and X.Y. Pham, Phys. Lett. B122 (1983) 297; Ann. Phys. (NY) 155 (1984) 202.
- [14] Y. Nir, Phys. Lett. B221 (1989) 184.
- [15] A. Czarnecki and M. Jezabek, Phys. Lett. B427 (1994) 3.
- [16] E. Bagan, P. Ball, V.M. Braun and P. Gosdzinsky, Nucl. Phys. B432 (1994) 3.
- [17] M.B. Voloshin, Int. J. Mod. Phys. A11 (1996) 4931.
- [18] M.B. Voloshin, Surv. High En. Phys. 8 (1995) 27.
- [19] P. Ball and V. Braun, Phys. Rev. D49 (1994) 2472.
- [20] M. Neubert, Trieste Summer School Lectures, Report CLNS 00/1660, Jan. 2000; [hep-ph/001334].
- [21] M. Neubert and C.T. Sachrajda, Nucl. Phys. B483 (1997) 339.
- [22] M.A. Shifman and M.B. Voloshin, Sov. J. Nucl. Phys. 45 (1987) 292.
- [23] M.B. Voloshin, Phys. Lett. B385 (1996) 369.

- [24] H.-Y. Cheng, Phys. Rev. D **56** (1997) 2783.
- [25] B. Guberina and B. Melić, Eur.Phys.J. C **2** (1998) 697.
- [26] Particle Data Group. *1999 WWW Update*, <http://pdg.lbl.gov/1999/bxxx.html>
- [27] UKQCD Collaboration: M. Di Pierro, C.T. Sachrajda, and C. Michael, Univ. of Southampton report SHEP 99-07, June 1999; [hep-lat/9906031].
- [28] M.B. Voloshin, Phys. Rep. **320** (1999) 275.
- [29] M.B. Voloshin, Phys.Rev. D **61** (2000) 074026.
- [30] M.B. Voloshin, Phys.Lett. B **476** (2000) 297.
- [31] A. J. Buras, M. Jamin and P. H. Weisz, Nucl. Phys. B **347**, 491 (1990).
- [32] C. Bernard, Nucl. Phys. Proc. Suppl. **94**, 159 (2001).
- [33] A. Stocchi, talk at *ICHEP 2000 Conference*, 7 Jul – 2 Aug 2000, Osaka, Japan.
- [34] M. Ciuchini *et al.*, hep-ph/0012308.
- [35] L. Wolfenstein, preprint no. NSF-ITP-90-29 (unpublished), and Phys. Rev. D **43** (1991) 151. A. J. Buras, M. E. Lautenbacher, G. Ostermaier, Phys. Rev. D **50** (1994) 3433.
- [36] M. Beneke, G. Buchalla, C. Greub, A. Lenz and U. Nierste, Phys. Lett. B **459**, 631 (1999).
- [37] S. Hashimoto and N. Yamada, hep-ph/0104080.
- [38] M. Beneke, G. Buchalla and I. Dunietz, Phys. Rev. D **54** (1996) 4419.
- [39] S. Hashimoto, Nucl. Phys. Proc. Suppl. **83-84** (2000) 3.
- [40] N. Yamada *et al.* (JLQCD coll.), contr. to the *18th Intern. Symposium on Lattice Field Theory (Lattice 2000)*, Bangalore, India, 17-22 Aug 2000, hep-lat/0010089.
- [41] K. Hartkorn and H. G. Moser, Eur. Phys. J. C **8** (1999) 381.
- [42] I. Bigi, B. Blok, M. Shifman, N. Uraltsev and A. Vainshtein, in *B decays*, ed. S. Stone, revised 2nd edition, p. 132–157, hep-ph/9401298. M. Neubert and C. T. Sachrajda, Nucl. Phys. B **483** (1997) 339. Y. Keum and U. Nierste, Phys. Rev. D **57** (1998) 4282.
- [43] R. Barate *et al.* [ALEPH coll.], Phys. Lett. B **486** (2000) 286.
- [44] R. Aleksan, A. Le Yaouanc, L. Oliver, O. Pène and J. C. Raynal, Phys. Lett. B **316** (1993) 567.
- [45] M. A. Shifman and M. B. Voloshin, Sov. J. Nucl. Phys. **47** (1988) 511.
- [46] I. Dunietz, R. Fleischer and U. Nierste, hep-ph/0012219.

- [47] Y. Grossman, Phys. Lett. **B380** (1996) 99.
- [48] Report of the b -decay Working Group of the Workshop *Standard Model Physics (and More) at the LHC*, P. Ball *et al.*, CERN-TH/2000-101 [hep-ph/0003238].
- [49] I. Dunietz, Phys. Rev. **D52** (1995) 3048.
- [50] F. Abe *et al.* [CDF Collaboration], Phys. Rev. **D59** (1999) 032004. A. Borgland *et al.* [DELPHI Collaboration], talk at *EPS-HEP 99 conference*, 15–21 Jul 1999, Tampere, Finland.
- [51] M. Acciarri *et al.* [L3 Collaboration], Phys. Lett. **B438** (1998) 417.
- [52] A. Lenz, U. Nierste and G. Ostermaier, Phys. Rev. D **59**, 034008 (1999).
- [53] H. Yamamoto, Nucl. Phys. Proc. Suppl. **65** (1998) 236; Phys. Lett. **B401** (1997) 91.
- [54] I. I. Bigi and N. G. Uraltsev, Nucl. Phys. B **592**, 92 (2001).
- [55] J. L. Rosner, Phys. Rev. D **42**, 3732 (1990).
- [56] A. S. Dighe, I. Dunietz, H. J. Lipkin and J. L. Rosner, Phys. Lett. **B369**, 144 (1996).
- [57] A. S. Dighe, I. Dunietz and R. Fleischer, Eur. Phys. J. C **6**, 647 (1999).
- [58] M. Paulini and K. Burkett, CDF/ANAL/BOTTOM/CDFR/4665 (1998).
- [59] I. Dunietz, H. R. Quinn, A. Snyder, W. Toki and H. J. Lipkin, Phys. Rev. D **43**, 2193 (1991).
- [60] A. S. Dighe and S. Sen, Phys. Rev. D **59**, 074002 (1999).
- [61] A. S. Dighe, I. Dunietz and R. Fleischer, Phys. Lett. **B433**, 147 (1998).
- [62] R. Fleischer and I. Dunietz, Phys. Rev. D **55**, 259 (1997).
- [63] P. Ball *et al.*, hep-ph/0003238.
- [64] G. Bonvicini *et al.*, CLEO conf 98-23, ICHEP98 852.
- [65] We note that this need not be the case in some specific scenarios, *e.g.*, supersymmetry with R-parity violation.
- [66] See, for example, J.L. Hewett, T. Takeuchi, S. Thomas, in *Electroweak Symmetry Breaking and Beyond the Standard Model*, ed. by T. Barklow, *et al.* (World Scientific, Singapore) 1996, hep-ph/9603391.
- [67] Y. Grossman, Y. Nir, M. Worah, Phys. Lett. **B407**, 307 (1997).
- [68] S. Bergmann and G. Perez, hep-ph/0103299; G. Eyal and Y. Nir, Jour. H. E. Phys. **9909**, 013 (1999); G. Barenboim, G. Eyal, and Y. Nir, Phys. Rev. Lett. **83**, 4486 (1999).

- [69] S.L. Glashow and E. Jenkins, *Phys. Lett.* **B196**, 223 (1987); V. Barger, J.L. Hewett, and R.J.N. Phillips, *Phys. Rev.* **D41**, 3421 (1990); A.J. Buras *et al.*, *Nucl. Phys.* **B337**, 284 (1990); J.F. Gunion and B. Grzadkowski, *Phys. Lett.* **B243**, 301 (1990).
- [70] For a review, see, Y. Okada, lectures given at *Int. Symp. on Supersymmetry, Supergravity and Superstrings*, Seoul, Korea, 23-26 Jun 1999, hep-ph/9910457.
- [71] G. Burdman, K. Lane, and T. Rador hep-ph/0012073; G. Buchalla, G. Burdman, C.T. Hill, and D. Kominis *Phys. Rev.* **D53**, 5185 (1996); G. Beall, M. Bander, and A. Soni, *Phys. Rev. Lett.* **48**, 848 (1982).
- [72] D. Atwood, L. Reina, and A. Soni, *Phys. Rev.* **D55**, 3156 (1997); Y. Nir and D. Silverman, *Phys. Rev.* **D42**, 1477 (1990); H. Dreiner in *Perspectives on Supersymmetry*, ed. by G.L. Kane, World Scientific, hep-ph/9707435.
- [73] A. Datta, *Z. Phys.* **C27**, 515 (1985); S. Nandi, L. Zhang, *Phys. Rev.* **D41**, 240 (1990).
- [74] E. Golowich, and A. Petrov, *Phys. Lett.* **B427**, 172 (1998); G. Burdman, hep-ph/9407378, hep-ph/9508349; H. Georgi, *Phys. Lett.* **B297**, 353 (1992); T. Ohl *et al.*, *Nucl. Phys.* **B403**, 605 (1993).
- [75] H. Nelson, talk given at the 19th *International Symposium on Lepton Photon Interactions at High Energies*, Stanford, CA, Aug 1999, hep-ex/9908021.
- [76] P. Sphicas, *A $b\bar{b}$ Monte Carlo Generator*, CDF Note 2655, (1999); K. Anikeev, P. Murat, Ch. Paus, *Description of Bgenerator II*, CDF Note 5092, (1999);
- [77] P. Nason, S. Dawson and R.K. Ellis, *Nucl. Phys.* **B303** (1988) 607; *Nucl. Phys.* **B327** (1989) 49.
- [78] C. Peterson *et al.*, *Phys. Rev.* **D27** (1983) 105.
- [79] P. Avery, K. Read and G. Trahern, Cornell Internal Note CSN-22, 1985 (unpublished).
- [80] T. A. Keaffaber, J. D. Lewis, M. W. Bailey, D. Bortoletto, S. Tkaczyk, A. F. Garginkel, *Measurement of the B Meson Differential Cross Section Using the Exclusive Decay $B \rightarrow J/\psi K$* , CDF Note 4911 (to be updated, 2000).
- [81] F. Abe *et al.*, The CDF Collaboration, *Phys. Rev.* **D60** (1999) 92005.
- [82] C. Caso, *et al.* [Particle Data Group], *Eur. Phys. Jor.* **C15** (2000) 1.
- [83] CDF Run II Technical Design Report.
- [84] The CDF Collaboration, Update to Proposal P-909: *Physics Performance of the CDF II Detector with An Inner Silicon Layer and A Time of Flight Detector*, Submitted to the Fermilab Director and PAC (1999)
- [85] S. Belforte *et al.*, *A Complete Minimum Bias Event Generator*, CDF Note 4219.
- [86] C. Caso, *et al.* [Particle Data Group], *Eur. Phys. Jor.* **C3** (1998) 1.

- [87] F. Parodi, P. Roudeau and A. Stocchi, *Nuovo Cim.* **A112** (1999) 833.
- [88] Particle Data Group, *Eur. Phys. J.* **C 15** (2000) 1.
- [89] F. Abe *et al.* [CDF Collaboration], *Phys. Rev.* **D59** (1999) 032004.
- [90] F. Abe *et al.* [CDF Collaboration], *Phys. Rev. Lett.* **82** (1999) 3576.
- [91] BTeV Preliminary Technical Design Report.
- [92] F. Abe *et al.* [The CDF Collaboration], *Phys. Rev.* **D54**, 6596 (1996).
- [93] P. McBride and S. Stone, *Nucl. Instrum. Meth.* **A368**, 38 (1995).
- [94] BTeV Collaboration, *Proposal for an Experiment to Measure Mixing, CP Violation and Rare Decays in Charm and Beauty Particle Decays at the Fermilab Collider – BTeV*, May 2000.
- [95] K.T. McDonald, *Maximum Likelihood Analysis of CP Violating Asymmetries*, PRINCETON-HEP-92-04, Sep 1992. 12pp, unpublished.
- [96] F. Abe *et al.* [CDF Collaboration], *Phys. Rev.* **D59** (1999) 032004.
- [97] F. Abe *et al.* [CDF Collaboration], *Phys. Rev. Lett.* **77** (1996) 1945.
- [98] F. Abe *et al.* [CDF Collaboration], *Phys. Rev. Lett.* **75** (1995) 3068, *Phys. Rev. Lett.* **85** (2000) 4668.
- [99] I. Dunietz, R. Fleischer, U. Nierste, *In Pursuit of New Physics with B_s Decays*, CERN-TH/2000-333 [hep-ph/0012219].
- [100] F. Abe *et al.*, *Phys. Rev. Lett.* **77**(1996)1945.
- [101] R. Aleksan, A. Le Yaouanc, L. Oliver, O. Pène, J.-C. Raynal, *Phys. Lett.* **B317** (1993) 173.
- [102] R. Aleksan, A. Le Yaouanc, L. Oliver, O. Pène, J.-C. Raynal, *Phys. Lett.* **B316** (1993) 567.
- [103] The ALEPH Collaboration, CERN-EP/2000-036, to be submitted to *Phys. Lett.* **B**.
- [104] T. Affolder *et al.*, CDF Collaboration, *Phys. Rev. Lett.* **85** (2000) 4668.
- [105] P. L. Frabetti *et al.*, E687 Collaboration, *Phys. Rev. Lett.* **70** (1993) 1755.
- [106] F. Abe *et al.*, *Phys. Rev. Lett.* **77**(1996)1945.
- [107] LEP B Lifetime Working Group, <http://home.cern.ch/~claires/lepblife.html>.
- [108] ALEPH Collaboration, R. Barate *et al.*, *Measurement of the b Baryon Lifetime and Branching Fractions in Z Decays*, *Eur. Phys. J.* **C2**, (1998) 197.

- [109] CDF Collaboration, F. Abe *et al.*, *Measurement of the Λ_b^0 Lifetime Using $\Lambda_b^0 \rightarrow \Lambda_c^+ \ell^- \bar{\nu}$* , Phys. Rev. Lett. **77**, (1996) 1439.
- [110] DELPHI Collaboration, P. Abreu *et al.*, *Determination of the Average Lifetime of b Baryons*, Z. Phys. **C71**, (1996) 199.
- [111] OPAL Collaboration, K. Ackerstaff *et al.*, *Measurements of the B_s^0 and Λ_b^0 Lifetimes*, Phys. Lett. **B426**, (1998) 161.